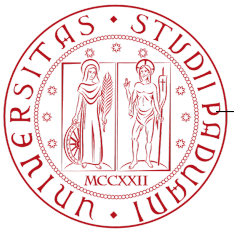

UNIVERSITÀ DEGLI STUDI DI PADOVA
DIPARTIMENTO DI INGEGNERIA INDUSTRIALE
DIPARTIMENTO DI FISICA E ASTRONOMIA

Corso di Laurea Magistrale in Ingegneria Aerospaziale

SOLAR RADIATION PRESSURE MODELING FOR THE QZS-1 SATELLITE

Studente

Francesco Darugna
Mat. 1106937

Relatore

Prof. Stefano Casotto
Università degli Studi di Padova

Correlatori

Dr. Oliver Montenbruck
Deutsches Zentrum für Luft- und Raumfahrt

Prof. Enrico Lorenzini
Università degli Studi di Padova

A.A. 2016/2017

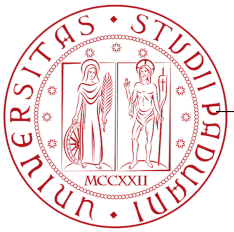

UNIVERSITÀ DEGLI STUDI DI PADOVA
DIPARTIMENTO DI INGEGNERIA INDUSTRIALE
DIPARTIMENTO DI FISICA E ASTRONOMIA

Corso di Laurea Magistrale in Ingegneria Aerospaziale

SOLAR RADIATION PRESSURE MODELING FOR THE QZS-1 SATELLITE

Studente

Francesco Darugna
Mat. 1106937

Relatore

Prof. Stefano Casotto
Università degli Studi di Padova

Correlatori

Dr. Oliver Montenbruck
Deutsches Zentrum für Luft- und Raumfahrt

Prof. Enrico Lorenzini
Università degli Studi di Padova

A.A. 2016/2017

To my parents, Franco and Patrizia.
Ai miei genitori, Franco e Patrizia.

ACKNOWLEDGEMENTS

This Master thesis assignment involved two different institutes: the German Space Operations Center (GSOC) of the Deutsches Zentrum für Luft und Raumfahrt (DLR) in Ober - pfaffenhofen (Munich, Germany) and the University of Padova (Italy). This thesis has in fact its roots in the research conducted at GSOC and at the University of Padova on the Solar Radiation Pressure modeling. First and foremost I would like to express my gratitude to my supervisors Dr. O.Montenbruck (DLR/GSOC) and Prof. S.Casotto (University of Padova) for the ideas and vision, the constant technical supervision, but especially for being an every day source of inspiration and for giving me this opportunity. In addition, I would like to thank the whole GNSS Technology and Navigation Group at DLR (GSOC/DLR) for the support during my period at DLR. Special credits to Dr. P.Steigenberger for the software testing support with the orbit determination and for the opportunity to manage real observed data and to Dr. B.Braun for the time as office mate during my period at DLR. Furthermore I would like to thank Dr. M.Bardella (University of Padova) for his programming support. Eventually I thank Prof. E.Lorenzini to contribute from the Department of Engineering (University of Padova) in providing me this opportunity. I have really enjoyed working together with the GNSS Group at GSOC, in this highly professional environment.

CONTENTS

LIST OF FIGURES

LIST OF TABLES

LIST OF SYMBOLS

ϵ	elongation
α	absorbed fraction of the incident radiation
$\bar{\mathbf{C}}$	correlation matrix
$\bar{E}$	energy of the particle
$\bar{F}$	force per unit area
β	Sun elevation
δ	diffusely reflected fraction of the incident radiation
$\boldsymbol{e}_n$	surface normal unit vector
$\boldsymbol{e}_\odot$	spacecraft to sun unit vector
$\mathbf{e}_s$	shear direction unit vector
$\mathbf{F}$	force due to SRP
μ	orbit angle
Ω	Right Ascension Ascending Node (RAAN)
ω	argument of perigee
Φ	solar flux
ρ	specularly reflected fraction of the incident radiation
θ	angle between incident radiation and the surface normal
$\boldsymbol{a}$	SRP acceleration
A	azimuth angle
a	semi-major axis
c	velocity of the light in vacuum
d$\mathbf{f}$	differential force due to SRP
dA	element area
E	elevation angle
e	eccentricity
f	frquency
h	Planck's constant
i	inclination
M	mean anomaly
m	total mass
m_0	rest mass
p	photon momentum
W	solar irradiance

Acronyms

ARPA	Aerodynamics and Radiation Pressure Analysis
CAD	Computer Aided Design
DLR	Deutsches Zentrum für Luft und Raum-fahrt
ECOM	Empirical CODE Orbit Model
GHOST	GPS High Precision Orbit Determination Software Tools
GLONASS	Global'naya Navigatsionnaya Sputnikovaya Sistema
GNSS	Global Navigation Satellite System
GPS	Global Positioning System
GSOC	German Space Operations Center
IGSO	Inclined Geosynchronous orbits
IRNSS	Indian Regional Navigation Satellite System
JAXA	Japan Aerospace Exploration Agency
NAPEOS	NAvigation Package for Earth Orbiting Satellites
ON	Orbit Normal
POD	Precise Orbit Determination
QZSS	Quasi Zenith Satellite System
SRP	Solar Radiation Pressure
YS	Yaw Steering

Abstract

Solar Radiation Pressure (SRP) is the dominant non-gravitational perturbation of Global Navigation Satellite Systems (GNSSs). The system considered in this thesis is the Japanese regional satellite navigation system QZSS that is currently made up of one single satellite, called QZS-1. Since the Earth gravity field is described with a good accuracy, the modeling of the non-gravitational perturbations is significant for the Precise Orbit Determination (POD). The SRP modeling is therefore fundamental to improve the navigation performance of a satellite such as QZS-1. The SRP depends on the surfaces of the satellite involved, in particular it depends on the optical and geometrical properties of the surfaces. In the absence of detailed information about these properties and, therefore, in the absence of detailed models, empirical SRP, such as the Empirical CODE Orbit Model (ECOM), are employed for GNSS orbit determination. An issue associated with the ECOM is that it requires a significant number of parameters to accurately describe the real motion. Two different models of the SRP are developed: an analytical model and a ray-tracing model. The first one is a generic box-wing model based on the previous work of DLR about the SRP analysis for the European Galileo system while the second one is based on the previous work about the SRP analysis for the GOCE satellite at the University of Padova. A new reference frame with respect to the previous works is introduced in the analytical description of the SRP in order to consider both the attitudes used by QZS-1, the Yaw-Steering mode and the Orbit-Normal mode. The box-wing model is related to the corresponding parameters of the ECOM. The validation of the box-wing model in a POD gives as result an adjusted model of the SRP for the QZS-1 satellite. The orbits obtained using this model show consistent improvements in the quality of the orbit for both Yaw-Steering and Orbit-Normal attitude modes, in terms of Day Boundary Discontinuities (DBDs), Satellite Laser Ranging (SLR) residuals and clock residuals. The ray-tracing approach gives an accurate model based on a CAD geometry of the spacecraft. The comparison between the two models in orbit determination suggests that a more accurate model, such as the ray-tracing model, could improve the POD of QZS-1 even more than a box-wing model. Nevertheless, to completely explain the remaining discrepancies between the analytical model and the observed orbital perturbations, a more detailed model of thermal re-radiation, more detailed information about the true attitude, and the offsets between the nominal and actual solar panels are needed.

1. INTRODUCTION

1.1 Context

The *Quasi Zenith Satellite System* QZSS is a Japanese navigation satellite system providing GPS compatible signals as well as integrity and correction for the users in Asia and the Pacific region [11]. It operates from inclined, elliptical geosynchronous orbits to achieve optimal high-elevation visibility in urban canyons and mountainous areas. The navigation system objective is to broadcast GPS-interoperable and augmentation signals as well as original Japanese (QZSS) signals from a four-spacecraft constellation since the beginning of 2018 [23, 27] and seven-spacecraft constellation after 2023 [23, 27]. As part of the GNSS satellites, its Precise Orbit Determination (POD) is an important goal to achieve the navigation performance. Since the Earth gravity field and luni-solar gravitational perturbations are, nowadays, described with a good accuracy, the non-gravitational perturbations (such as the solar radiation pressure) represent the most important source of error for orbit determination. This thesis primary aims at modeling of the Solar Radiation Pressure (SRP) for the QZS-1 satellite, which is the first one launched in 2010, as a technological validation for the enhancement of GPS availability and performance. The Solar Radiation Pressure is not easy to model. This difficulty is due to its direct relation with the geometry and the optical properties of the spacecraft which often, as well as in this particular case, are not not properly defined. Within the present study an analytical SRP model is investigated and then validated in a orbit determination procedure. In absence of detailed surface models empirical SRP models are considered and the improvement offered by the addition of an analytical model are presented. At the same time the SRP effect on the satellite is considered with a ray-tracing technique, which simulates the interaction of the photons coming from the Sun with the satellite surfaces, considering a more accurate geometrical description of the spacecraft with respect to the analytical model. Then the model obtained from the ray-tracing approach is compared to the analytical model. The difference between the two is used as the SRP model in the orbit determination in order to analyze the effect of this difference on the orbit accuracy. The work of this thesis presents a complete analysis of the Solar Radiation Pressure modeling and estimates what are the benefits on the quality of the orbit determination modeling this particular non-gravitational perturbation. Furthermore part of the results obtained during this work has been published in the scientific journal *Advances in Space Research* [28].

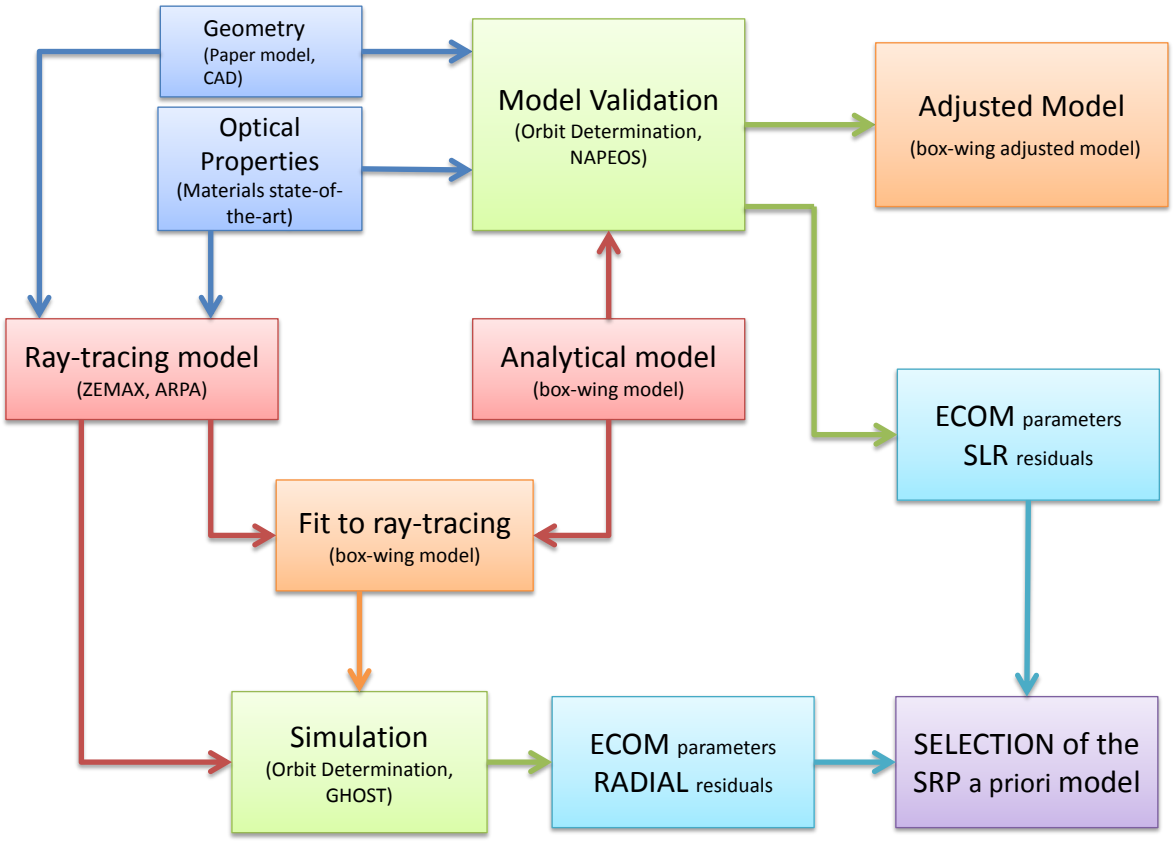

Figure 1.1: Operative path of the thesis work.

1.2 Thesis outline

Figure 1.1 shows the outline of the work of this thesis highlighting the main points. The analytical model is developed as a box-wing model based on the previous DLR's work for Galileo satellites [24]. As well as the name suggests the box-wing model considers the satellite as sum of two components: a box, which represents the body of the spacecraft and wings, that represent the solar panels. It is very simple and its simplicity causes also an approximation (concerning the geometry), but it gives the opportunity to understand the behaviour and to manage the different contributions to the Solar Radiation Pressure. The analytical model, in fact, allows to consider the contribution of the different optical properties to the total amount of the SRP. The optical properties are represented by the fractions of absorbed as well as diffusely and specularly reflected photons of the incident radiation [1]. In this way the analytical model is parametrized with parameters that depend on the geometry and the optical fractions. Furthermore the analytical model allows to considered averaged components of the SRP acceleration over an orbit, that are useful to fit the model to real observed data. The validation of the model in a Precise Orbit Determination gives an adjusted analytical model of the SRP with the minimum number of parameters needed to describe this particular magnitude. This adjusted model is the best analytical model which fits the observed data. The parameters of this model are compared to the expected values calculated with the analytical model and considerations about the geometry and the optical properties. These considerations are based on a Computer Aided Design (CAD) model (realized with SolidWorks®), based on a paper model furnished by JAXA [35], and on the state-of-the-art of the materials used in this field [21, 3]. The geometrical and optical characterization is needed also for a first guess in the adjusting process of the model within POD. The parametrized analytical model allows to con-

sider also the relation between the contributions related to different optical properties and the components of the SRP acceleration considering real observed data. Moreover, the application of a simple box-wing model in the GNSS data processing gives significant improvements to the quality of the estimated QZS-1 orbits [28]. Nevertheless, this thesis develops also a more accurate model with a ray-tracing approach, with the purpose to understand if it could give a relevant improvement to the quality of the estimated orbits with respect to a simple box-wing model. The software used for the ray-tracing is the commercial software ZEMAX® which allows to consider CAD geometry to simulate the spacecraft. The program developed by the University of Padova ARPA [19], upgraded in the SRP analysis with new features in the context of this thesis, is used to compute the SRP acceleration. The goal of ARPA is to translate the binary output of ZEMAX into results with physical meaning. The ray-tracing approach gives in output tabulated accelerations for different configurations between Sun and spacecraft. The analytical model can be fitted to the ray-tracing model in order to consider the box-wing model which best fits the data obtained from the ray-tracing. The difference between the last two models is considered as an a priori model into the orbit determination, whose performances (represented by the empirical parameters ECOM [2] and the position error in the radial direction) are compared to the performances (represented by the empirical parameters ECOM and the Satellite Laser Ranging SLR residuals) of the POD obtained from the model validation. Eventually the comparison of the two performances gives an idea about the potential improvement of the application of ray-tracing model in the GNSS data processing with respect to the simple analytical model. The thesis closes with a critical assessment about the entire work and with recommendations for further improvements.

2. GNSS AND QZSS OVERVIEW

2.1 GNSS

The term *Global Navigation Satellite System* (GNSS) refers to a constellation of satellites providing signals from space with positioning and timing data. A constellation of satellite consists of multiple satellites that orbit the Earth in similar, but suitably shifted or rotated trajectories. There are two GNSSs operative: the American GPS that is the first and oldest system and the Russian GLONASS. The European Galileo is under develop in this period. Other countries had effort in developing a navigation satellite system. In fact there are also the Japanese QZSS, the Chinese BeiDou and the Indian IRNSS. The last three offer only a regional coverage instead of a global one. The primary advantages of using $GNSS$ with respect to other satellite geodesy technique such as SLR or VLB are cost and mobility.

GPS The Navstar GPS (NAVigation System with Time and Ranging Global Positioning System) is a satellite-based radio navigation, positioning,and time - transfer system. It is completely operative since 1995. It consists of three segments: the space segment, the control segment and the user segment. The space segment comprises 24 satellites in six different orbital planes with a 55° inclination angle. The GPS is set at an altitude of 20 200 km.

GLONASS GLONASS is the Russian equivalent of the GPS. It was developed by the governmental "Academician Reshetnev Research and Production Association of Applied Mechanics", which then became the Joint Stock Company "Information Satellite Systems (ISS) - Reshetnev Company" [25]. As well as GPS it consists in the space segment, the control segment and the user segment. The space segment consists in three different types of spacecraft and it comprises 24 satellites on three different orbital planes. The orbital inclination is 64.5°. The orbits are almost circular and the orbital period is shorter than the GPS one since GLONASS is on lower orbits.

Galileo Galileo is Europe's own global navigation satellite system, providing a highly accurate, guaranteed global positioning service under civilian control. It is interoperable with GPS and GLONASS, the US and Russian global satellite navigation systems. By offering dual frequencies as standard, Galileo is set to deliver real-time positioning accuracy down to the metre range[32]. The Galileo system consists of 24 operational satellites plus six in-orbit spares, positioned in three circular Medium Earth Orbit (MEO) planes at 23 222 km altitude above the Earth, and at an inclination of the orbital planes of 56 degrees to the equator. This new European GNSS the 15^{th} December 2016 at the ceremony in Brussels titled *Galileo Goes Live*, has been declared operationally ready, it means that Galileo satellites and ground infrastructure can now offer their services, even if they are just Initial Service. The Initial Service are three: the Open Service for users (chip-sets for smartphones, car navigation systems), the Galileo's Public Regulated Service (for government-authorized users) and the Search and Rescue Service (International emergency beacon location). The Galileo navigation signals will provide good coverage even at latitudes up to 75 degrees north, which corresponds to Norway's North Cape, the most northerly tip of Europe, and beyond. The large number of satellites together with the carefully-optimised constellation design, plus the availability of the three active spare satellites per orbital plane, will ensure that the loss of one satellite should have no discernible effect on the user [32].

QZSS The Quasi Zenith Satellite System (QZSS) is a Japanese regional satellite navigation system. The first navigation system objective is to broadcast GPS-interoperable and augmentation signals as well as original Japanese (QZSS) signals from a three-spacecraft constellation in inclined, elliptical geosynchronous orbits. With this system concept, users in and around Japan and Oceania/Australia can use seamless positioning, navigation, and timing services, even in urban canyons and mountainous areas.

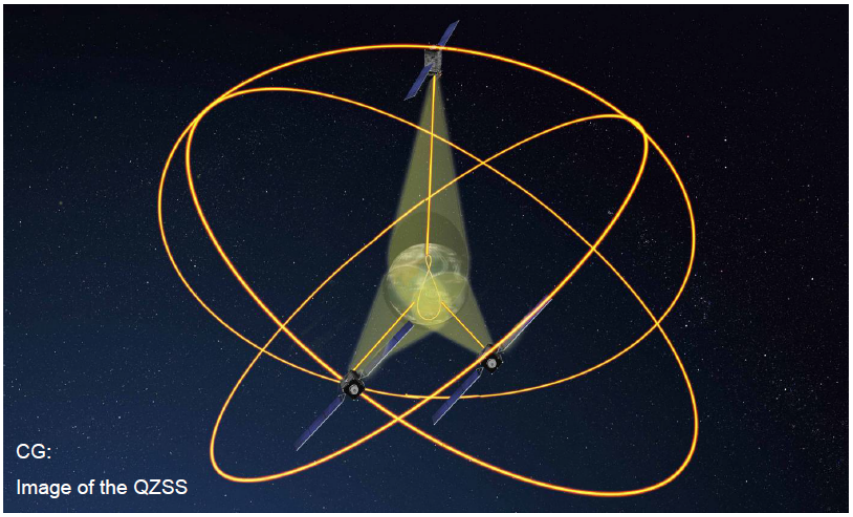

Figure 2.1: The QZSS aims to deploy three satellites on orbit so as to always have one flying near the zenith over Japan. By doing so, the system can provide a highly accurate satellite positioning service covering close to 100% of Japan even in urban canyons and mountainous areas. Reproduced from [36].

QZSS satellites will occupy inclined elliptical geosynchronous orbits for optimal high-elevation visibility in the area of coverage. QZSS consists of multiple satellites that fly in an orbit passing through the near zenith over Japan (hence the name *Quasi Zenith*). Satellites on the slightly eccentric orbits have a slower speed in the northern hemisphere by moving away from the earth, and a faster speed in the southern hemisphere by coming closer to the earth, as the QZSS website points out. The quasi-zenith orbit is a *figure-eight shaped* orbit with north-south asymmetry. Satellites spend approximately 13 hours in the northern hemisphere and roughly 11 hours in the southern hemisphere, allowing them to remain near Japan for a long period of time. The QZSS constellation (when completed) will operate more like independently - operating GPS or Galileo navigation satellites. QZSS currently is made up of one single satellite, called QZS-1 or *Michibiki* which means *guide* or *show the way* [30]. It is the prototype of this kind of satellite and it has to test the key technologies. It will be introduced in this chapter. Three more QZSS satellites have been ordered in April 2013. QZS-2 and QZS-3 will also operate from the inclined geosynchronous orbit, while QZS-4 will augment the system from a geostationary orbit since the beginning of 2018 [23]. In order to enable continuous and more sustainable positioning after 2023 the constellation will be completed into a seven-spacecraft constellation [23, 37].

BeiDou BeiDou Navigation Satellite System is China's global navigation satellite system which has been developed independently. BeiDou Navigation Satellite System is composed of three parts: the space section, the ground section and the user section. The space section contains 5 geostationary orbit satellites and 30 non-geostationary orbit satellites. Unlike GPS, GLONASS and Galileo, in fact, it is made of a mixture of different satellite: MEO, IGSO and GEO, in order to achieve a regional and, in the future, global navigation service [25]. The ground section consists of a certain number of stations: including the main control stations, the injection stations and the monitoring stations. Furthermore the user section includes terminals of BeiDou system and it is compatible with other navigation satellite systems [29].

IRNSS The Indian Regional Navigation Satellite System (IRNSS) is an autonomous regional satellite navigation system which covers only the Indian subcontinent and the adjacent regions. The final configuration of this satellite system will comprise seven satellites: three geostationary satellites and four geosynchronous satellites in moderately inclined orbits [25]. The Indian Space Research Organization (ISRO) for small meteoreological and communication satellites in geostationary orbit already developed INSAT-1000 (I-1K) and all the spacecraft of IRNSS make use of its satellite bus.

2.2 Reference frames

Two essential information for the processing of observations from Global (and Regional) Navigation Satellite Systems in precise orbit determination and precise point positioning applications are the geometry and orientation. In order to take into account this aspect, it is useful to introduce some reference frames [24]. The various constellations of navigation satellites have different configurations and orbits. Usually for a global coverage medium-altitude Earth orbits (MEO) are used, while to cover a regional area geosynchronous orbits are employed. The geosynchronous orbits are divided into two groups: the inclined geosynchronous orbits (IGSO) and the geostationary orbits (GEO) with a very small inclination.

The two main objectives that the inertial attitude of a GNSS satellite needs to guarantee are:

- to point the navigation antenna toward the Earth;
- to keep the solar panels oriented to the Sun.

In order to achieve these goals the satellite performs a rotation about the Earth-pointing *yaw* axis such as to keep the solar panel axis perpendicular to the Sun direction. This idea, adopted for the first time by the GPS, is commonly known as *yaw-steering* (YS) attitude mode [24]. However it has a disadvantage when the Sun is close to the orbital plane, because in this case it requires a rapid yaw-slews of up to 180°. For this particular case a mode in which the spacecraft body is fixed in the local orbital frame and the solar panel rotation axis is kept perpendicular to the orbital plane is often favored. It is called *orbit-normal* (ON) mode [24] . Sometimes (as well as QZS-1) both attitudes modes may be employed depending on the angle between the Sun and the orbital plane (usually denoted as β). Since there are different possible ways to describe the attitude (maybe differing only by a permutation of axes), the *International GNSS Service* (IGS) has adopted a common body-fixed reference frame $R_{BF,IGS}$ [25]:

- The $+z_{BF,IGS}$-axis is the principal body axis closest to the antenna boresight direction (i.e., the direction of the maximum beam intensity)[25].
- The $y_{BF,IGS}$-axis is parallel to the rotation axis of the solar panels. The positive $y_{BF,IGS}$-direction is set by the corresponding $x_{BF,IGS}$-axis orientation [25].
- The $+x_{BF,IGS}$ direction is chosen such that the $+x_{IGS}$-panel is permanently sunlit during the nominal yaw-steering, while the $-x_{IGS}$-panel remains dark[25].

Local orbital frame The local orbital frame is defined by the radial (**R**), along-track (**T**) and cross-track (**N**) directions. Considering the position **r** relative to the center of the Earth and an inertial velocity **v** of a satellite the corresponding unit vector of the RTN frame are obtained as [25]:

$$\begin{aligned} \mathbf{e}_R &= \frac{\mathbf{r}}{|\mathbf{r}|}, \\ \mathbf{e}_T &= \mathbf{e}_N \times \mathbf{e}_R, \\ \mathbf{e}_N &= -\frac{\mathbf{r}\times\mathbf{v}}{|\mathbf{r}\times\mathbf{v}|}. \end{aligned} \tag{2.1}$$

Yaw-steering frame The yaw-steering frame defines the reference orientation for a nadir-pointing GNSS satellite with Sun-oriented solar panels [25]. It is defined by the three unit vectors:

$$\begin{aligned} \mathbf{e}_{x,YS} &= \mathbf{e}_{y,YS} \times \mathbf{e}_{z,YS}, \\ \mathbf{e}_{y,YS} &= \frac{\mathbf{e}_\odot \times \mathbf{r}}{|\mathbf{e}_\odot \times \mathbf{r}|}, \\ \mathbf{e}_{z,YS} &= -\frac{\mathbf{r}}{|\mathbf{r}|}, \end{aligned} \tag{2.2}$$

where $\mathbf{e}_\odot$ is the unit Sun vector pointing from the satellite to the Sun. The vector $\mathbf{e}_{z,YS}$ points toward the center of the Earth and $\mathbf{e}_{y,YS}$ is perpendicular to the Sun and nadir direction. The

above definitions imply that $\mathbf{e}_{\odot} \cdot \mathbf{e}_{x,YS} > 0$, therefore the unit vector in Sun direction and the +x-axis of this frame are always part of the same hemisphere [25].

Considering the empirical accelerations, used in absence of detailed surface models for SRP, a Sun-oriented reference frame appears more suitable for the treatment of solar radiation pressure perturbations and a right-handed DYB frame which is aligned with the satellite-Sun direction and the nominal solar panel axis in yaw steering mode is introduced [25]:

$$\begin{aligned} \mathbf{e}_D &= \mathbf{e}_{\odot}, \\ \mathbf{e}_Y &= -\mathbf{e}_N, \\ \mathbf{e}_B &= \mathbf{e}_D \times \mathbf{e}_Y. \end{aligned} \tag{2.3}$$

Orbit-normal frame The orbit-normal frame defines the reference orientation of a spacecraft aligned with the orbital frame and its axes are parallel (or antiparallel) to those of the local orbital frame, but the naming and the direction of individual axes is chosen to match those of the body-fixed frame for a spacecraft in nominal orbit-normal mode [25]. Therefore the z_{ON}-axis points to the center of the Earth and the y_{ON}-axis is perpendicular to the orbital plane. Two subcases may be defined considering the x_{ON}-axis toward the velocity (ON^+ frame) or opposite to the velocity (ON^- frame) [25]. In this work the first one is considered. Consequently the three unit vectors that define the orbit normal mode are [25]:

$$\begin{aligned} \mathbf{e}_{x,ON} &= +\mathbf{e}_T, \\ \mathbf{e}_{y,ON} &= -\mathbf{e}_N, \\ \mathbf{e}_{z,ON} &= -\mathbf{e}_R. \end{aligned} \tag{2.4}$$

It is important to underline the meaning of two different angles: the over mentioned β angle and the μ angle. The first is the elevation of the Sun over the orbital plane and the second one is the orbit angle μ measured relative to the midnight point [25]. Another important angle needs to introduced: the elongation ϵ. The elongation is the angle between the z-axis and the Sun vector and it can be defined by [25]:

$$\cos\epsilon = \cos\beta\cos\mu. \tag{2.5}$$

2.3 QZS-1 (*Michibiki*)

Once given the complete framework about GNSS, what GNSS means, the different GNSSs present in the world and introduced the reference frames used in this kind of environment, the satellite considered in this work can be introduced in detail. As already mentioned QZS-1 is the first demonstrative satellite of the Japanese Quasi Zenith Satellite System. It was launched in September 11, 2010 and it enhances the GPS services mainly into two ways [16]:

- improving the availability of the GPS signals;
- increasing the accuracy and reliability of GPS signals.

For this particular work it would be very important to have the geometric and optical properties of the spacecraft but the information available is very poor: no published data about the optical properties of the material used in the satellite and few information about the geometry (just about the external dimensions). The information available is reported in Fig. 2.2. As can be observed the distance from a tip of a solar panel to another is 25.3m and the length of the envelope of the body is 6.2m. It means that this satellite has a very large span of the solar panels. JAXA furnishes also the box shape at the time of launch: 2.9m×3.1m×6.2m. These dimensions take into account the complete envelope in a particular direction, therefore also the undeployed solar arrays that are only in one direction and it could explain the difference in the first two dimensions.

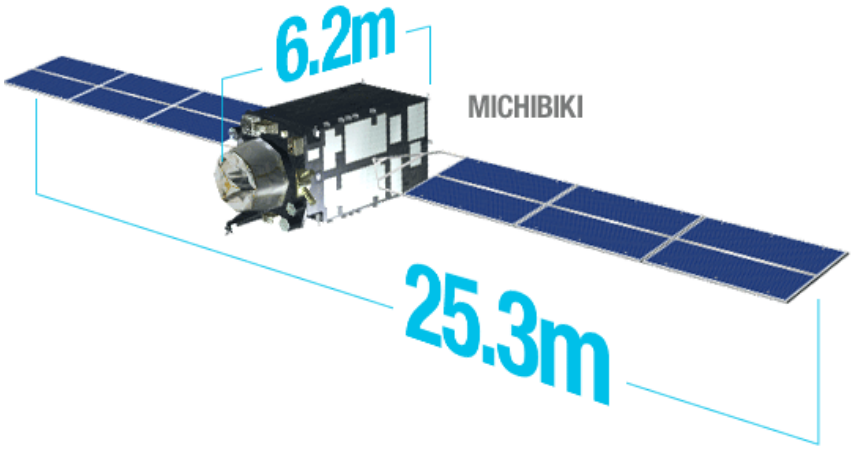

Figure 2.2: Representation of QZS-1 with information about the external dimension furnished by JAXA (from [34]).

The properties of the satellite are shown in [11] and shown in Table 2.1

Table 2.1: Performances of QZS-1.

Parameter	performance
Dry mass	1800 kg
Separated mass	4100 kg
Life time	> 10 years
Solar array power	5300 W at 10 years
Pointing accuracy	0.1 deg
Reliability	
Bus	>0.8
Payload	>0.7

2.3.1 Orbit and ground track

The orbit has the same period of the traditional equatorial geostationary orbit but with an higher inclination and it is elliptical. The orbital elements are showed in Table 2.2. Concerning the

Table 2.2: Orbital elements of QZS-1.

Element	value
Semi-Major axis (a)	42 164 km (average)
Eccentricity (e)	0.075 ± 0.015
Inclination (i)	43 deg ± 4 deg
RAAN (Ω)	195 deg (initial)
Argument of Perigee (ω)	270 deg ± 2 deg
Mean anomaly (M)	305 deg (initial)

ground track an important parameter which has to be satisfy is the *Central Longitude of Ground Track*. The ground track of Michibiki is a sort of eight (see Fig. 2.3) which covers the Asian area from Japan to Australia.

Figure 2.3: Ground track of QZS-1 created with the System Tool Kit (STK) of Analytical Graphics Inc. AGI. The day selected for the plot is January, 15 2017.

The central longitude of ground trace is the center of the 8-figure ground trace, and is the center of two longitudes of ascending and descending. The longitude value is maintained 135 deg East 5 deg [16].

2.3.2 Reference frame and attitude

QZS-1 employs two different attitudes: the Orbit Normal mode and the Yaw Steering mode depending on the Sun elevation above the orbital plane, angle called β [12]:

- Orbit Normal mode (ON) for $|\beta|$<20 deg;
- Yaw Steering mode (YS) for $|\beta|$>20 deg.

However the changing from the YS attitude to the ON attitude mode does not take place exactly at 20deg, but when the yaw-angle in the two attitude modes differ least [18, 25]. Considering the aforementioned β angle and the orbit angle μ (measured relative to the midnight point) [25] the nominal yaw-angle is given by:

$$\psi_{IGS} = \text{atan2}(-\tan\beta, \sin\mu), \tag{2.6}$$

where atan2 is used in order to consider the right quadrant to determine the angle. The orientation of the body of the spacecraft described by the R_{BF} body reference frame is the same of $R_{BF,IGS}$ but with the x and y axes inverted [25].

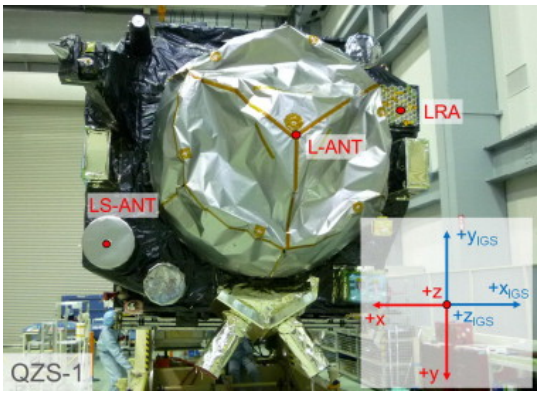

Figure 2.4: Orientation of the spacecraft body with respect to the IGS reference frame. The red frame is the manufacturing JAXA-proposed frame while the blue frame is the IGS frame. Reproduced from [25].

2.3.3 Signals

On QZS-1 are mounted: an L-band transmission antenna (L-ANT), an L1-SAIF transmission antenna (LS-ANT), TTC antennas, and a Ku-band Time Transfer Antenna (Ku-ANT). The L-ANT is made up of a helical antenna array. The gain curve formed by this array is designed to provide signals with constant power levels at any location on the ground by compensating for the Earth's

surface shape [16]. Michibiki's purpose is to cooperate with GPS signals and to ensure this interoperability it uses modernized GPS civil signals as a base, transmitting the L1C/A, L1C, L2C and L5 signals [16]. QZSS further improves standalone GPS accuracy by means of ranging correction data provided through the transmission of submeter-class performance enhancement signals L1-SAIF and LEX from QZS [16]. The L1-SAIF antenna is an auxiliary antenna for transmission of the so-called SAIF (Submeter-class Augmentation with Integrity Function) signal [25].

Table 2.3: QZS-1, GPS and Galileo transmitted signals. The L- denomination is used for the GPS' signals while the E-denomination for the Galileo's signals.

Signal	QZS-1	GPS	Galileo
L1-E1 (1575.42 MHz):	x	x	x
LEX-E6 (1278.75 MHz):	x		x
L2 (1227.60 MHz):	x	x	
E5b (1207.14 MHz):			x
L5-E5a (1176.45 MHz):	x	x	x

Additionally, L1C and L5 of the signals transmitted by QZSS have interoperability with not only GPS but also Galileo and other GNSS in future multi-GNSS era [16]. Table 2.3 gives a comparison of the transmitted signals of QZS, GPS and Galileo [22]. It shows what could be the cooperation between these systems.

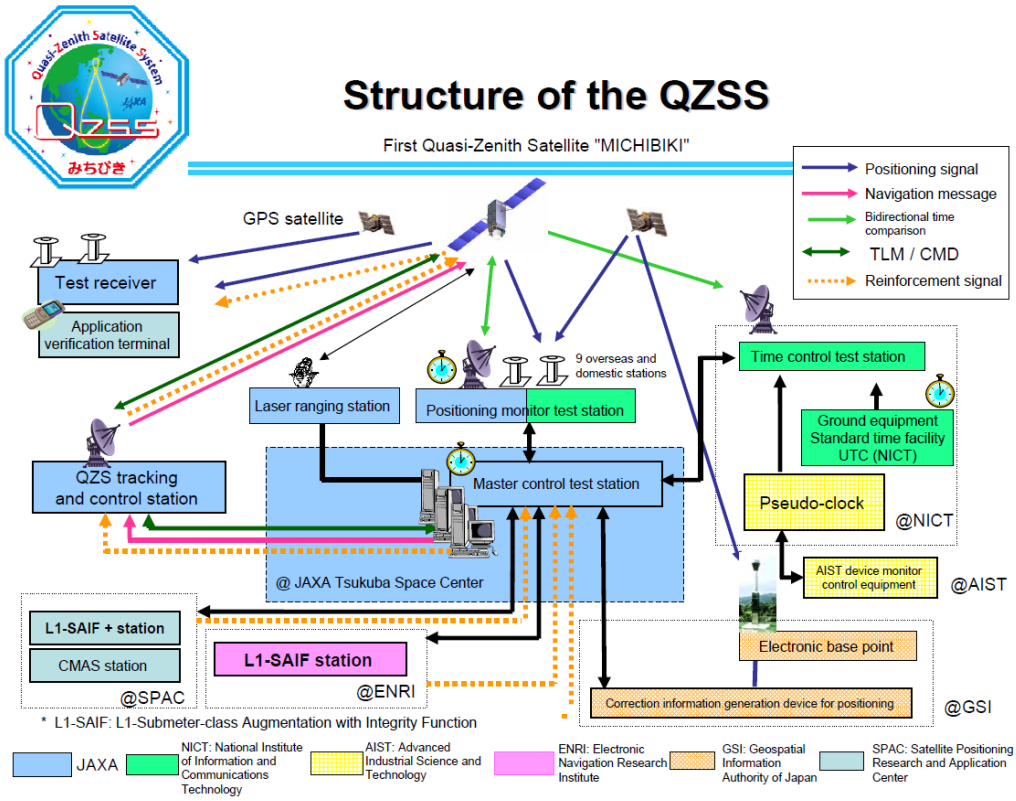

Figure 2.5: Operation of QZS-1. It involves three dfferent segments: the space segment, the control segment and the user segment. Reproduced from [36].

3. SOLAR RADIATION PRESSURE: LITERATURE OVERVIEW

With an effect next to the gravitational attraction of the Earth, Moon and Sun, the Solar Radiation Pressure represents the dominating source of acceleration acting on GNSS satellites [24]. It has a representative magnitude of $100\,\mathrm{nm/s^2}$ which means to introduce an orbital perturbations at the level of 100 m over time scales of one orbital revolution [24]. As already mentioned SRP is very difficult to model also for its dependence on the optical and geometrical properties and its orientation with respect to the incident radiation.

3.1 Solar Radiation Pressure SRP

The theoretical basis of solar analytical solar radiation pressure modeling finds its foundation in the Einstein's special theory of relativity:

$$\bar{E} = \sqrt{(cp)^2 + (m_0 c^2)^2}, \tag{3.1}$$

where:

- $\bar{E}$ is the energy of the particle;
- c is the velocity of the light in vacuum;
- p is the momentum;
- m_0 is the rest mass.

For a photon m_0 =0, therefore $\bar{E} = pc$. Einstein, considering the ideas of Max Planck, proposed also a corpuscular theory of light in which every photon has an associated energy proportional to its frequency $\bar{E} = hf$, where h is the Planck's constant. Therefore is seen that $p = hf/c$, that is photon's momentum is proportional to its frequency. It means that if a photon is absorbed by a surface of a body, the momentum of the photon is transferred to the body. Hence, considering an average number of particles of frequency f which impinge unit area of surface per second at one astronomical unit $n(f)$, the integral over the solar electromagnetic spectrum gives:

$$\bar{F} = \int_{EM} d\bar{F}\, df = \int_{EM} \frac{dp_{n(f)}}{dt}\, df = \int_{EM} \frac{h}{c} n(f) f\, df. \tag{3.2}$$

But:

$$\int_{EM} \frac{h}{c} n(f) f\, df = W, \tag{3.3}$$

where W is the solar irradiance in $\mathrm{J/(sm^2)}$. Hence the force $\bar{F}$ per unit area is:

$$\bar{F} = \frac{W}{c}. \tag{3.4}$$

The solar radiation may be modeled as a radiative force which can be absorbed, specularly reflected or diffusely reflected [24, 5, 7]. It means that none of the radiation is transmitted through the spacecraft. For each surface of element dA the following coefficients are considered:

- α is the fraction of the incident radiation that is absorbed;
- δ is the fraction of the incident radiation that is diffusely reflected;
- ρ is the fraction of the incident radiation that is specularly reflected.

For each surface area these optical parameters are related by the following expression:

$$\alpha + \delta + \rho = 1. \tag{3.5}$$

The following considerations are therefore made [1]:

1. the spacecraft transmissivity is zero (as already mentioned) and implied by Eq. 3.5;
2. the diffusion is Lambertian. It means that the net force perpendicular to the surface is proportional to 2/3 the incident radiation scaled by the factor $\cos\theta$ where θ is the angle between the direction of the incident radiation and the normal to the surface;
3. the surface area dA behaves as well as a linear combination of a black body, a lambertian diffuser and a perfect mirror. It means that the three parameters α, δ and ρ completely described the optical properties of the surface and they do not vary with the, already mentioned, angle θ.

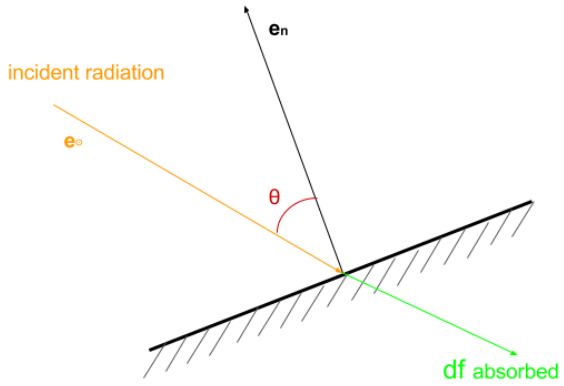

Figure 3.1: Scheme of the incident radiation absorbed

From these assumptions the absorbed, specularly reflected and diffusely reflected contribution of the force can be calculated as follow:

$$d\mathbf{f}_{abs} = -\frac{\Phi}{c} dA \cos\theta \cdot \alpha \boldsymbol{e}_{\odot}, \tag{3.6}$$

$$d\mathbf{f}_{ref} = -\frac{\Phi}{c} dA \cos\theta \cdot 2\cos\theta \rho \boldsymbol{e}_{n}. \tag{3.7}$$

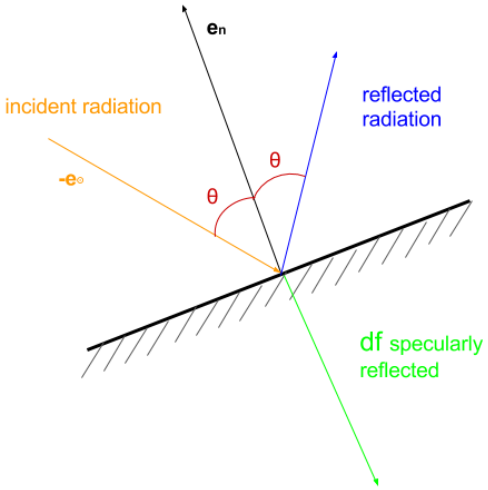

Figure 3.2: Scheme of the incident radiation specularly reflected

The diffusive reflection gives a contribution both in the $-\boldsymbol{e}_{\odot}$ direction and in the $-\boldsymbol{e}_{n}$ direction. It is due to the fact that this part of radiation is first absorbed, transferring momentum along the $\boldsymbol{e}_{\odot}$ direction and then re-emitted according with Lambert's law.

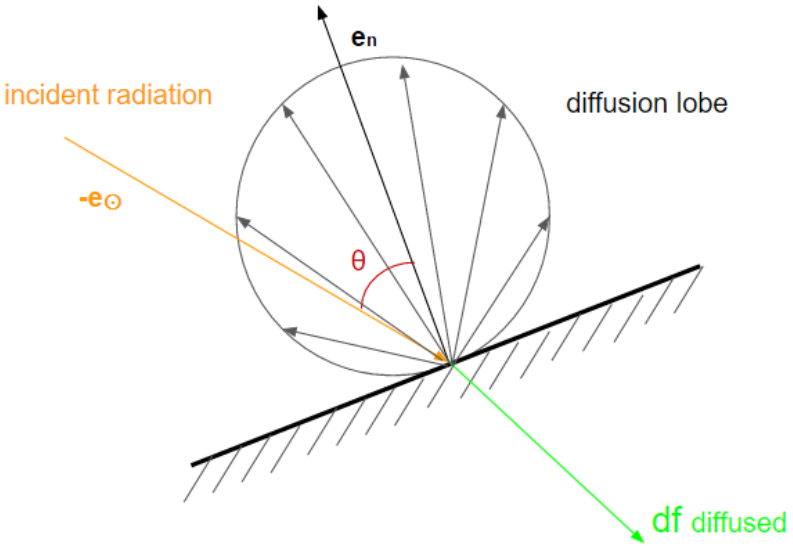

Figure 3.3: Scheme of the incident radiation diffusely reflected

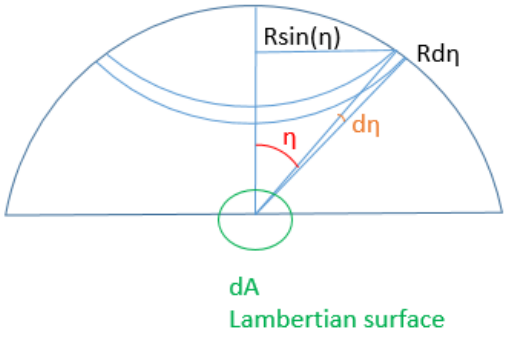

Figure 3.4: Representation of Hemispherical interception of Radial Flux from a Lambertian surface.

The contribution in the normal to the surface direction can be found integrating the diffusive radiation intensity over an hemisphere external to dA [7].

Looking at figure 3.4 can be observed that the total amount of the diffusive force over the hemisphere is given by:

$$\int_0^{\frac{\pi}{2}} 2\pi \sin\eta \cos\eta \, d\eta = \pi. \tag{3.8}$$

Considering the Lambert's law the component in the direction perpendicular to the surface is:

$$\int_0^{\frac{\pi}{2}} 2\pi \sin\eta \cos^2\eta \, d\eta = \frac{2}{3}\pi. \tag{3.9}$$

Hence the contribution of the diffusive force in the direction normal to the elementary surface is $\frac{2}{3}$ of the total amount and the diffusive contribution is therefore given by:

$$d\mathbf{f}_{diff} = -\frac{\Phi}{c} dA \cos\theta \cdot \delta\left(\boldsymbol{e}_{\odot} + \frac{2}{3}\boldsymbol{e}_n\right), \tag{3.10}$$

where in these expressions:

- d**f** is the differential force due to the solar radiation pressure on the surface element considered measured in N;
- dA is the elementary area of the spacecraft, m^2;
- Φ is the solar flux, W/m^2;
- $\boldsymbol{e}_{\odot}$ spacecraft to sun unit vector;
- $\boldsymbol{e}_n$ elementary surface normal unit vector;
- θ angle between $\boldsymbol{e}_{\odot}$ and $\boldsymbol{e}_n$;
- dA $\cos\theta$ is the cross-section of the bundle of light that illuminates dA;
- α is the absorbed fraction of the incident radiation;
- δ is the diffusely reflected fraction;
- ρ is the specularly reflected fraction.

Hence the total differential force due to the SRP on a surface element is given by the sum of the three different contributions:

$$d\mathbf{f} = -\frac{\Phi}{c} dA \cos\theta \cdot \left[(\alpha+\delta)\boldsymbol{e}_{\odot} + \frac{2}{3}\delta\boldsymbol{e}_n + 2\rho\cos\theta\boldsymbol{e}_n\right]. \tag{3.11}$$

3.2 Box-wing model

For high-precision applications, which are required for geodetic space missions, a simplified macro model may consist of a *box-wings* satellite shape. The box, with six flat plates, represents the satellite body, instead the wings represent the two solar panels [4]. Therefore in this case the model is made by the summation of the effect of different flat plates. Considering the final result obtained in the previous section the force due to the solar radiation pressure over a flat plate is given by [1, 7, 24]:

$$\mathbf{F} = -\frac{\Phi}{c} A \cos\theta \cdot \left[(\alpha + \delta)\boldsymbol{e}_{\odot} + \frac{2}{3}\delta \boldsymbol{e}_n + 2\rho \cos\theta \boldsymbol{e}_n \right]. \tag{3.12}$$

The Equation 3.12 is the fundamental equation for the box-wing model. In fact the total SRP force acting over a satellite represented with a box-wing model is given by:

$$\mathbf{F} = -\frac{\Phi}{c} \sum_{i=1}^{n} A_i \cos\theta_i \cdot \left[(\alpha_i + \delta_i)\boldsymbol{e}_{\odot} + \frac{2}{3}\delta_i \boldsymbol{e}_{ni} + 2\rho_i \cos\theta_i \boldsymbol{e}_{ni} \right]. \tag{3.13}$$

Here $i = 1, .., n$ represents the ith surface (flat plate) of the model. The work that is presented in this thesis mainly follows the force model proposed in [24]. When multi-layer insulation (MLI) is used as thermal protection, the absorbed radiation does not enter in the surfaces covered by MLI but it is almost instantaneously re-radiated ([28, 9, 14, 15]). The absorbed radiation instantaneously re-radiated in accord with Lambert's law is given by:

$$F = -\frac{\Phi}{c} \cdot A \cos\theta \cdot \left[\frac{2}{3}\alpha \boldsymbol{e}_n \right]. \tag{3.14}$$

Hence the equation of the force for the box is given by:

$$\mathbf{F} = -\frac{\Phi}{c} A \cos\theta \cdot \left[(\alpha + \delta) \left(\boldsymbol{e}_{\odot} + \frac{2}{3}\boldsymbol{e}_n \right) + 2\rho \cos\theta \boldsymbol{e}_n \right]. \tag{3.15}$$

Therefore for the box the SRP force acting on body of a spacecraft represented with a box-wing model yelds:

$$\mathbf{F} = -\frac{\Phi}{c} \sum_{i=1}^{n} A_i \cos\theta_i \cdot \left[(\alpha_i + \delta_i) \left(\boldsymbol{e}_{\odot} + \frac{2}{3}\boldsymbol{e}_{ni} \right) + 2\rho_i \cos\theta_i \boldsymbol{e}_{ni} \right]. \tag{3.16}$$

Equation 3.12 is instead applied for the solar panels because thermal re-emission creates a negligible contribution to the overall acceleration for a mostly balanced thermal re-emission form the front- and back-side of the panel ([28, 9, 14, 15]).

3.3 Box-wing-hat model

The work of *Ikari* of the *University of Tokyo* [33] proposes an alternative box-wing model considering also the L-band antenna, that is on the top of the satellite in the +z direction (see Fig. 2.5) as a combination of a circular cylinder and a circular truncated cone. It makes sense for the particular case of QZS-1 because of its very large antenna. The SRP acceleration acting on a surface of a circular cylinder and a circular truncated cone are derived analytically. The expressions developed in [33] are presented here using the notation assumed in this work based on Eq. 3.5.

SRP model of the circular cylinder

SRP acting on a circular cylinder surface is derived by surface integration of the SRP acting on the micro flat surface in the illuminated region. The expression of this acceleration is:

$$\mathbf{a_{cy}} = -\frac{\Phi LR}{mc} \cdot \begin{bmatrix} 0 \\ (1 + \frac{1}{3}\rho)\cos^2\psi + \frac{\pi}{6}\delta\cos\psi \\ (1-\rho)\cos\psi sin\psi \end{bmatrix}, \tag{3.17}$$

where ρ, δ are the specularly and diffusely reflected fractions of the cylinder and ψ is the angle between the sun direction and the perpendicular to the symmetry axis. L and R have the meaning observed in Fig. 3.5, that are respectively the length and the radius of the circular cylinder.

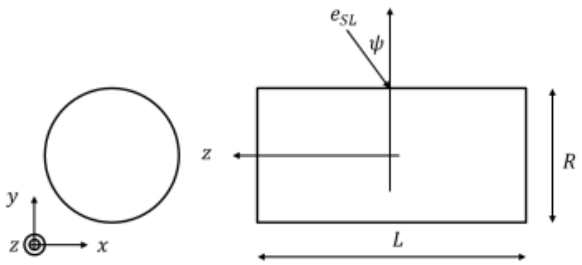

Figure 3.5: Definition of parameters and coordinate of circular cylinder. Reproduced from [33].

SRP model of the truncated cone

The SRP acting on the side surface of the circular truncated cone is derived by surface integration. The components of the acceleration are:

$$\begin{aligned}
a_{tc,x} &= -2\tfrac{\phi A_l}{mc}\big[\cdot C_3 c_\psi (c_{\bar\omega} c\psi + \tfrac{\pi}{2} s_{\bar\omega} s_\psi) \\
&\quad + c_{\bar\omega}\big(\tfrac{2}{3} C_{13} c_{\bar\omega}^2 c_\psi^2 \\
&\quad + \tfrac{\pi}{4}(2C_{13} s_{\bar\omega} c_{\bar\omega} s_\psi c_\psi + C_2 c_{\bar\omega} c_\psi) \\
&\quad + C_{13} s_{\bar\omega}^2 c_\psi^2 + C_2 s_{\bar\omega} s_\psi\big)\big], \\
a_{tc,y} &= -2\tfrac{\phi A_l}{mc}\big[\cdot C_3 c_\psi (c_{\bar\omega} c\psi + \tfrac{\pi}{2} s_{\bar\omega} s_\psi) \\
&\quad + c_{\bar\omega}\big(\tfrac{2}{3} C_{13} c_{\bar\omega}^2 c_\psi^2 \\
&\quad + \tfrac{\pi}{4}(2C_{13} s_{\bar\omega} c_{\bar\omega} s_\psi c_\psi + C_2 c_{\bar\omega} c_\psi) \\
&\quad + C_{13} s_{\bar\omega}^2 c_\psi^2 + C_2 s_{\bar\omega} s_\psi\big)\big], \\
a_{tc,z} &= -2\tfrac{\phi A_l}{mc} \cdot \big[C_3 s_\psi (c_{\bar\omega} c\psi + \tfrac{\pi}{2} s_{\bar\omega} s_\psi) \\
&\quad + s_{\bar\omega}\big(\tfrac{\pi}{4} C_{13} c_{\bar\omega}^2 c_\psi^2 + 2C_{13} s_{\bar\omega} c_{\bar\omega} s_\psi c_\psi \\
&\quad + C_2 c_{\bar\omega} c_\psi) \\
&\quad + \tfrac{\pi}{2} C_{13} s_{\bar\omega}^2 s_\psi^2 + C_2 s_{\bar\omega} s_\psi\big)\big],
\end{aligned} \tag{3.18}$$

where:

$$C_1 = 1 + \rho, \tag{3.19a}$$
$$C_2 = \frac{2}{3}\delta, \tag{3.19b}$$
$$C_3 = 1 - \rho, \tag{3.19c}$$
$$C_{13} = C_1 - C_3 = 2\rho, \tag{3.19d}$$
$$A_l = \frac{1}{4}\sqrt{1 + \frac{R_l - R_u}{2}}(R_l + R_u)L, \tag{3.19e}$$
$$c_\psi = \cos\psi, \tag{3.19f}$$
$$s_\psi = \sin\psi, \tag{3.19g}$$
$$c_{\bar\omega} = \cos\bar\omega, \tag{3.19h}$$
$$s_{\bar\omega} = \sin\bar\omega. \tag{3.19i}$$

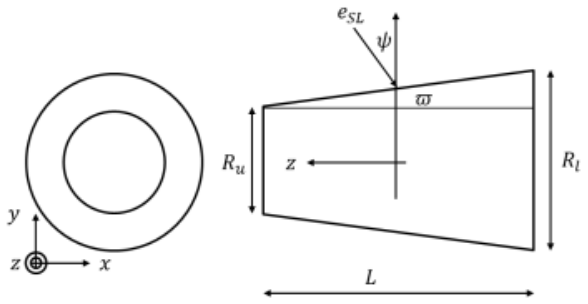

Figure 3.6: Definition of parameters and coordinate of truncated cone. Reproduced from [33].

The angle ψ is defined as well as in the cylindrical case.

3.4 Empirical SRP-model

In the absence of a detailed, physics-based SRP model, the *Precise Orbit Determination* (POD) for GNSS satellites studies have typically made use of an empirical SRP model, the Empirical CODE Orbit model (named after the Center for Orbit Determination in Europe that first established its use for GPS) [2]. The CODE allows for the adjustment of constant and orbit-periodic accelerations along three orthogonal axes aligned with the Sun and solar panel direction. Within the CODE model the empirical accelerations in the right-handed DYB frame are calculated as:

$$\begin{aligned} a_{\text{emp,D}} &= D_0 + D_c \cdot \cos u + D_s \cdot \sin u, \\ a_{\text{emp,Y}} &= Y_0 + Y_c \cdot \cos u + Y_s \cdot \sin u, \\ a_{\text{emp,B}} &= B_0 + B_c \cdot \cos u + B_S \cdot \sin u. \end{aligned} \tag{3.20}$$

In other words the acceleration in DYB direction at 1 AU is parametrized in terms of three constants accelerations (D_0, Y_0, B_0) and up to six accelerations ($D_{c,s}$,Y_{cs},$B_{c,s}$) varying with a 1/rev periodicity. There is also an alternative formulation with the empirical acceleration as function of the angle μ:

$$\begin{aligned} a_{\text{emp,D}} &= D_0 + D_c^* \cdot \cos\mu + D_s^* \cdot \sin\mu, \\ a_{\text{emp,Y}} &= Y_0 + Y_c^* \cdot \cos\mu + Y_s^* \cdot \sin\mu, \\ a_{\text{emp,B}} &= B_0 + B_c^* \cdot \cos\mu + B_S^* \cdot \sin\mu. \end{aligned} \tag{3.21}$$

The two set of parameters are related by:

$$\begin{aligned} B_c^* &= -B_c \cdot \cos u_\odot - B_s \cdot \sin u_\odot, \\ B_c^* &= +B_c \cdot \sin u_\odot - B_s \cdot \cos u_\odot. \end{aligned} \tag{3.22}$$

There are corresponding expressions for D and Y terms, where $u_\odot$ denotes the argument of latitude of the Sun. As well as in [24] in this work will be considered only five ECOM parameters: D_0, Y_0, B_0, B_C^* and B_S^*. Hence the empirical acceleration considered is given by:

$$\begin{aligned} a_{\text{emp,D}} &= D_0, \\ a_{\text{emp,Y}} &= Y_0, \\ a_{\text{emp,B}} &= B_0 + B_c^* \cdot \cos\mu + B_s^* \cdot \sin\mu. \end{aligned} \tag{3.23}$$

3.5 Ray-tracing analysis

The ray-tracing is a very interesting technique which allows to consider the real geometry of the satellite instead of a model, i.e. the box-wing model. The idea of the ray tracing is to simulate the Sun as an array of pixels which is normal to the sun-vector and rotates around the satellite. From

each pixel a ray starts and it moves towards the satellite along the Sun direction. If the ray really impinges a component of the body it is saved and considering the area of the pixel, the normal of the surface of the component impinged and the instantaneous direction of the ray the force is calculated. Repeating it for each pixel of the array and summing all the effects of the rays which impinge the satellite the total force due to the solar radiation pressure is calculated.

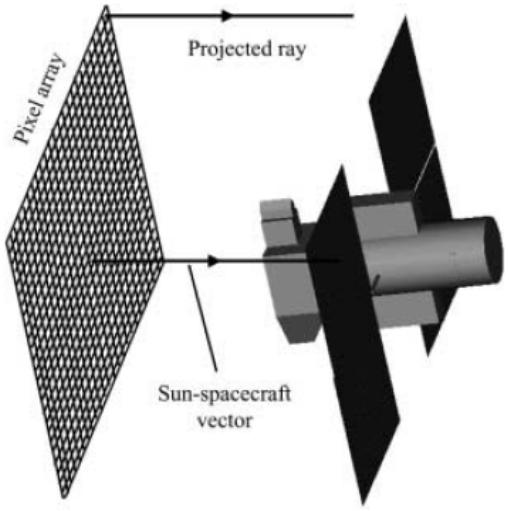

Figure 3.7: Pixel array orthogonal to the Sun-spacecraft direction. Reproduced from [6].

3.5.1 Ray-tracing at the University of London

One of the most important application of the ray-tracing technique was developed by M.Ziebart [5, 6, 8]. In his works he divided the surfaces into three typologies:

- regular and irregular planar polygonal elements;
- circular elements;
- cylindrical elements.

The force model used by Ziebart is based on the same physical interpretation presented in the previous section but it is expressed in a different way, that is considering the direction normal to the surface and the shear direction ($\mathbf{e}_s$). The equations of the force model are presented with the notation assumed in this work based on Eq. 3.5, following [1].

$$\begin{aligned} \mathbf{F}_n &= -\frac{\phi A \cos\theta}{c}\left[(1+\rho)\cos\theta + \frac{2}{3}\delta\right]\boldsymbol{e}_n, \\ \mathbf{F}_s &= -\frac{\phi A \cos\theta \sin\theta}{c}\left[1-\rho\right]\mathbf{e}_s, \end{aligned} \tag{3.24}$$

where ρ, δ are the specularly and diffusely reflected fractions of the surface involved. Ziebart's method considers a test which checks if the a ray intersects an object of the spacecraft. The requirements for this kind of ray tracing are:

- a description of the geometry and of the optical properties of the spacecraft;
- the attitude used by the satellite as function of known parameters;
- parameters which describe the radiation environment during the life of the spacecraft.

The final aim of the Ziebart's work is to furnish a model which describes the SRP effect as a function of the only angle which describes the problem: the elongation ϵ given by Eq. 2.5.

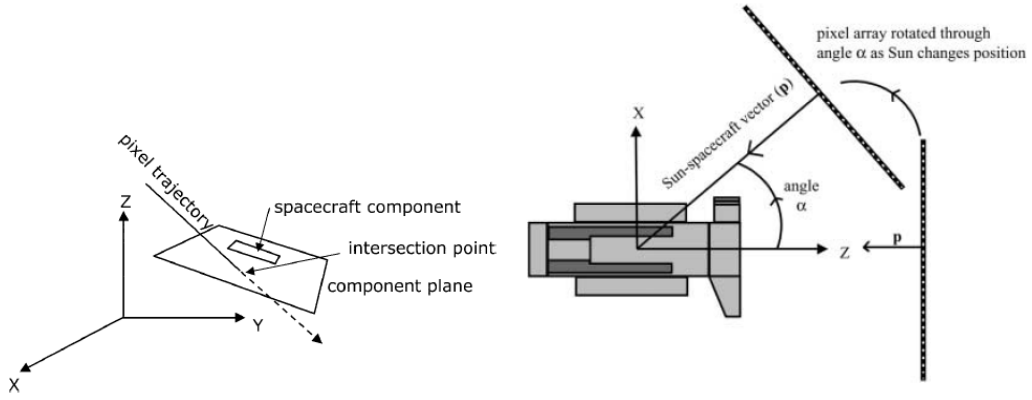

(a) *Intersection.* (b) *Array rotation.*

Figure 3.8: Conceptual idea of the ray-tracing technique in Ziebart's work [5] [6] [8]. (a) shows the simulation of the intersection of the ray with a component and how to select a ray which really impinges a component. (b) illustrates the rotation of the pixel array around the spacecraft.

It is enough to describe the SRP acceleration for the satellite considered by Ziebart, GLONASS, because it uses a configuration in which the Sun is always in the x-z satellite plane . But it is not enough for example for the QZS-1 satellite because it uses also the Orbit-Normal mode which implies an elevation of the Sun over the plane of the orbit. In the case treated by Ziebart the acceleration is always in the x-z plane. The x and z components represent two periodic functions of ϵ and Ziebart models them with a Fourier series [5]:

$$f(x) = \frac{a_0}{2} + \sum_{n=1}^{\infty} [a_n \cos(nx) + b_n \sin(nx)]. \tag{3.25}$$

The final product is therefore two tables with the a_n and b_n for x and z coefficients which give the model description of the acceleration due to the SRP. The Ziebart's code is very good for spacecraft with a geometry well described with polygonal, circular and cylindrical elements and for satellite whose relative position with the Sun is defined just by one angle. In order to consider the geometry with its full complexity there are commercial optical software which allow to do ray-tracing over a CAD-model of the spacecraft.

3.5.2 Ray tracing at the University of Padova

F. Gini of the University of Padua in his PhD thesis [19] used the commercial software ZEMAX®. It is an essential software platform for optical engineers capable of combining sequential lens design, optical physics, non-sequential optical system design and it allows also an integration with a Computer Aided Design (CAD) program [38]. It is a software which can be used for tolerancing, analysis and optimization. Its main purpose is hence to design and optimize optical paths, and is usually adopted in the design of complex lens systems such as telescopes and satellite onboard cameras [19]. Gini focuses on the non-gravitational forces acting on the GOCE spacecraft. The steps followed by Gini are:

- to realize a CAD model of the spacecraft;
- to analyze with a ray tracing technique the CAD model in ZEMAX;
- to calculate the Solar and Earth radiation pressure, the thermal re-rediation and the Aerodynamics forces and torques thanks to the ARPA software of the University of Padua.

ARPA, *Aerodynamics and Radiation Pressure Analysis*, is the software designed and implemented at the University of Padova to compute forces and torques on satellites due to the non-gravitational perturbations: Solar Radiation Pressure (SRP), Earth Radiation Pressure (ERP) for the albedo and infrared components, the satellite Thermal Re-Radiation (TRR), and the aerodynamics. The CAD model is the input for the raytracing software which simulates the interaction of the

photons coming from the Sun or the Earth with the satellite surfaces. The raytracing software creates files which contain the geometric information of the rays reflections on the spacecraft. These files are then read by the ARPA software which, together with the satellite surface properties, computes the physical interaction of the photons with the satellite surfaces, computing forces and torques for the SRP and ERP components. The forces are then converted into coefficients and are used to create a database which will be the input for the Precise Orbit Determination (POD) software [19]. Concerning the force model that one used by Gini in his work is the same considered by Ziebart, i.e. Eq. 3.24. The input parameters for ARPA are [19]:

- **ID** : a progressive number which indicates each surface;
- **Obj** : the name of the object, as called in the ray-tracing software;
- **Obj ID**: is the progressive number associated to each object, as in the ray-tracing software;
- **Face ID**: the progressive number associated to each face of an object, as in the ray-tracing software. Each object is in fact subdivided into different faces;
- **Type**: provides additional information about the face, to avoid eventual confusion in the surface identification;
- **Material** : describes the material which forms or covers the surface;
- $\mathbf{T}_{NoEcl}$: is the mean temperature of the surface when the satellite is not in eclipse;
- $\mathbf{T}_{Ecl}$: is the mean temperature of the surface when the satellite is in eclipse;
- $\alpha_{\mathbf{BOL}}$:is the coefficient of absorption of the surface at the satellite Beginning Of Life (BOL), specific for the optical band;
- $\alpha_{\mathbf{EOL}}$: is the coefficient of absorption of the surface at the satellite End Of Life (EOL), specific for the optical band;
- $\bar{\epsilon}$: is the emissivity of the surface, specific for the infrared band (thermal band);
- $\gamma_{\mathbf{opt}}$: is the reflectivity of the surface, specific for the optical band;
- $\gamma_{\mathbf{IR}}$: is the reflectivity of the surface, specific for the infrared band.

In particular, for the SRP effect the temperature and the parameters related to the infrared are not considered. The NAPEOS (NAvigation Package for Earth Observation Satellites) software, developed and maintained at ESA/ESOC, was upgraded to make use of the new ARPA inputs and adopted to perform the tests on GOCE [19]. A POD sequence has been set up to carried out the tests. The tests on GOCE were performed on 30 consecutive daily arcs, starting at the beginning of the GOCE science phase on 1st November 2009. The results for the radiation test cases show a significant reduction of the empirical accelerations, especially in the cross-track direction, of about the 20% for the SRP, 12% for the ERP albedo, 13% for the ERP infrared and 20% for the TRR with respect to the standard NAPEOS force modeling (cannon-ball) [19]. For the aerodynamics, an important reduction of the post-fit RMS from 7:6 to 7:3 mm has been observed with the new ARPA model, and a reduction from 4:6 to 4:2 cm of the distance of the orbits computed with ARPA from the official reduced-dynamics GOCE orbits (Precise Science Orbit) has been computed [19]. The obtained results confirm the goodness of the modeling and techniques of ARPA for all the non-gravitational perturbations computed for GOCE [19].

4. FUNDAMENTALS OF ORBIT DETERMINATION

This Chapter would like to give an idea about what is the context in which this work about the solar radiation modeling is inserted. The field in which it founds its application is the orbit determination. The purpose here is to give an introduction about the fundamentals of statistical orbit determination. It consists in a set of techniques which allows to estimate parameters of a spacecraft during its motion around the Earth or, more generally, of a celestial body during its motion in the solar system. The basic assumption made in the classic orbit determination problem is that the motion of the body is ruled by a central force. Given an initial state vector, composed by position and velocity, at a certain time it can be integrated obtaining the trajectory if the motion of this body at any time. But in real condition the initial state vector is never known exactly and the mathematical models of the forces acting on the body and some constants are known with a certain value of approximation. Therefore something to obtain a better estimation is needed. It is the observations. In the GNSS case, for instance, the observations are given by the tracking of the ground stations. Generally the trajectory must be tracked by ground stations or satellites whose position is well known (e.g. the GNSS themselves). The observations need to estimate in a better way the initial state and then, therefore, to calculate the state vector at any time different from the initial epoch considered. However also the observations are affected by errors and hence the estimation is never perfect, but what can be calculate is the best estimation. The estimated values can differ from the true values for different reasons [19]:

- approximation involved in the mathematical models of the forces acting on the body (e.g. SRP force);
- observations errors;
- computational errors in the solution process.

As already mentioned in the introduction the work of this thesis is focused on improving the description of a model for the non-gravitational SRP force in order to decrease the errors due to the modeling of this force in the orbit determination. In order to obtain a better estimate it is important to have available a sufficient number of observations in the time span considered. The main goal is to reduce the residuals obtain between the observations and the calculated values with the mathematical expressions. The most used technique to do it is the least squares approach. There are essentially two ways to update the state vector:

- *the sequential* estimation if a new state vector is estimated after each observation;
- *the batch* estimation which accumulates all the measurements and then processes it to obtain the estimate state vector at a certain epoch.

The method used in the work of this thesis is the batch processor.

4.1 Dynamical systems

The dynamical state vector of a celestial body during its motion in the solar system is given by its position and velocity:

$$\mathbf{X}(t) = (\mathbf{r}(t), \mathbf{v}(t))^T. \tag{4.1}$$

The orbit described by the motion of the body depends also on parameters that describe the force model. Therefore the governing relations that involve nonlinear dynamical equations for the n-dimensional dynamical state $\mathbf{X}(t)$ are given by [17] :

$$\dot{\mathbf{X}}(t) = \mathbf{F}(\mathbf{X}, \mathbf{P}, t), \tag{4.2}$$

where $\mathbf{P}$ is a n dimensional vector of parameters describing the force model, $\mathbf{X}$ is the state vector at a time t. Since the knowledge of the true state (position and velocity, and other parameters) of

the considered body will never be absolute, statistical techniques are necessary. In particular, the least squares approach is used to minimize the differences between observations and a model of them. The measurements can be modeled in the following way:

$$\dot{\mathbf{Y}}(t) = \mathbf{G}(\mathbf{X}, \mathbf{Q}, t) + \epsilon(t), \tag{4.3}$$

where $\mathbf{Y}(t)$ is a p-dimensional vector of observations made on the system at time t, $\mathbf{Q}$ is a vector of constant, non-dynamical, or *geometric parameters* and $\epsilon(t)$ is a vector of measurement errors. The observations $\mathbf{Y}_i = \mathbf{Y}(t_i)$ are obtained at discrete times t_i with i=1,...,l. Therefore in general the number of observations $m = p \times l \gg n$. But Eqs. 4.2, 4.3 are characterized by [17]:

- the inability to observe the state directly;
- nonlinear relations between the observations and the state;
- fewer observations at any time epoch than there are state vector components (p<n);
- errors in the observations represented by ϵ_i.

In this work is assumed a *Bayesian maximum likelihood estimation approach* which means that a reasonable reference trajectory is available and the true and reference trajectories remain sufficiently close throughout the time interval of interest [17]. In this case the trajectory for the actual motion can be expanded in a Taylor's series about the reference trajectory at each point of time. Truncating this expansion to eliminate the higher order terms, then the deviation in the state from the reference trajectory can be described by a set of linear differential equations with time-dependent coefficients. Hence the nonlinear orbit determination problem in which the complete state vector is to be estimated can be replaced by a linear orbit determination problem in which *the deviation* from some reference solution has to be determined. Moreover, since a Baesyan approach has been assumed, the measurements and measurement errors and the state variables are assumed to be realizations of appropriate *stochastic processes*. Therefore the problem now is to estimate the best variation to the given initial state vector to obtain the best initial state vector. Furthermore the process is used to estimate also the best variation of the parameters $\mathbf{P}$ and $\mathbf{Q}$ above mentioned.

4.2 Linearization of the problem and least squares application

The linearization of the problem is obtained introducing the variations $\delta\mathbf{X}$, $\delta\mathbf{Y}$, $\delta\mathbf{P}$, $\delta\mathbf{Q}$ of the state vector, the observations and the parameters [17]. It gives the following expressions:

$$\mathbf{X}(t) = \mathbf{X}^*(t, \mathbf{P}^*) + \delta\mathbf{X}, \tag{4.4a}$$
$$\mathbf{Y}(t) = \mathbf{G}(\mathbf{X}^*, \mathbf{Q}^*, t) + \delta\mathbf{Y}, \tag{4.4b}$$
$$\mathbf{P} = \mathbf{P}^* + \delta\mathbf{P}, \tag{4.4c}$$
$$\mathbf{Q} = \mathbf{Q}^* + \delta\mathbf{Q}, \tag{4.4d}$$

where the index * represents the reference values at a certain epoch t_0. Now expanding the eq. 4.4 to the first order about the reference values yields:

$$\mathbf{F}(\mathbf{X}, \mathbf{P}, t) = \mathbf{F}(\mathbf{X}^*, \mathbf{P}^*, t) + \left[\frac{\partial \mathbf{F}}{\partial \mathbf{X}}\right]^* \delta\mathbf{X}(t) + \left[\frac{\partial \mathbf{F}}{\partial \mathbf{X}}\right]^* \delta\mathbf{P}, \tag{4.5a}$$
$$\mathbf{G}(\mathbf{X}_i, t_i) = \mathbf{G}(\mathbf{X}_i^*, \mathbf{Q}^*, t_i) + \left[\frac{\partial \mathbf{G}}{\partial \mathbf{X}}\right]_i^* \delta\mathbf{X}(t_i) + \left[\frac{\partial \mathbf{G}}{\partial \mathbf{X}}\right]_i^* \delta\mathbf{Q}. \tag{4.5b}$$

Upon substitutions into Eqs. 4.2, 4.3 the *differential equations of the dynamics* are obtained as follow:

$$\delta\dot{\mathbf{X}}(t) = \left[\frac{\partial \mathbf{F}}{\partial \mathbf{X}}\right]^* \delta\mathbf{X}(t) + \left[\frac{\partial \mathbf{F}}{\partial \mathbf{X}}\right]^* \delta\mathbf{P}, \tag{4.6a}$$
$$\delta\mathbf{Y}_i = \left[\frac{\partial \mathbf{G}}{\partial \mathbf{X}}\right]_i^* \delta\mathbf{X}(t_i) + \left[\frac{\partial \mathbf{G}}{\partial \mathbf{X}}\right]_i^* \delta\mathbf{Q}. \tag{4.6b}$$

For convenience and to maintain the description clear the following positions are introduced:

$$\mathbf{x} = \delta\mathbf{X}, \tag{4.7a}$$

$$\mathbf{y}_i = \delta\mathbf{Y}_i, \tag{4.7b}$$

$$\mathbf{p} = \delta\mathbf{P}, \tag{4.7c}$$

$$\mathbf{q} = \delta\mathbf{Q}. \tag{4.7d}$$

Hence Eq. 4.6 can be rewritten as:

$$\dot{\mathbf{x}}(t) = \mathbf{A}(t)\mathbf{x}(t) + \mathbf{B}(t)\mathbf{p}, \tag{4.8a}$$

$$\mathbf{y}_i = \tilde{\mathbf{H}}_i\mathbf{x}_i + \mathbf{K}_i\mathbf{q} + \boldsymbol{\epsilon}_i, \tag{4.8b}$$

where:

$$\mathbf{A}(t) = \left[\frac{\partial\mathbf{F}(t)}{\partial\mathbf{X}(t)}\right]^*, \tag{4.9a}$$

$$\mathbf{B}(t) = \left[\frac{\partial\mathbf{F}(t)}{\partial\mathbf{P}}\right]^*, \tag{4.9b}$$

$$\tilde{\mathbf{H}}_i = \left[\frac{\partial\mathbf{G}}{\partial\mathbf{X}}\right]_i^*, \tag{4.9c}$$

$$\mathbf{K}_i = \left[\frac{\partial\mathbf{G}}{\partial\mathbf{Q}}\right]_i^*, \tag{4.9d}$$

with i=1,...,l as already explained. The application of the least squares technique for this particular problem needs a relation between the measurement deviation $\mathbf{y}_i$ at time t_i and the state deviation $\mathbf{x}_0$ at epoch t_0 and the parameter deviation $\mathbf{p}$. It can be done by mapping the linear state deviation with the differential relationship:

$$\delta\mathbf{X} = \frac{\partial\mathbf{X}}{\partial\mathbf{X}_0}\delta\mathbf{X}_0 + \frac{\partial\mathbf{X}}{\partial\mathbf{P}}\delta\mathbf{P}. \tag{4.10}$$

It may be recognized that the sensitivity to the initial state $\frac{\partial\mathbf{X}}{\partial\mathbf{X}_0}$ is the *dynamical state transition matrix* $\boldsymbol{\Phi}_{\boldsymbol{xx}}(\boldsymbol{t}, \boldsymbol{t_0})$. The ratio $\frac{\partial\mathbf{X}}{\partial\mathbf{P}}\delta\mathbf{P}$ instead represents the *parameter state transition matrix* $\boldsymbol{\Phi}_{\boldsymbol{xp}}(\boldsymbol{t}, \boldsymbol{t_0})$. Together these two matrix define the *state transition matrix* $\boldsymbol{\Phi}(\boldsymbol{t}, \boldsymbol{t_0})$. The presence of this State Transition Matrix STM is very important because it allows to relate a state description at epoch t_0 to any epoch desired. That is the possibility to write the solution of the *Variational Equations* VE as:

$$\mathbf{x}(t) = \boldsymbol{\Phi}_{\boldsymbol{xx}}(t, t_0)\mathbf{x}_0 + \tilde{\mathbf{H}}_\mathbf{i}\boldsymbol{\Phi}_{xp}(t, t_0)\mathbf{p}. \tag{4.11}$$

Hence from 4.8 it can be written:

$$\mathbf{y}_i \quad = \quad \tilde{\mathbf{H}}_i\boldsymbol{\Phi}_{\boldsymbol{xx}}(\boldsymbol{t}, \boldsymbol{t_0})\mathbf{x}_0 + \tilde{\mathbf{H}}_\mathbf{i}\boldsymbol{\Phi}_{xp}(t, t_0)\mathbf{p} + \mathbf{K}_i\mathbf{q} + \boldsymbol{\epsilon}_i. \tag{4.12}$$

For i = 1,...,l . Now, considering the following points:

- it may happened that some parameters may be both dynamical and geometrical, therefore are introduced two new matrix: $\mathbf{K}_i^p$ matrix of geometric partial of dual-nature parameters and $\mathbf{K}_i^q$ matrix of geometric partial of the purely geometric parameters, hence $\mathbf{K}_i = \mathbf{K}_i^p + \mathbf{K}_i^q$;
- in order to compact the equation two new matrices can be defined:
  - $\mathbf{H}_i^x = \tilde{\mathbf{H}}_i\boldsymbol{\Phi}_{xx}(t, t_0)$;
  - $\mathbf{H}_i^p = \tilde{\mathbf{H}}_i\boldsymbol{\Phi}_{xp}(t, t_0) + \mathbf{K}_i^p$.
- It is introduced a new vector: the initial *system deviation vector:*

$$\tilde{\mathbf{x}}_0 = (\mathbf{x}_0 \quad \mathbf{p} \quad \mathbf{q})^T. \tag{4.13}$$

Moreover considering 4.12 the final relationship between measurement deviation and sytem deviation vector can be written as:

$$\mathbf{y}_i = \mathbf{H}_i\tilde{\mathbf{x}}_0 + \boldsymbol{\epsilon}_i, \qquad i = 1, ..., l, \tag{4.14}$$

where $\mathbf{H}_i = (\mathbf{H}_i^x \quad \mathbf{H}_i^p \quad \mathbf{K}_i^q)$.

State transition Matrix The State Transition Matrix needs to be compute in order to play its role. The differential equations that rule the STM are given by [17]:

$$\dot{\mathbf{\Phi}}_{xx}(t,t_0) = \mathbf{A}(t)\mathbf{\Phi}_{xx}(t,t_0), \tag{4.15a}$$

$$\dot{\mathbf{\Phi}}_{xp}(t,t_0) = \mathbf{A}(t)\mathbf{\Phi}_{xp}(t,t_0) + \mathbf{B}(t). \tag{4.15b}$$

These equations have to be introduce in the general integration program where also the state vector is determined. The initial condition for the numerical integration of the STM is the identity matrix:

$$\mathbf{\Phi}(t,t_0) = \mathbf{I}. \tag{4.16}$$

Least squares implementation

The least squares approach is used to estimate the best correction for the reference initial values which minimizes the residuals between observations and calculated values. Here it is introduced a *weighted least squares estimate* . It is because, when it is possible, a weight is associated to the observation errors. The amount of the weight depends on the available data or on the accuracy that the user retain right to consider. The measurement weight matrix $\mathbf{W}$ is a block diagonal matrix with the weights on the diagonal. The system of equations used in the least squares problem is given by Eq. 4.14 in the following way:

$$\mathbf{y} = \mathbf{H}\tilde{\mathbf{x}}_0 + \boldsymbol{\epsilon}, \tag{4.17}$$

where $\mathbf{y}$ is a $m \times 1$ vector, $\mathbf{x}$ is an $n \times 1$ vector, $\boldsymbol{\epsilon}$ a $m \times 1$ vector and $\mathbf{H}$ is a m matrix that is the so called design matrix for the least squares method. As already mentioned $m = p$ is the total number of the observations. In this work the system of observations has to be overdetermined and therefore p or l has to be sufficiently large. The weighted least squares solution selects the estimate $\hat{\mathbf{x}}_0$ of $\tilde{\mathbf{x}}_0$ which minimizes the sum of the squares of the calculated observation residuals. Hence $\hat{\mathbf{x}_0}$ is that one minimizes the *performance index* :

$$J(\tilde{\mathbf{x}}_0) = \frac{1}{2}\boldsymbol{\epsilon}^T\boldsymbol{\epsilon} = \sum_{i=1}^{l}\frac{1}{2}\epsilon_i^T\mathbf{w}_i\boldsymbol{\epsilon}_i. \tag{4.18}$$

Substituting 4.17 into 4.18 the performance index can be rewritten as:

$$J(\tilde{\mathbf{x}}_0) = \frac{1}{2}\mathbf{y} - \mathbf{H}\tilde{\mathbf{x}}^T\mathbf{y} - \mathbf{H}\tilde{\mathbf{x}}_\mathbf{0}. \tag{4.19}$$

The minimum of this function is obtained setting its first derivative equal to zero $\frac{\partial J}{\partial \tilde{\mathbf{x}}} = 0$. The expression resulting from this position gives the *normal equations* in the least squares formulation:

$$(\mathbf{H}^T\mathbf{W}\mathbf{H})\tilde{\mathbf{x}}_0 = \mathbf{H}^T\mathbf{W}\mathbf{y}. \tag{4.20}$$

Hence, if the *normal matrix* $\mathbf{H}^T\mathbf{W}\mathbf{H}$ is positive definite, the weighted least squares estimate $\hat{\mathbf{x}}_0$ that minimizes the sum of squares of the weighted observation errors is :

$$\hat{\mathbf{x}}_0 = (\mathbf{H}^T\mathbf{W}\mathbf{H})^{-1}\mathbf{H}^T\mathbf{W}\mathbf{y}, \tag{4.21}$$

where the matrix $\mathbf{H}^T\mathbf{W}\mathbf{H}^{-1}$ represents the solution covariance matrix $\mathbf{C}$ which gives an idea of the accuracy of the estimation and shows the relation through the different parameters estimated. In fact, in general, the larger the magnitude of the elements of the covariance matrix the less accurate the estimate.

If an *a priori value* $\bar{\mathbf{x}}_0$ with the associate weighting matrix $\bar{\mathbf{W}}$ is available (usually an a priori estimate value), the desired best estimate $\hat{\mathbf{x}_0}$ is that one which minimizes the following performance index:

$$J(\tilde{\mathbf{x}_0}) = \frac{1}{2}\mathbf{y} - \mathbf{H}\tilde{\mathbf{x}}^T\mathbf{y} - \mathbf{H}\tilde{\mathbf{x}}_\mathbf{0} + \frac{1}{2}(\bar{\mathbf{x}} - \tilde{\mathbf{x}}_\mathbf{0})^T\bar{\mathbf{W}}(\bar{\mathbf{x}}_\mathbf{0} - \tilde{\mathbf{x}}_\mathbf{0}). \tag{4.22}$$

Hence the solution of the least squares problem is in this case:

$$\hat{\mathbf{x}}_0 = (\mathbf{H}^T\mathbf{W}\mathbf{H} + \bar{\mathbf{W}})^{-1}(\mathbf{H}^T\mathbf{W}\mathbf{y} + \bar{\mathbf{W}}\bar{\mathbf{x}}_\mathbf{0}). \tag{4.23}$$

4.3 Batch processor

As already mentioned in this work to update the state vector a batch processor is used . Considering the final Eq. 4.23 $\mathbf{W}$ can be substituted with the inverse of the covariance matrix of the observations $\mathbf{C}^{-1}$ and $\bar{\mathbf{W}}$ with the covariance matrix of the a priori information $\mathbf{C_0}^{-1}$. That is:

$$\hat{\mathbf{x}}_0 = (\mathbf{H}^T\mathbf{C}^{-1}\mathbf{H} + \mathbf{C_0^{-1}})^{-1}(\mathbf{H}^T\mathbf{C}^{-1}\mathbf{y} + \mathbf{C_0^{-1}}\bar{\mathbf{x}}_\mathbf{0}). \tag{4.24}$$

All the quantities of 4.24 are assumed mapped through the state transition matrix. The batch estimation works accumulating the measurements and processing it to obtain the estimate state vector at a certain epoch. The quantities that have to be accumulated are: $\mathbf{H}^T\mathbf{C}^{-1}\mathbf{H}$ and $\mathbf{H}^T\mathbf{C}^{-1}\mathbf{y}$. These matrices may be accumulated in a simply way as follows:

$$\mathbf{H}^T\mathbf{C}^{-1}\mathbf{H} = \sum_{i=1}^{l} \mathbf{H}_i^T\mathbf{C}_i^{-1}\mathbf{H}_i, \tag{4.25a}$$

$$\mathbf{H}^T\mathbf{C}^{-1}\mathbf{y} = \sum_{i=1}^{l} \mathbf{H}_i^T\mathbf{C}_i^{-1}\mathbf{y}_i, \tag{4.25b}$$

where $\mathbf{H}_i$ has the same meaning as in 4.14. The entire sequence of computations are repeated until the estimation process has converged. The procedure yields a minimum value of the performance index:

$$J(\tilde{\mathbf{x}_0}) = (\hat{\mathbf{x}_0} - \bar{\mathbf{x}_0})^T\bar{\mathbf{C}}_0^{-1} + \sum_{i=1}^{l} \hat{\boldsymbol{\epsilon}}_i^T\mathbf{C}_i^{-1}\hat{\boldsymbol{\epsilon}}_i, \tag{4.26}$$

where $\hat{\boldsymbol{\epsilon}}_i = \mathbf{y_i} - \mathbf{H_i}\hat{\mathbf{x}}_\mathbf{0}$ is the best estimate of the observation error. The Root Mean Square of the observation residuals may be used as a measure of convergence: when the RMS no larger changes the solution is assumed to be converged. The RMS computation is given by:

$$RMS = \sqrt{\frac{\sum_{i=1}^{l} \hat{\boldsymbol{\epsilon}}_\boldsymbol{i}^\boldsymbol{T}\mathbf{C}_i^T\hat{\boldsymbol{\epsilon}}_\boldsymbol{i}}{m}}. \tag{4.27}$$

5. SRP ANALYTICAL MODEL FOR QZS-1

The develop of an analytical model is a fundamental step of this thesis. The analytical model is a box-wing model (Sec. 3.2) that is simple and it can be parametrized. The analytical model evaluates the SRP acceleration and it can be fitted both to real observation data and to a more accurate model (see Chapter 6), such as a ray-tracing model (see Chapter 7). The parameters of the analytical model are *characteristic accelerations* that depend on the optical and geometric properties of the surfaces of the box-wing model. The model is described in different reference frames in order to consider both the attitudes of QZS-1. In particular a new reference frame is introduced to define in a useful way the SRP acceleration in the ON mode. Furthermore, the geometrical and optical properties of the spacecraft are defined: a CAD model is, in fact, realized and assumptions on the optical properties based on the state-of -the-art are made. Eventually the parameters of a box-wing model based on the geometry and on the assumptions on the optical properties are presented.

5.1 Reference frames

As already said in the first chapter, QZS-1 adopts two different attitude modes: Yaw-Steering mode and Orbit-Normal mode. In order to consider both the modes two angles are now defined:

- the elevation angle E of the Sun on the satellite x,z plane;
- the azimuth angle A between the z-axis of the satellite frame and the projection of the Sun-vector on the satellite x-z plane.

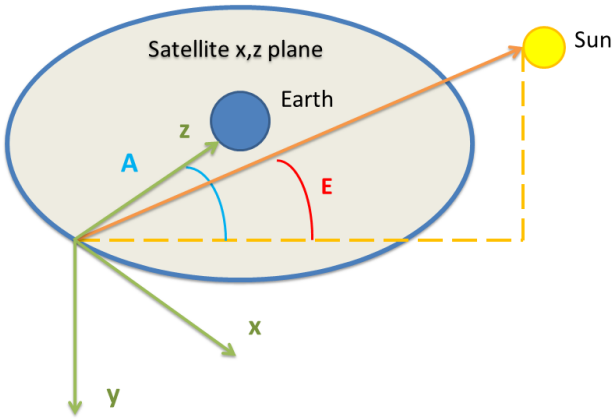

Figure 5.1: Generic description of the problem. E is the elevation of the Sun on the satellite x,z plane and A represents the angle between the z-axis and the projection of the Sun on the x,z plane.

In this way, as may be recognized comparing Figures 5.1 and 5.2 in the YS mode $E = 0\,\text{deg}$ and $A = \epsilon$ while in the ON mode $E = \beta$ and $A = \mu$. Taking into account these considerations the unit vectors and the direction cosines needed to describe the SRP force are defined in the YS and ON attitude modes.

Yaw steering mode

A nominal Yaw Steering mode implies that, as already mentioned in Sec. 2.2, the unit vector in Sun direction and the +x-axis are always part of the same hemisphere and the solar panels are maintained perpendicular to the Sun direction. Therefore the surfaces involved in this case are four: ±z, +x and the solar panels. Therefore the relative configuration Sun-satellite is always given in the satellite x-z plane that means that the x and z directions can be described by just an angle: the elongation ϵ. Hence the direction cosines of the Sun direction are given by [28]:

$$\cos\theta_x = +\sqrt{1-\cos^2\epsilon}, \tag{5.1a}$$
$$\cos\theta_y = 0, \tag{5.1b}$$
$$\cos\theta_z = +\cos\epsilon, \tag{5.1c}$$
$$\cos\theta_{sp} = 1, \tag{5.1d}$$

where $+\sqrt{1-\cos^2\epsilon} = \sin\epsilon$ because $0\,\text{deg} \leq \epsilon \leq 180\,\text{deg}$. The unit vectors of the Sun direction and consequently of the normal to the solar panels yield:

$$\boldsymbol{e}_\odot = +\sin\epsilon\cdot\boldsymbol{e}_{+x} + \cos\epsilon\cdot\boldsymbol{e}_{+z}, \tag{5.2a}$$
$$\boldsymbol{e}_{sp} = \boldsymbol{e}_\odot. \tag{5.2b}$$

In order to compare the SRP acceleration with the empirical acceleration of Eq. 3.23, the DYB frame of Eq. 2.3 has to be considered. The unit vectors of the DYB frame are defined with respect to the satellite x,y,z frame in the following way:

$$\mathbf{e}_D = +\sin\epsilon\cdot\boldsymbol{e}_{+x} + \cos\epsilon\cdot\boldsymbol{e}_{+z}, \tag{5.3a}$$
$$\mathbf{e}_Y = \mathbf{e}_{y,YS}, \tag{5.3b}$$
$$\mathbf{e}_B = -\cos\epsilon\cdot\boldsymbol{e}_{+x} + \sin\epsilon\cdot\boldsymbol{e}_{+z}. \tag{5.3c}$$
$$\tag{5.3d}$$

Orbit Normal mode

The Orbit Normal mode assumed is the ON^+ frame described by Eq. 2.4. The satellite x,y,z frame is therefore aligned with the ON^+ frame. In this fixed attitude mode all the surfaces of the box-wing model are involved in the contribution to the SRP acceleration: ±x,±y,±z and the solar panels. It is important to remark that the azimuth angle of the Sun is exactly the orbit angle, i.e. $A = \mu$, and the elevation angle of the Sun above the satellite x-z plane is equivalent to the elevation above the orbital plane, i.e. $E = \beta$. Moreover the normal to the surface of the solar panels is assumed in the direction of the projection of the Sun vector on the orbital plane. Consequently the direction cosines of the Sun direction in the ON mode are given by [28]:

$$\cos\theta_x = +\cos\beta\sin\mu, \tag{5.4a}$$
$$\cos\theta_y = -\sin\beta, \tag{5.4b}$$
$$\cos\theta_z = +\cos\beta\cos\mu, \tag{5.4c}$$
$$\cos\theta_{sp} = +\cos\beta. \tag{5.4d}$$

In order to compare the SRP acceleration with the empirical acceleration in the ON mode a new right-handed reference frame $\overline{DYB}$ [28]. It is given by[28]:

$$\begin{aligned} \mathbf{e}_{\bar{D}} &= \bar{\mathbf{e}}_\odot, \\ \mathbf{e}_{\bar{Y}} &= \mathbf{e}_{y,ON}, \\ \mathbf{e}_{\bar{B}} &= \mathbf{e}_{\bar{D}} \times \mathbf{e}_{\bar{Y}}, \end{aligned} \tag{5.5}$$

where $\bar{\mathbf{e}}_\odot$ is the projection of the sun vector on the plane of the orbit. With the introduction of the $\overline{DYB}$ frame, as may be observed from Fig. 5.2, the study of the two different attitudes is very

similar. In fact the $\bar{D}$ and $\bar{B}$ axes are in the satellite x-z plane(that in this case is coincident with orbital plane) as well as the D and B axes in the YS mode, and the $\bar{Y}$ axis is perpendicular to this plane as well as the Y axis in the YS mode. In other words the $\overline{DYB}$ frame in the ON mode is the analog of the DYB frame of the YS mode. Furthermore with this notation the normal to the solar panels is exactly in the $\bar{D}$ direction, i.e. $\mathbf{e_{sp}} = \mathbf{e}_{\bar{D}}$.

The unit vector of the Sun direction in the satellite x,y,z frame in this case has a component also in the y-direction:

$$\boldsymbol{e}_{\odot} = +\cos\beta\sin\mu\cdot\boldsymbol{e}_{+x} - \sin\beta\cdot\boldsymbol{e}_{+y} + \cos\beta\cos\mu\cdot\boldsymbol{e}_{+z}. \tag{5.6}$$

The expressions of the unit vectors of this frame with respect to the satellite x,y,z frame are given by:

$$\mathbf{e}_{\bar{D}} = +\sin\mu\cdot\boldsymbol{e}_{+x} + \cos\mu\cdot\boldsymbol{e}_{+z}, \tag{5.7a}$$
$$\mathbf{e}_{\bar{Y}} = \mathbf{e}_{y,ON}, \tag{5.7b}$$
$$\mathbf{e}_{\bar{B}} = -\cos\mu\cdot\boldsymbol{e}_{+x} + \sin\mu\cdot\boldsymbol{e}_{+z}. \tag{5.7c}$$

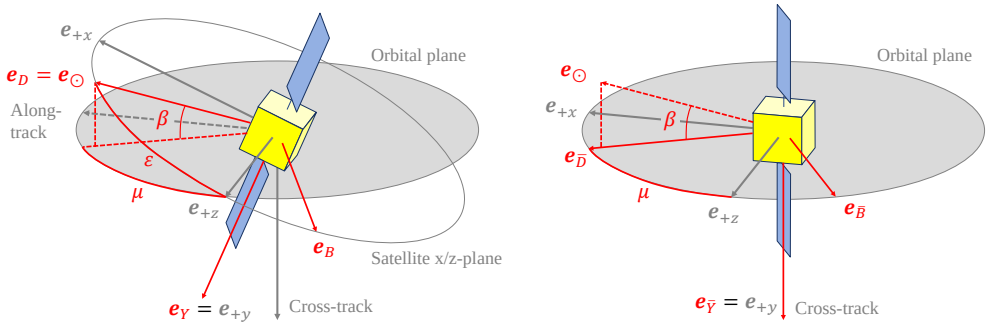

(a) *YS mode.* (b) *ON mode.*

Figure 5.2: The two different attitude modes of the satellite QZS-1. In both cases the z-direction is pointing the Earth. Note that in the ON mode $\mu = A$ and $\beta = E$. Reproduced from [28].

Furthermore the introduction of the $\overline{DYB}$ frame implies a new expression of the ECOM model [28]:

$$a_{\text{emp},\bar{D}} = \bar{D}_0, \tag{5.8a}$$
$$a_{\text{emp},\bar{Y}} = \bar{Y}_0, \tag{5.8b}$$
$$a_{\text{emp},\bar{B}} = \bar{B}_0 + \bar{B}_C^*\cdot\cos\mu + \bar{B}_S^*\cdot\sin\mu. \tag{5.8c}$$

5.2 Geometric and optical properties of QZS-1

Geometric features The absence of official data about the size of the surfaces and optical properties constrains to do some assumptions deduced by the analysis of the available images and the information furnished by the *QZS-vision website*[35] . This website provides a summary description of the components of the surfaces and a useful scaled (1:50) paper model [35]. The paper model allows to define a CAD model that is realized with the Computer Aided Design software SolidWorks® and it is useful to compute the size of the flat surfaces summarized in Table 5.1. The frame chosen to define the geometry is the manufacturing JAXA-proposed frame (see Fig. 2.5) which corresponds to the ON$^+$ frame defined by Eq. 2.4.

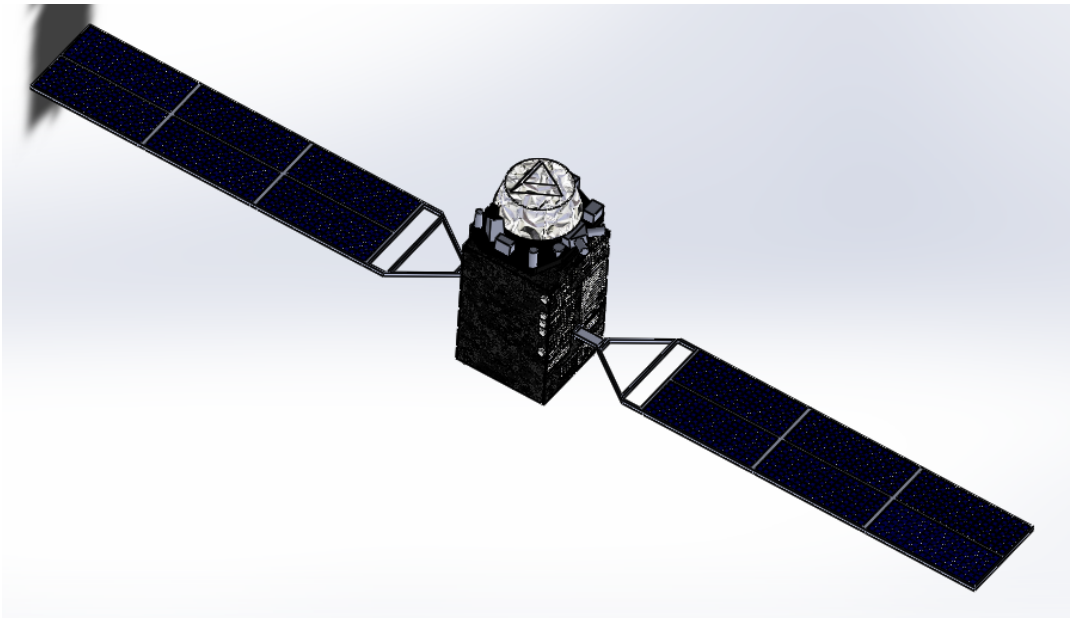

Figure 5.3: QZS-1 3D CAD representation.

Table 5.1: Flat surfaces of QZS-1 for the box-wing model ([28]).

Surface	m^2
A_x :	12.2
A_y :	12.6
A_z :	6.0
A_{sp}:	40.0

The values of Table 5.1 are referred to the cross sections, therefore for the x and y surfaces a cross section which includes also an effect of the strange part between the end of the box shaped body and the antenna is considered. A 2D draw realized with SolidWorks helps in the visualization of the complete geometry and the distances between every piece of the satellite (Fig. 5.4).

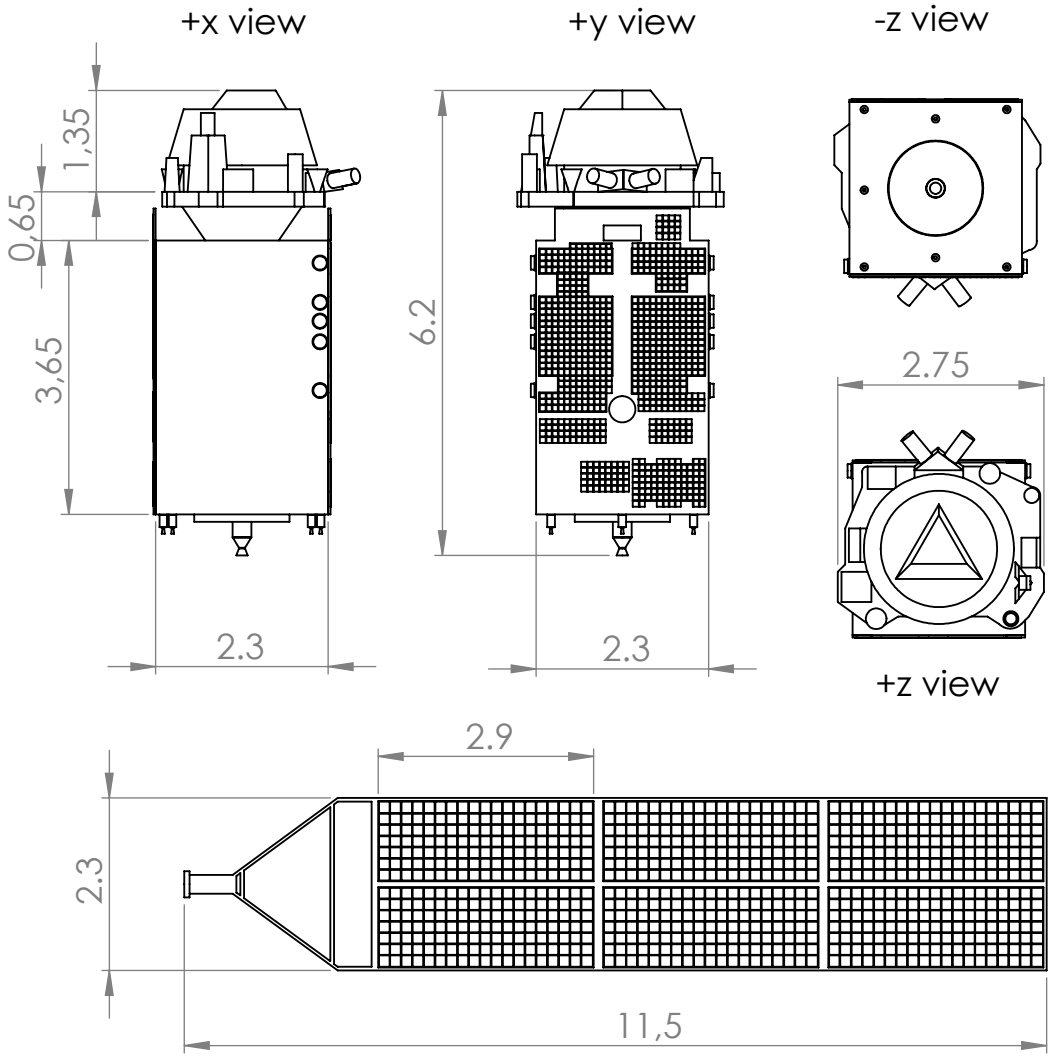

Figure 5.4: QZS-1 2D CAD representation. All dimensions in m and rounded to 5 cm. The reference frame considered is the spacecraft frame used is the manufactured frame, not the IGS frame (see fig. 2.5). Reproduced from [28]

As may be observed from Fig. 5.4 the body of the spacecraft has its longest dimension in the z-direction. Furthermore from the figure the relevant size of the L-band antenna (1.35m) with respect to the envelop of the complete satellite in the z-direction (6.2m) is evident. It means that the antenna represents ≈22% of the total envelop of the satellite. The antenna is even more relevant comparing it with the *box-shaped* part of the body of the satellite whose sizes are 2.3m × 2.3m × 3.65m. From Fig. 5.4 the different composition of the +z-surface and -z surface can be recognized. In fact the +z-surface comprises the L-band antenna and other components (like sun-sensors), while the -z surface is made by the bottom of the box-shaped body with the exception of the thrusters. Figure 5.4 shows also that the solar panels have a long arm for the deployment, that is 2.5m while the total length is 11.5m and it has implications in the possible relative shadows between body of the spacecraft and solar panels (Sec. 5.4).

Optical properties Michibiki appears like a mostly black body with parts that seem to be of a sort of alloy similar to aluminum or a metal alloy which has a silver colour. In fact the material of the body is MLI with a carbon-filled outer layer that prevents electrostatic charging [28]. The *silver* material which covers the large L-band antenna seems to be *radome* made from a different type of radio frequency (RF) transparent MLI with an higher reflectivity [28].

(a) *South payload panel (+y).* (b) *North payload panel (-y).*

Figure 5.5: Representation of the y panels of QZS-1 furnished by JAXA [34]. In correspondence of the circles the heat pipes are set.

(a) *South payload panel (+y).* (b) *North payload panel (-y).*

Figure 5.6: Representation of the y panels of QZS-1 furnished by JAXA [34]. In correspondence of the circles the optical solar reflectors are installed.

Moreover the QZS-vision website [34] describes the y-surfaces like surfaces that have the role to maintain the temperature constant and declares the presence of optical solar reflectors. The optical solar reflector is a reflective layer typical used with the radiators. Consequently an high specular reflectivity is assumed for this mirror-like part of the y-surfaces. Concerning the solar panels the values of the solar panels are considered similar to different GPS and GLONASS satellites described in [20].

Table 5.2: Optical properties of the QZS-1 materials (from [28]).

Material	Absorption α	Diffuse reflectivity δ	Specular reflectivity ρ
black	0.94	0.06	0.00
silver	0.44	0.46	0.10
radiator	0.06	0.00	0.94
solar panels	0.75	0.04	0.21

Table 5.3: Values of the area covered by optical solar reflectors or by mirror like materials on the y surfaces. All values m^2.

surface	area
+y	5.329
-y	4.109

The realization of a CAD geometry allows to better understand the dimensions and the amount of the areas of the spacecraft. Table 5.3 shows the area covered by the optical solar reflector and the *mirror-like* material of the y surfaces computed with the CAD model. Furthermore Table 5.3 shows an asymmetry in the amount of the mirror-like part between the two y-sides and conse-

quently an optical asymmetry. Considering the area covered by the radiator on the y-surfaces (Table 5.3) and the total areas calculated with the CAD model (Table 5.1) the surfaces of the box are divided in their *black*,*silver* and *radiator* fractions as summarized in Table 5.4. Table 5.4 shows that

Table 5.4: Black, silver and radiator fraction of the six surfaces of the box of the model for QZS-1.

Surface	Black Fraction	Silver Fraction	Radiator Fraction
A_{+z}	0.30	0.70	0.00
A_{-z}	1.00	0.00	0.00
A_{+x}	0.80	0.20	0.00
A_{-x}	0.80	0.20	0.00
A_{+y}	0.32	0.30	0.38
A_{-y}	0.46	0.33	0.21

the x-surfaces are mostly black while the y-surfaces are mostly non-black. Furthermore Table 5.4 highlights a relevant ±z-asymmetry due to the different materials of the two surfaces. Weighting the black and non-black area (silver and mirror-like) contributions the optical properties of QZS-1 can be assumed as in Table 5.5 ([28]). As may be recognized looking at Tables 5.1 and 5.4 the ±x

Table 5.5: Optical properties of panels of the complete box-wing model

Surface	Absorption α	Diffuse reflectivity δ	Specular reflectivity ρ
+z	0.790	0.180	0.030
-z	0.940	0.060	0.000
+x	0.840	0.140	0.020
-x	0.840	0.140	0.020
+y	0.456	0.157	0.387
-y	0.590	0.180	0.230

asymmetry can be neglected, while there are ±y and ±z asymmetries.

5.3 QZS-1 a priori SRP model

5.3.1 Analytical derivation

Equations 3.15, 3.12 provide the basis of *box-wing* radiation pressure models respectively for the body of the spacecraft and for the solar panels. Considering a box-shaped body of mass m made up of multiple flat surfaces A_i ($i = 1, ..., n$), the resulting acceleration due to the radiation pressure is obtained by summation over all surface elements:

$$\boldsymbol{a} = -\sum_{i=1}^{n} \frac{\Phi}{mc} \cdot A_i \cos\theta_i \cdot H(\cos\theta_i) \left[(1-\rho_i) \left(\boldsymbol{e}_\odot + \frac{2}{3}\boldsymbol{e}_{ni} \right) + 2\rho \cos\theta_i \cdot \boldsymbol{e}_{ni} \right]. \tag{5.9}$$

The step (or Heaviside) function $H(x)$ introduced in this relation is equal to 1 for $x \geq 0$ but otherwise zero. It accounts for the fact that only surface elements with $\theta_i = \arccos(\boldsymbol{e}_D^T \boldsymbol{e}_{ni}) > 0$ are considered to be illuminated while $\theta_i < 0$ implies a shaded surface. Accordingly with Sec. 3.2 for the solar panels the acceleration is instead computed as:

$$\boldsymbol{a} = -\frac{\Phi}{mc} A \cos\theta \cdot \left[(\alpha+\delta)\boldsymbol{e}_\odot + \frac{2}{3}\delta \boldsymbol{e}_n + 2\rho\cos\theta \boldsymbol{e}_n \right]. \tag{5.10}$$

Hence the generic expression of the SRP acceleration $\boldsymbol{a}$ with a box-wing model is given by:

$$
\begin{aligned}
\boldsymbol{a} \quad = \quad & -\frac{\Phi}{mc}\cdot A_{+x}\cdot(+\cos\theta_x)\cdot H(+\cos\theta_x)\cdot\left[(1-\rho_{+x})\left(\boldsymbol{e}_\odot+\tfrac{2}{3}\boldsymbol{e}_{+x}\right)+2\rho_{+x}\cdot\sin\epsilon\cdot\boldsymbol{e}_{+x}\right] \\
& -\frac{\Phi}{mc}\cdot A_{-x}\cdot(-\cos\theta_x)\cdot H(-\cos\theta_x)\cdot\left[(1-\rho_{-x})\left(\boldsymbol{e}_\odot+\tfrac{2}{3}\boldsymbol{e}_{-x}\right)-2\rho_{-x}\cdot\cos\epsilon\cdot\boldsymbol{e}_{-x}\right] \\
& -\frac{\Phi}{mc}\cdot A_{+y}\cdot(\cos\theta_y)\cdot H(\cos\theta_y)\quad\cdot\left[(1-\rho_{+y})\left(\boldsymbol{e}_\odot+\tfrac{2}{3}\boldsymbol{e}_{+y}\right)-2\rho_{+y}\cdot\sin E\cdot\boldsymbol{e}_{+y}\right] \\
& -\frac{\Phi}{mc}\cdot A_{-y}\cdot(-\cos\theta_y)\cdot H(-\cos\theta_y)\cdot\left[(1-\rho_{-y})\left(\boldsymbol{e}_\odot+\tfrac{2}{3}\boldsymbol{e}_{-y}\right)+2\rho_{-y}\cdot\sin E\cdot\boldsymbol{e}_{-y}\right] \\
& -\frac{\Phi}{mc}\cdot A_{+z}\cdot(\cos\theta_z)\cdot H(\cos\theta_z)\quad\cdot\left[(1-\rho_{+z})\left(\boldsymbol{e}_\odot+\tfrac{2}{3}\boldsymbol{e}_{+z}\right)+2\rho_{+z}\cdot\cos\epsilon\cdot\boldsymbol{e}_{+z}\right] \\
& -\frac{\Phi}{mc}\cdot A_{-z}\cdot(-\cos\theta_z)\cdot H(-\cos\theta_z)\cdot\left[(1-\rho_{-z})\left(\boldsymbol{e}_\odot+\tfrac{2}{3}\boldsymbol{e}_{-z}\right)-2\rho_{-z}\cdot\cos\epsilon\cdot\boldsymbol{e}_{-z}\right] \\
& -\frac{\Phi}{mc}\cdot A_{\mathrm{sp}}\cdot\cos\theta_{sp}\qquad\qquad\cdot\left[(1-\rho_{sp})\boldsymbol{e}_\odot+\tfrac{2}{3}\delta_{sp}\boldsymbol{e}_{sp}+2\rho_{sp}\cos E\right]\quad .
\end{aligned}
\tag{5.11}
$$

Assuming that there is not ±x asymmetry, for the ease of notation, the partial accelerations are introduced:

$$
\begin{aligned}
a_x^{\alpha\delta} &= \frac{\Phi}{mc}\cdot A_x\cdot(1-\rho_x), & a_{+z}^{\alpha\delta} &= \frac{\Phi}{mc}\cdot A_{+z}\cdot(1-\rho_{+z}), & a_{-z}^{\alpha\delta} &= \frac{\Phi}{mc}\cdot A_{-z}\cdot(1-\rho_{-z}), \\
a_x^{\rho} &= \frac{\Phi}{mc}\cdot A_x\cdot\rho_x, & a_{+z}^{\rho} &= \frac{\Phi}{mc}\cdot A_{+z}\cdot\rho_{+z}, & a_{-z}^{\rho} &= \frac{\Phi}{mc}\cdot A_{-z}\cdot\rho_{-z}, \\
a_{+y}^{\alpha\delta} &= \frac{\Phi}{mc}\cdot A_y\cdot(1-\rho_{+y}), & a_{-y}^{\alpha\delta} &= \frac{\Phi}{mc}\cdot A_y\cdot(1-\rho_{-y}), & a_{sp}^{\alpha\delta} &= \frac{\Phi}{mc}\cdot A_{\mathrm{sp}}\cdot\left(1-\rho_{\mathrm{sp}}\right), \\
a_{+y}^{\rho} &= \frac{\Phi}{mc}\cdot A_y\cdot\rho_{+y}, & a_{-y}^{\rho} &= \frac{\Phi}{mc}\cdot A_y\cdot\rho_{-y}, & a_{sp}^{\delta} &= \frac{\Phi}{mc}\cdot A_{\mathrm{sp}}\cdot\delta_{\mathrm{sp}}, \\
a_{sp}^{\rho} &= \frac{\Phi}{mc}\cdot A_{\mathrm{sp}}\cdot\rho_{\mathrm{sp}}. & & & & \\
\end{aligned}
\tag{5.12}
$$

Considering the geometric and optical properties of the satellite , i.e. Tables 5.2 and 5.1, the partial accelerations are computed and shown in Table 5.6. The values of the partial accelerations of this

Table 5.6: Reference values of partial accelerations from body and solar panel surfaces of Michibiki. All values in nm/s^2.

	nm/s^2
$a_x^{\alpha\delta}$	+27.3
a_x^{ρ}	+0.0
$a_{+y}^{\alpha\delta}$	+16.8
a_{+y}^{ρ}	+12.0
$a_{-y}^{\alpha\delta}$	+19.3
a_{-y}^{ρ}	+9.4
$a_{+z}^{\alpha\delta}$	+12.8
a_{+z}^{ρ}	+0.9
$a_{-z}^{\alpha\delta}$	+13.7
a_{-z}^{ρ}	+0.9
$a_{sp}^{\alpha\delta}$	+72.1
a_{sp}^{ρ}	+19.2
a_{sp}^{δ}	+3.6

chapter are computed considering a total mass of the spacecraft $m = 2000$ kg which means taking into account a mass of 200 kg of fuel left after launch for orbit keeping and end-of-life operations [28]. As may be observed from Table 5.6 the specular reflective contribution has an important role only for the ±y-surface, represented by the a_{+y}^{ρ} and a_{-y}^{ρ}.

With the introduced partial accelerations the solar radiation pressure acceleration can now be

expressed as:

$$\begin{aligned}
\boldsymbol{a} \;=\; & -|\cos\theta_x|\cdot H(+\cos\theta_x)\cdot\left[a_x^{\alpha\delta}\cdot\boldsymbol{e}_\odot+\tfrac{2}{3}a_x^{\alpha\delta}\cdot\boldsymbol{e}_{+x}+2a_x^{\rho}\cdot|\cos\theta_x|\cdot\boldsymbol{e}_{+x}\right]\\
& -|\cos\theta_x|\cdot H(-\cos\theta_x)\cdot\left[a_x^{\alpha\delta}\cdot\boldsymbol{e}_\odot-\tfrac{2}{3}a_x^{\alpha\delta}\cdot\boldsymbol{e}_{+x}-2a_x^{\rho}\cdot|\cos\theta_x|\cdot\boldsymbol{e}_{+x}\right]\\
& -|\cos\theta_y|\cdot H(\cos\theta_y)\quad\cdot\left[a_{+y}^{\alpha\delta}\cdot\boldsymbol{e}_\odot+\tfrac{2}{3}a_{+y}^{\alpha\delta}\cdot\boldsymbol{e}_{+y}+2a_{+y}^{\rho}\cdot|\cos\theta_y|\cdot\boldsymbol{e}_{+y}\right]\\
& -|\cos\theta_y|\cdot H(-\cos\theta_y)\cdot\left[a_{-y}^{\alpha\delta}\cdot\boldsymbol{e}_\odot-\tfrac{2}{3}a_{-y}^{\alpha\delta}\cdot\boldsymbol{e}_{+y}-2a_{-y}^{\rho}\cdot|\cos\theta_y|\cdot\boldsymbol{e}_{+y}\right]\\
& -|\cos\theta_z|\cdot H(+\cos\theta_z)\cdot\left[a_{+z}^{\alpha\delta}\cdot\boldsymbol{e}_\odot+\tfrac{2}{3}a_{+z}^{\alpha\delta}\cdot\boldsymbol{e}_{+z}+2a_{+z}^{\rho}\cdot|\cos\theta_z|\cdot\boldsymbol{e}_{+z}\right]\\
& -|\cos\theta_z|\cdot H(-\cos\theta_z)\cdot\left[a_{-z}^{\alpha\delta}\cdot\boldsymbol{e}_\odot-\tfrac{2}{3}a_{-z}^{\alpha\delta}\cdot\boldsymbol{e}_{+z}-2a_{-z}^{\rho}\cdot|\cos\theta_z|\cdot\boldsymbol{e}_{+z}\right]\\
& -\cos\theta_{sp}\qquad\qquad\cdot\left[a_{sp}^{\alpha\delta}\cdot\boldsymbol{e}_\odot+\tfrac{2}{3}a_{sp}^{\delta}\cdot\boldsymbol{e}_{sp}+2a_{sp}^{\rho}\cos\theta_{sp}\cdot\boldsymbol{e}_{sp}\right].
\end{aligned}\tag{5.13}$$

Now, in order to isolate the impact of asymmetric and symmetric contributions from the ± z and ± y surfaces, the mean value and the semi difference are introduced as follows:

$$\begin{aligned}
a_z^{\alpha\delta} &= \tfrac{1}{2}(a_{+z}^{\alpha\delta}+a_{-z}^{\alpha\delta}), & \Delta a_z^{\alpha\delta} &= \tfrac{1}{2}(a_{+z}^{\alpha\delta}-a_{-z}^{\alpha\delta}),\\
a_z^{\rho} &= \tfrac{1}{2}(a_{+z}^{\rho}+a_{-z}^{\rho}), & \Delta a_z^{\rho} &= \tfrac{1}{2}(a_{+z}^{\rho}-a_{-z}^{\rho}),\\
a_y^{\alpha\delta} &= \tfrac{1}{2}(a_{+y}^{\alpha\delta}+a_{-y}^{\alpha\delta}), & \Delta a_y^{\alpha\delta} &= \tfrac{1}{2}(a_{+y}^{\alpha\delta}-a_{-y}^{\alpha\delta}),\\
a_y^{\rho} &= \tfrac{1}{2}(a_{+y}^{\rho}+a_{-y}^{\rho}), & \Delta a_y^{\rho} &= \tfrac{1}{2}(a_{+y}^{\rho}-a_{-y}^{\rho}) \quad .
\end{aligned}\tag{5.14}$$

The values of these new partial accelerations are computed and tabulated in Table 5.7 considering the geometric and optical properties of the satellite aforementioned. The introduction of parameters that consider the symmetric and asymmetric contributions highlights that the asymmetric contribution has a lower impact with respect to the symmetric contribution.

Table 5.7: Reference values of partial accelerations of the symmetric and asymmetric contributions. All values in nm/s^2.

	nm/s^2
$a_y^{\alpha\delta}$	+18.1
a_y^{ρ}	+10.7
$\Delta a_y^{\alpha\delta}$	-1.3
Δa_y^{ρ}	+1.3
$a_z^{\alpha\delta}$	+13.3
a_z^{ρ}	+0.45
$\Delta a_z^{\alpha\delta}$	-0.45
Δa_z^{ρ}	+0.45

Introducing the partial accelerations of the symmetric and asymmetric contributions in Eq. 5.13

the SRP acceleration is given by :

$$\begin{aligned}
\boldsymbol{a} \;=\; & -|\cos\theta_x|\cdot\big[\; +a_x^{\alpha\delta}\cdot\boldsymbol{e}_\odot \qquad\qquad\qquad\qquad\quad\big] \\
& -\cos\theta_x\cdot\big[\qquad\qquad +\tfrac{2}{3}a_x^{\alpha\delta}\cdot\boldsymbol{e}_{+x} \quad +2a_x^{\rho}\cdot|\cos\theta_x|\cdot\boldsymbol{e}_{+x}\big] \\
& -|\cos\theta_y|\cdot\big[\; +a_y^{\alpha\delta}\cdot\boldsymbol{e}_\odot \quad +\tfrac{2}{3}\Delta a_y^{\alpha\delta}\cdot\boldsymbol{e}_{+y} \quad +2\Delta a_y^{\rho}\cdot|\cos\theta_y|\cdot\boldsymbol{e}_{+y}\big] \\
& -\cos\theta_y\cdot\big[+\Delta a_y^{\alpha\delta}\cdot\boldsymbol{e}_\odot \quad +\tfrac{2}{3}a_y^{\alpha\delta}\cdot\boldsymbol{e}_{+y} \quad +2a_y^{\rho}\cdot|\cos\theta_y|\cdot\boldsymbol{e}_{+y}\big] \\
& -|\cos\theta_z|\cdot\big[\; +a_z^{\alpha\delta}\cdot\boldsymbol{e}_\odot \quad +\tfrac{2}{3}\Delta a_z^{\alpha\delta}\cdot\boldsymbol{e}_{+z} \quad +2\Delta a_z^{\rho}\cdot|\cos\theta_z|\cdot\boldsymbol{e}_{+z}\big] \\
& -\cos\theta_z\cdot\big[+\Delta a_z^{\alpha\delta}\cdot\boldsymbol{e}_\odot \quad +\tfrac{2}{3}a_z^{\alpha\delta}\cdot\boldsymbol{e}_{+z} \quad +2a_z^{\rho}\cdot|\cos\theta_z|\cdot\boldsymbol{e}_{+z}\big] \\
& -\cos\theta_{sp}\cdot\big[\; +a_{sp}^{\alpha\delta}\cdot\boldsymbol{e}_\odot \quad +\tfrac{2}{3}a_{sp}^{\delta}\cdot\boldsymbol{e}_{sp} \quad +2a_{sp}^{\rho}\cos\theta_{sp}\cdot\boldsymbol{e}_{sp}\big].
\end{aligned} \tag{5.15}$$

The purpose now is to allow a comparison between the analytical box-wing model and real observation data,comparing it to the ECOM acceleration. Therefore the DYB and $\overline{DYB}$ reference frames have to be considered. Furthermore the acceleration will be computed also in the satellite x,y,z frame for a complete description of the SRP. The formulation of the acceleration is now developed, considering the two specific YS and ON attitude modes.

Yaw Steering mode

Considering Eqs. 5.1 and 5.2 and projecting Eq. 5.15 in the spacecraft system, the x,y,z components of the acceleration in the YS mode yield:

$$\begin{aligned}
a_x = \boldsymbol{a}^T\boldsymbol{e}_{+x} \;=\; & -\tfrac{2}{3}a_x^{\alpha\delta}\cdot\cos\epsilon\sin\epsilon \\
& -\left(a_x^{\alpha\delta}+2a_x^{\rho}\right)|\sin\epsilon|\sin\epsilon \\
& -a_z^{\alpha\delta}|\cos\epsilon|\sin\epsilon \\
& -\Delta a_z^{\alpha\delta}\cos\epsilon\sin\epsilon \\
& -a_{sp}^{\alpha\delta}\sin\epsilon \\
& -\left(\tfrac{2}{3}a_{sp}^{\delta}+2a_{sp}^{\rho}\right)\sin\epsilon, \\
a_y = 0, & \\
a_z = \boldsymbol{a}^T\boldsymbol{e}_{+z} \;=\; & -\tfrac{2}{3}a_z^{\alpha\delta}\cdot\cos\epsilon-\tfrac{2}{3}\Delta a_z^{\alpha\delta}\cdot|\cos\epsilon| \\
& -\left(2\Delta a_z^{\rho}+\Delta a_z^{\alpha\delta}\right)\cdot\cos^2\epsilon-\left(a_z^{\alpha\delta}+2a_z^{\rho}\right)\cdot|\cos\epsilon|\cos\epsilon \\
& -a_x^{\alpha\delta}\cdot\cos\epsilon|\sin\epsilon| \\
& -a_{sp}^{\alpha\delta}\cos\epsilon \\
& -\left(\tfrac{2}{3}a_{sp}^{\delta}+2a_{sp}^{\rho}\right)\cos\epsilon.
\end{aligned} \tag{5.16}$$

While in the DYB frame the acceleration results as:

$$\begin{aligned}
a_D = \boldsymbol{a}^T \boldsymbol{e}_D \quad &= \quad -\left(a_z^{\alpha\delta}|\cos\epsilon| + \Delta a_z^{\alpha\delta}\cos\epsilon\right) \\
&\quad -\tfrac{2}{3}\left(a_z^{\alpha\delta}\cos\epsilon + \Delta a_z^{\alpha\delta}|\cos\epsilon|\right)\cos\epsilon \\
&\quad -2\left(a_z^{\rho}\cos\epsilon + \Delta a_z^{\rho}|\cos\epsilon|\right)\cos\epsilon|\cos\epsilon| \\
&\quad -a_x^{\alpha\delta}|\sin\epsilon| \\
&\quad -\left(\tfrac{2}{3}a_x^{\alpha\delta} + 2a_x^{\rho}|\sin\epsilon|\right)\sin^2\epsilon \\
&\quad -\left(a_{sp}^{\alpha\delta} + \tfrac{2}{3}a_{sp}^{\delta} + 2a_{sp}^{\rho}\right), \\
a_Y = \boldsymbol{a}^T \boldsymbol{e}_Y = 0, & \\
a_B = \boldsymbol{a}^T \boldsymbol{e}_B \quad &= \quad +\left(\tfrac{2}{3}a_x^{\alpha\delta} \quad + 2a_x^{\rho}|\cos\theta_x|\right)\cos\epsilon\sin\epsilon \\
&\quad -\left(\tfrac{2}{3}\Delta a_z^{\alpha\delta} + 2\Delta a_z^{\rho}|\cos\epsilon|\right)\sin\epsilon|\cos\epsilon| \\
&\quad -\left(\tfrac{2}{3}a_z^{\alpha\delta} \quad + 2a_z^{\rho}|\cos\epsilon|\right)\sin\epsilon\cos\epsilon.
\end{aligned} \tag{5.17}$$

Now, in order to take into account also the x-z asymmetry, the SRP model will be parametrize in terms of the sum and difference:

$$\begin{aligned}
a_{zx}^{\alpha\delta} &= \tfrac{1}{2}(a_z^{\alpha\delta} + a_x^{\alpha\delta}), \qquad \Delta a_{zx}^{\alpha\delta} &= \tfrac{1}{2}(a_z^{\alpha\delta} - a_x^{\alpha\delta}), \\
a_{zx}^{\rho} &= \tfrac{1}{2}(a_z^{\rho} + a_x^{\rho}), \qquad \Delta a_{zx}^{\rho} &= \tfrac{1}{2}(a_z^{\rho} - a_x^{\rho}).
\end{aligned} \tag{5.18}$$

Considering the geometric and optical properties of the QZS-1 satellite the new parameters of the x-z asymmetry can be computed and their values are shown in Table 5.8. From Table 5.8 is

Table 5.8: Reference values of partial accelerations of the symmetric and asymmetric contributions concerning the x-z asymmetry. All values in nm/s^2.

	nm/s^2
$a_{zx}^{\alpha\delta}$	+20.3
$\Delta a_{zx}^{\alpha\delta}$	-7.0
a_{zx}^{ρ}	+0.5
Δa_{zx}^{ρ}	+0.0

evident that, with the assumptions made in this chapter about geometry and optical properties, the two relevant parameters of the x-z symmetry and asymmetry are only $a_{zx}^{\alpha\delta}$ and $\Delta a_{zx}^{\alpha\delta}$. The introduction of the x-z asymmetry parametrization implies a new expression of the acceleration

in the spacecraft frame:

$$
\begin{aligned}
a_x = \boldsymbol{a}^T \boldsymbol{e}_{+x} \quad = \quad & -a_{zx}^{\alpha\delta} \cdot \left((|\cos\epsilon| + |\sin\epsilon| + \tfrac{2}{3}) \cdot \sin\epsilon \right) \\
& -\Delta a_{zx}^{\alpha\delta} \cdot \left((|\cos\epsilon| - |\sin\epsilon| - \tfrac{2}{3}) \cdot \sin\epsilon \right) \\
& -2a_{zx}^{\rho} \cdot (|\sin\epsilon| \sin\epsilon) \\
& +2\Delta a_{zx}^{\rho} \cdot (|\sin\epsilon| \sin\epsilon) \\
& -\Delta a_{z}^{\alpha\delta} \cdot (\cos\epsilon \sin\epsilon) \\
& -a_{sp}^{\alpha\delta} \cdot \sin\epsilon \\
& -\left(\tfrac{2}{3} a_{sp}^{\delta} + 2a_{sp}^{\rho} \right) \cdot \sin\epsilon, \\
a_y = 0, & \\
a_z = \boldsymbol{a}^T \boldsymbol{e}_{+z} \quad = \quad & -a_{zx}^{\alpha\delta} \cdot \left((|\cos\epsilon| + |\sin\epsilon| + \tfrac{2}{3}) \cdot \cos\epsilon \right) \\
& -\Delta a_{zx}^{\alpha\delta} \cdot \left((|\cos\epsilon| - |\sin\epsilon| + \tfrac{2}{3}) \cdot \cos\epsilon \right) \\
& -2a_{zx}^{\rho} \cdot (|\cos\epsilon| \cos\epsilon) \\
& -2\Delta a_{z}^{\rho} \cdot (|\cos\epsilon| \cos\epsilon) \\
& -\Delta a_{z}^{\alpha\delta} \cdot \left(\tfrac{2}{3} |\cos\epsilon| + \cos^2\epsilon \right) \\
& -2\Delta a_{z}^{\rho} \cdot \left(\cos^2\epsilon \right) \\
& -a_{sp}^{\alpha\delta} \cdot \cos\epsilon \\
& -\left(\tfrac{2}{3} a_{sp}^{\delta} + 2a_{sp}^{\rho} \right) \cdot \cos\epsilon.
\end{aligned}
\tag{5.19}
$$

In the same way in the *DYB* frame:

$$
\begin{aligned}
a_D = \boldsymbol{a}^T \boldsymbol{e}_D \quad = \quad & -a_{zx}^{\alpha\delta} \cdot \left(|\cos\epsilon| + \sin\epsilon + \tfrac{2}{3} \right) \\
& -\Delta a_{zx}^{\alpha\delta} \cdot \left(|\cos\epsilon| - \sin\epsilon - \tfrac{4}{3}\sin^2\epsilon + \tfrac{2}{3} \right) \\
& -2a_{zx}^{\rho} \cdot \left(|\cos\epsilon| \cos^2\epsilon + \sin^3\epsilon \right) \\
& -2\Delta a_{zx}^{\rho} \cdot \left(|\cos\epsilon| \cos^2\epsilon - \sin^3\epsilon \right) \\
& -\Delta a_{z}^{\alpha\delta} \cdot \left(\cos\epsilon + \tfrac{2}{3} |\cos\epsilon| \cos\epsilon \right) \\
& -2\Delta a_{z}^{\rho} \cdot (|\cos\epsilon|^2 \cos\epsilon) \\
& -a_{\mathrm{sp}}, \\
a_Y = \boldsymbol{a}^T \boldsymbol{e}_Y = 0, & \\
a_B = \boldsymbol{a}^T \boldsymbol{e}_B \quad = \quad & -\tfrac{4}{3} \Delta a_{zx}^{\alpha\delta} \cdot (\cos\epsilon \sin\epsilon) \\
& -2a_{zx}^{\rho} \cdot ((|\cos\epsilon| - \sin\epsilon) \cos\epsilon \sin\epsilon) \\
& -2\Delta a_{zx}^{\rho} \cdot ((|\cos\epsilon| + \sin\epsilon) \cos\epsilon \sin\epsilon) \\
& -\tfrac{2}{3} \Delta a_{z}^{\alpha\delta} \cdot (|\cos\epsilon| \sin\epsilon) \\
& -2\Delta a_{z}^{\rho} \cdot \left(|\cos\epsilon|^2 \sin\epsilon \right),
\end{aligned}
\tag{5.20}
$$

where $a_{sp} = a_{sp}^{\alpha\delta} + \frac{2}{3} a_{sp}^{\delta} + 2a_{sp}^{\rho}$. At this point the parametrized expressions of the acceleration both in the spacecraft frame and in the DYB frame are obtained.

Now the data extracted from the orbit determination process will be used in order to improve the a priori model and to better understand the real QZS-1 dimensions and optical properties. The purpose is to give an analytical expression of the coefficients of the ECOM parameters. But, in order to compare the model with the data, also the acceleration average over one orbit has to be considered. The averaged components of the acceleration in the D and B direction are given

by:

$$\begin{aligned} \bar{a}_D &= \tfrac{1}{\pi}\int_0^{\pi} a_D(\epsilon(\beta,\mu)\,d\mu, \\ \bar{a}_B &= \tfrac{1}{\pi}\int_0^{\pi} a_B(\epsilon(\beta,\mu)\,d\mu. \end{aligned} \tag{5.21}$$

The elongation ϵ in turn is, in fact, a function of β and of the orbit angle μ as Eq. 2.5 shows. The averaged values are obtained assuming a circular orbit with constant angular velocity [28]. This averaged acceleration corresponds to the constant part of the ECOM parameters D_0, Y_0 and B_0 (see Eq. 3.21). Considering, furthermore, that $\epsilon(\beta,\pi-\mu)=\pi-\epsilon(\beta,\mu)$, it may be recognized that partial accelerations varying with $\cos\epsilon$ exhibit a vanishing mean across the orbit. Accordingly, $\Delta a_z^{\alpha\delta}$ and Δa_z^{ρ} do not contribute to the average acceleration in D-direction. Likewise, $a_{zx}^{\alpha\delta}$, $\Delta a_{zx}^{\alpha\delta}$, a_{zx}^{ρ}, and Δa_{zx}^{ρ} do not contribute a mean B-acceleration. Therefore β-dependent mean acceleration is given by:

$$\begin{aligned} \bar{a}_D = \overline{\boldsymbol{a}^T\boldsymbol{e}_D} \quad = \quad & -a_{zx}^{\alpha\delta}\cdot\left(\tfrac{2}{\pi}|\cos\beta| + \tfrac{2}{\pi}E(\cos\beta) + \tfrac{2}{3}\right) \\ & -\Delta a_{zx}^{\alpha\delta}\cdot\left(\tfrac{2}{\pi}|\cos\beta| - \tfrac{2}{\pi}E(\cos\beta) + \tfrac{2}{3}\cos^2\beta - \tfrac{2}{3}\right) \\ & -2a_{zx}^{\rho}\cdot\left(\tfrac{4}{3\pi}\cos^3\beta - \tfrac{2}{3\pi}\sin^2\beta F(\cos\beta) + \tfrac{4}{3\pi}(1+\sin^2\beta)E(\cos\beta)\right) \\ & -2\Delta a_{zx}^{\rho}\cdot\left(\tfrac{4}{3\pi}\cos^3\beta + \tfrac{2}{3\pi}\sin^2\beta F(\cos\beta) - \tfrac{4}{3\pi}(1+\sin^2\beta)E(\cos\beta)\right) \\ & -a_{\mathrm{sp}}, \\ \bar{a}_B = \overline{\boldsymbol{a}^T\boldsymbol{e}_B} \quad = \quad & -\tfrac{2}{3}\Delta a_z^{\alpha\delta}\cdot\left(\tfrac{1}{\pi}\sin^2(\beta)\log(\tfrac{1+\cos\beta}{|\sin\beta|}) + \tfrac{1}{\pi}\cos\beta\right) \\ & -2\Delta a_z^{\rho}\cdot\left(\tfrac{2}{3\pi}\sin^2(\beta)F(\cos\beta) - \tfrac{2}{3\pi}(1-2\cos^2\beta)E(\cos\beta)\right). \end{aligned} \tag{5.22}$$

Where $F(k)$ and $E(k)$ are respectively the complete elliptic integral of first and second kind for k:

$$E(k) = \int_0^{\frac{\pi}{2}} \sqrt{1-k^2\sin^2 x}\,dx, \tag{5.23a}$$

$$F(k) = \int_0^{\frac{\pi}{2}} \frac{1}{\sqrt{1-k^2\sin^2 x}}\,dx \tag{5.23b}$$

In order to give the complete view of the expression of the acceleration for the YS mode considering the ECOM parameters involved in this work, in a similar way also the two harmonic coefficients B_C^* and B_S^* are calculated.

$$\begin{aligned} B_C^* = \overline{a_B\cdot 2\cos\mu} \quad = \quad & -\tfrac{4}{3}\Delta a_{zx}^{\alpha\delta}\cdot\left(\tfrac{4}{3\pi}\tfrac{\sin^2\beta}{\cos\beta}F(\cos\beta) - \tfrac{4}{3\pi}EI(\cos\beta)\right) \\ & -2a_{zx}^{\rho}\cdot\Big(-\tfrac{1}{2\pi}\tfrac{(1-\cos^2\beta)(1+3\cos^2\beta)}{\cos\beta}\log\sqrt{\tfrac{1-\cos\beta}{1+\cos\beta}} \\ & \quad -\tfrac{1}{2\pi}(1-3\cos^2\beta) - (\cos\beta - \tfrac{3}{4}\cos^3\beta)\Big) \\ & -2\Delta a_{zx}^{\rho}\cdot\Big(\tfrac{1}{2\pi}\tfrac{(1-\cos^2\beta)(1+3\cos^2\beta)}{\cos\beta}\log\sqrt{\tfrac{1-\cos\beta}{1+\cos\beta}} \\ & \quad -\tfrac{1}{2\pi}(1-3\cos^2\beta) + (\cos\beta - \tfrac{3}{4}\cos^3\beta)\Big), \\ B_S^* = \overline{a_B\cdot 2\sin\mu} \quad = \quad & 0. \end{aligned} \tag{5.24}$$

Orbit Normal mode

The develop of the expression of the acceleration in the ON mode follow the same steps of the YS mode analysis. Therefore considering Eqs. 5.4 and 5.6 and projecting Eq. 5.15 in the spacecraft

system, the x,y,z components of the acceleration in the ON mode yield:

$$\begin{aligned}
a_x = \boldsymbol{a}^T \boldsymbol{e}_{+x} &= -\tfrac{2}{3} a_x^{\alpha\delta} \cdot \cos\beta \sin\mu \\
&\quad -\left(a_x^{\alpha\delta} + 2a_x^{\rho}\right) |\cos\beta \sin\mu| \cos\beta \sin\mu \\
&\quad -a_z^{\alpha\delta} |\cos\beta \cos\mu| \cos\beta \sin\mu \\
&\quad -\Delta a_z^{\alpha\delta} \cos^2\beta \cos\mu \sin\mu + \Delta a_y^{\alpha\delta} \sin\beta \cos\beta \sin\mu \\
&\quad -a_y^{\alpha\delta} |\sin\beta| \cos\beta \sin\mu \\
&\quad -a_{sp}^{\alpha\delta} \cos^2\beta \sin\mu \\
&\quad -\left(\tfrac{2}{3} a_{sp}^{\delta} + 2a_{sp}^{\rho} |\cos\beta|\right) \cos\beta \sin\mu, \\
a_y = \boldsymbol{a}^T \boldsymbol{e}_{+y} &= +\tfrac{2}{3} a_y^{\alpha\delta} \cdot \sin\beta - \tfrac{2}{3} \Delta a_y^{\alpha\delta} \cdot |\sin\beta| \\
&\quad -\left(2\Delta a_y^{\rho} + \Delta a_y^{\alpha\delta}\right) \cdot \sin^2\beta + \left(a_y^{\alpha\delta} + 2a_y^{\rho}\right) \cdot |\sin\beta| \sin\beta \\
&\quad +a_x^{\alpha\delta} |\cos\beta \sin\mu| \sin\beta \\
&\quad +a_z^{\alpha\delta} |\cos\beta \cos\mu| \sin\beta + \Delta a_z^{\alpha\delta} \cos\beta \cos\mu \sin\beta \\
&\quad +a_{sp}^{\alpha\delta} \cos\beta \sin\beta, \\
a_z = \boldsymbol{a}^T \boldsymbol{e}_{+z} &= -\tfrac{2}{3} a_z^{\alpha\delta} \cdot \cos\beta \cos\mu - \tfrac{2}{3} \Delta a_z^{\alpha\delta} \cdot |\cos\beta \cos\mu| \\
&\quad -\left(2\Delta a_z^{\rho} + \Delta a_z^{\alpha\delta}\right) \cdot \cos^2\beta \cos^2\mu - \left(a_z^{\alpha\delta} + 2a_z^{\rho}\right) \cdot |\cos\beta\mu| \cos\beta\mu \\
&\quad -a_x^{\alpha\delta} \cdot \cos\beta \cos\mu |\cos\beta \sin\mu| \\
&\quad -a_y^{\alpha\delta} \cdot \cos\beta \cos\mu |\sin\beta| + \Delta a_y^{\alpha\delta} \sin E \cos\beta \cos\mu \\
&\quad -a_{sp}^{\alpha\delta} \cos^2\beta \cos\mu \\
&\quad -\left(\tfrac{2}{3} a_{sp}^{\delta} + 2a_{sp}^{\rho} |\cos\beta|\right) \cos\beta \cos\mu.
\end{aligned} \tag{5.25}$$

While in the $\overline{DYB}$ frame the acceleration results as:

$$\begin{aligned}
a_{\bar{D}} = \boldsymbol{a}^T \boldsymbol{e}_{\bar{D}} &= -\left(a_z^{\alpha\delta} |\cos\beta \cos\mu| + \Delta a_z^{\alpha\delta} \cos\beta \cos\mu\right) \cos\beta \\
&\quad -\tfrac{2}{3} \left(a_z^{\alpha\delta} \cos\beta \cos\mu + \Delta a_z^{\alpha\delta} |\cos\beta \cos\mu|\right) \cos\mu \\
&\quad -2 \left(a_z^{\rho} \cos\beta \cos\mu + \Delta a_z^{\rho} |\cos\beta \cos\mu|\right) \cos\mu |\cos\beta \cos\mu| \\
&\quad -a_x^{\alpha\delta} |\cos\beta \sin\mu| \cos\beta \\
&\quad -\left(\tfrac{2}{3} a_x^{\alpha\delta} + 2a_x^{\rho} |\cos\beta \sin\mu|\right) \cos\beta \sin\mu \sin\mu \\
&\quad -\left(a_y^{\alpha\delta} |\sin\beta| - \Delta a_y^{\alpha\delta} \sin\beta\right) \cos\beta \\
&\quad -a_{sp}^{\alpha\delta} |\cos\beta| \cos\beta \\
&\quad -\left(\tfrac{2}{3} a_{sp}^{\delta} + 2a_{sp}^{\rho} |\cos\beta|\right) \cos\beta, \\
a_{\bar{Y}} &= a_y, \\
a_{\bar{B}} = \boldsymbol{a}^T \boldsymbol{e}_{\bar{B}} &= +\left(\tfrac{2}{3} a_x^{\alpha\delta} \quad + 2a_x^{\rho} |\cos\beta \sin\mu|\right) \cos\mu \cos\beta \sin\mu \\
&\quad -\left(\tfrac{2}{3} \Delta a_z^{\alpha\delta} + 2\Delta a_z^{\rho} |\cos\beta \cos\mu|\right) \sin\mu |\cos\beta \cos\mu| \\
&\quad -\left(\tfrac{2}{3} a_z^{\alpha\delta} \quad + 2a_z^{\rho} |\cos\beta \cos\mu| \quad\right) \sin\mu \cos\beta \cos\mu.
\end{aligned} \tag{5.26}$$

Introducing now the parameters of the x-z symmetry and asymmetry, i.e. Eq. 5.18, the x,y,z components of the acceleration become:

$$
\begin{aligned}
a_x = \boldsymbol{a}^T \boldsymbol{e}_{+x} \quad = \quad & -a_{zx}^{\alpha\delta} \cdot \left((|\cos\beta\cos\mu| + |\cos\beta\sin\mu| + \tfrac{2}{3}) \cdot \cos\beta\sin\mu \right) \\
& -\Delta a_{zx}^{\alpha\delta} \cdot \left((|\cos\beta\cos\mu| - |\cos\beta\sin\mu| - \tfrac{2}{3}) \cdot \cos\beta\sin\mu \right) \\
& -2a_{zx}^{\rho} \cdot \left(|\cos\beta\sin\mu| \cos\beta\sin\mu \right) \\
& +2\Delta a_{zx}^{\rho} \cdot \left(|\cos\beta\sin\mu| \cos\beta\sin\mu \right) \\
& -\Delta a_{z}^{\alpha\delta} \cdot \left(\cos\beta\cos\mu\cos\beta\sin\mu \right) \\
& -a_{y}^{\alpha\delta} \cdot |\sin\beta| \cos\beta\sin\mu \\
& +\Delta a_{y}^{\alpha\delta} \cdot \sin\beta\cos\beta\sin\mu \\
& -a_{sp}^{\alpha\delta} \cdot \cos\beta\sin\mu|\cos\beta| \\
& -\left(\tfrac{2}{3} a_{sp}^{\delta} + 2a_{sp}^{\rho} |\cos\beta| \right) \cdot \cos\beta\sin\mu, \\
a_y = \boldsymbol{a}^T \boldsymbol{e}_{+y} \quad = \quad & +a_{zx}^{\alpha\delta} \cdot \left(|\cos\beta\cos\mu| + |\cos\beta\sin\mu| \right) \cdot \sin\beta \\
& +\Delta a_{zx}^{\alpha\delta} \cdot \left(|\cos\beta\cos\mu| - |\cos\beta\sin\mu| \right) \cdot \sin\beta \\
& +\Delta a_{z}^{\alpha\delta} \cdot \cos\beta\cos\mu\sin\beta \\
& +\tfrac{2}{3} a_{y}^{\alpha\delta} \cdot \sin\beta \\
& +\left(a_{y}^{\alpha\delta} + 2a_{y}^{\rho} \right) \cdot |\sin\beta| \sin\beta \\
& -\tfrac{2}{3} \Delta a_{y}^{\alpha\delta} \cdot |\sin\beta| \\
& -\left(2\Delta a_{y}^{\rho} + \Delta a_{y}^{\alpha\delta} \right) \cdot \sin^2\beta \\
& +a_{sp}^{\alpha\delta} \cdot \sin\beta|\cos\beta|, \\
a_z = \boldsymbol{a}^T \boldsymbol{e}_{+z} \quad = \quad & -a_{zx}^{\alpha\delta} \cdot \left((|\cos\beta\cos\mu| + |\cos\beta\cos\mu| + \tfrac{2}{3}) \cdot \cos\beta\cos\mu \right) \\
& -\Delta a_{zx}^{\alpha\delta} \cdot \left((|\cos\beta\cos\mu| - |\cos\beta\sin\mu| + \tfrac{2}{3}) \cdot \cos\beta\sin\mu \right) \\
& -2a_{zx}^{\rho} \cdot \left(|\cos\beta\cos\mu| \cos\beta\cos\mu \right) \\
& -2\Delta a_{z}^{\rho} \cdot \left(|\cos\beta\cos\mu| \cos\beta\cos\mu \right) \\
& -\Delta a_{z}^{\alpha\delta} \cdot \left(\tfrac{2}{3} |\cos\beta\cos\mu| + \cos^2\beta\cos\mu \right) \\
& -2\Delta a_{z}^{\rho} \cdot \left(\cos^2\beta\cos^2\mu \right) \\
& -a_{y}^{\alpha\delta} \cdot \cos\beta\cos\mu|\sin\beta| \\
& +\Delta a_{y}^{\alpha\delta} \cdot \sin\beta\cos\beta\cos\mu \\
& -a_{sp}^{\alpha\delta} \cdot \cos\beta\cos\mu|\cos\beta| \\
& -\left(\tfrac{2}{3} a_{sp}^{\delta} + 2a_{sp}^{\rho} |\cos\beta| \right) \cdot \cos\beta\cos\mu.
\end{aligned}
\tag{5.27}
$$

While in the $\overline{DYB}$ the expressions of the components are:

$$
\begin{aligned}
a_{\bar{D}} = \boldsymbol{a}^T \boldsymbol{e}_{\bar{D}} \quad = \quad & -a_{zx}^{\alpha\delta} \cdot \left[\left(|\cos\beta\cos\mu| + |\cos\beta\sin\mu| \right) \cos\beta + \tfrac{2}{3} \left(\cos\beta\cos^2\mu + \cos\beta\sin^2\mu \right) \right] \\
& -\Delta a_{zx}^{\alpha\delta} \cdot \left[\left(|\cos\beta\cos\mu| - |\cos\beta\sin\mu| \right) \cos\beta + \tfrac{2}{3} \left(\cos\beta\cos^2\mu - \cos\beta\sin^2\mu \right) \right] \\
& -2a_{zx}^{\rho} \cdot \left(|\cos\beta\cos\mu| \cos\beta\cos^2\mu + |\cos\beta\sin\mu| \cos\beta\sin^2\mu \right) \\
& -2\Delta a_{zx}^{\rho} \cdot \left(|\cos\beta\cos\mu| \cos\beta\cos^2\mu - |\cos\beta\sin\mu| \cos\beta\sin^2\mu \right) \\
& -\Delta a_{z}^{\alpha\delta} \cdot \left(\cos\beta^2 \cos\mu + \tfrac{2}{3} |\cos\beta\cos\mu| \cos\mu \right) \\
& -2\Delta a_{z}^{\rho} \cdot |\cos\beta\cos\mu|^2 \cos\mu \\
& -a_{y}^{\alpha\delta} \cdot |\sin\beta| \cos\beta \\
& +\Delta a_{y}^{\alpha\delta} \cdot \sin\beta\cos\beta \\
& -\left(a_{sp}^{\alpha\delta} + 2a_{sp}^{\rho} \right) \cdot |\cos\beta| \cos\beta \\
& -\tfrac{2}{3} a_{sp}^{\delta} \cdot \cos\beta, \\
a_{\bar{Y}} = a_y, & \\
a_{\bar{B}} = \boldsymbol{a}^T \boldsymbol{e}_{\bar{B}} \quad = \quad & -\tfrac{2}{3} a_{zx}^{\alpha\delta} \cdot \left(\cos\beta\cos\mu\sin\mu - \cos\beta\sin\mu\cos\mu \right) \\
& -\tfrac{2}{3} \Delta a_{zx}^{\alpha\delta} \cdot \left(\cos\beta\cos\mu\sin\mu + \cos\beta\sin\mu\cos\mu \right) \\
& -2a_{zx}^{\rho} \cdot \left(|\cos\beta\cos\mu| \cos\beta\cos\mu\sin\mu - |\cos\beta\sin\mu| \cos\beta\sin\mu\cos\mu \right) \\
& -2\Delta a_{zx}^{\rho} \cdot \left(|\cos\beta\cos\mu| \cos\beta\cos\mu\sin\mu + |\cos\beta\sin\mu| \cos\beta\sin\mu\cos\mu \right) \\
& -\tfrac{2}{3} \Delta a_{z}^{\alpha\delta} \cdot |\cos\beta\cos\mu| \sin\mu \\
& -2\Delta a_{z}^{\rho} \cdot |\cos\beta\cos\mu|^2 \sin\mu.
\end{aligned}
\tag{5.28}
$$

The average acceleration in the $\overline{DYB}$ frame is given by:

$$
\begin{aligned}
\bar{a}_{\bar{D}} &= \tfrac{1}{\pi} \int_0^{\pi} a_{\bar{D}}(\beta,\mu)\, d\mu, \\
\bar{a}_{\bar{Y}} &= \tfrac{1}{\pi} \int_0^{\pi} a_{\bar{Y}}(\beta,\mu)\, d\mu, \\
\bar{a}_{\bar{B}} &= \tfrac{1}{\pi} \int_0^{\pi} a_{\bar{B}}(\beta,\mu)\, d\mu.
\end{aligned}
\tag{5.29}
$$

Hence the β-dependent mean components of the acceleration are given by:

$$\begin{aligned}
\bar{a}_{\bar{D}} = \overline{\boldsymbol{a}^T \boldsymbol{e}_{\bar{D}}} \quad = \quad & -a_{zx}^{\alpha\delta} \cdot \left[\tfrac{4}{\pi}|\cos\beta| + \tfrac{2}{3}\right]\cos\beta \\
& -2\tfrac{8}{3\pi} a_{zx}^{\rho} \cdot \cos^2\beta \\
& -a_{y}^{\alpha\delta} \cdot |\sin\beta|\cos\beta \\
& +\Delta a_{y}^{\alpha\delta} \cdot \sin\beta\cos\beta \\
& -\left(a_{sp}^{\alpha\delta} + 2a_{sp}^{\rho}\right) \cdot |\cos\beta|\cos\beta \\
& -\tfrac{2}{3} a_{sp}^{\delta} \cdot \cos\beta, \\
\bar{a}_{\bar{Y}} = \overline{\boldsymbol{a}^T \boldsymbol{e}_{\bar{Y}}} \quad = \quad & +\tfrac{4}{\pi} a_{zx}^{\alpha\delta} \cdot \sin\beta|\cos\beta| \\
& +\tfrac{2}{3} a_{y}^{\alpha\delta} \cdot \sin\beta \\
& +\left(a_{y}^{\alpha\delta} + 2a_{y}^{\rho}\right) \cdot |\sin\beta|\sin\beta \\
& -\tfrac{2}{3}\Delta a_{y}^{\alpha\delta} \cdot |\sin\beta| \\
& -\left(2\Delta a_{y}^{\rho} + \Delta a_{y}^{\alpha\delta}\right) \cdot \sin^2\beta \\
& +a_{sp}^{\alpha\delta} \cdot \sin\beta|\cos\beta|, \\
\bar{a}_{\bar{B}} = \overline{\boldsymbol{a}^T \boldsymbol{e}_{\bar{B}}} \quad = \quad & -\tfrac{4}{3}\Delta a_{zx}^{\alpha\delta} \cdot \cos\mu\sin\mu\cdot\cos\beta \\
& -2a_{zx}^{\rho} \cdot \left(|\cos\mu| - |\sin\mu|\right)\cos\mu\sin\mu\cdot\cos^2\beta \\
& -2\Delta a_{zx}^{\rho} \cdot \left(|\cos\mu| + |\sin\mu|\right)\cos\mu\sin\mu\cdot\cos^2\beta \\
& -\tfrac{2}{3}\Delta a_{z}^{\alpha\delta} \cdot |\cos\mu|\sin\mu\cdot\cos\beta \\
& -2\Delta a_{z}^{\rho} \cdot \cos^2\mu\sin\mu\cdot\cos^2\beta.
\end{aligned} \tag{5.30}$$

While the harmonic coefficients $\bar{B}_C^*$ and $\bar{B}_S^*$ yield:

$$\begin{aligned}
\bar{B}_c^* = \overline{a_B \cdot 2\cos\mu} \quad = \quad & +\tfrac{2}{3} a_{x}^{\alpha\delta} \cdot \tfrac{4}{3\pi}\cos\beta \\
& +2a_{x}^{\rho} \cdot \tfrac{1}{4}\cos^2\beta, \\
\bar{B}_s^* = \overline{a_B \cdot 2\cos\mu} \quad = \quad & -\tfrac{2}{3} a_{x}^{\alpha\delta} \cdot \tfrac{4}{3\pi}\cos\beta \\
& -2a_{x}^{\rho} \cdot \tfrac{1}{4}\cos^2\beta.
\end{aligned} \tag{5.31}$$

5.3.2 Summary

Table 5.9: Characteristic accelerations of the box-wing SRP model and considering the body dimensions and the assumed optical properties as well as an assumed mass of 2000kg [28].

Parameter	value [nm/s^2]
$a_{zx}^{\alpha\delta}$	+20.3
a_{zx}^{ρ}	+0.5
$\Delta a_{zx}^{\alpha\delta}$	-7.0
$a_{y}^{\alpha\delta}$	+18.1
a_{y}^{ρ}	+10.7
$\Delta a_{y}^{\alpha\delta}$	-1.3
Δa_{y}^{ρ}	+1.3
$a_{sp}^{\alpha\delta}$	+72.1
a_{sp}^{ρ}	+19.2
a_{sp}^{ρ}	+3.6

The analytical model for QZS-1 is obtained. It is parametrized with respect to geometric and optical properties through partial accelerations that take into account the asymmetries of the spacecraft. The partial accelerations can be called characteristic accelerations of the box-wing

SRP model and, considering the body dimensions and the assumed optical properties of Tables 5.1 and 5.2 as well as an assumed mass of 2000kg, they can be computed as shown in Table 5.9. The values of Table 5.9 and those obtained in Tables 5.6, 5.7 and 5.8 are used as guideline in the validation process of the following chapter (Chapter 6). The parametrization of the analytical box-wing model allows to evaluate the impact of the absorbed and diffusely reflected (i.e. $\alpha + \delta$) contribution as well as the specularly reflected (i.e. ρ) contribution and it is useful to understand the validity of the model assumptions in a POD validation process. Furthermore the introduction of the use of the angles A,E and of the $\overline{DYB}$ gives continuity between the analyses of the two YS and ON attitude modes.

5.4 Solar panels shadows

The relative shadowing between body of the spacecraft and solar panels could have effects on the SRP acceleration. But there is a separation between the solar panel and the body, that is the bracket of the deployment. Therefore if the shadow caused by a plate of the same length of the bracket is greater than every distance between the attachment of the bracket and the border of the surface there is no shadow effect of the solar panel on the surface.

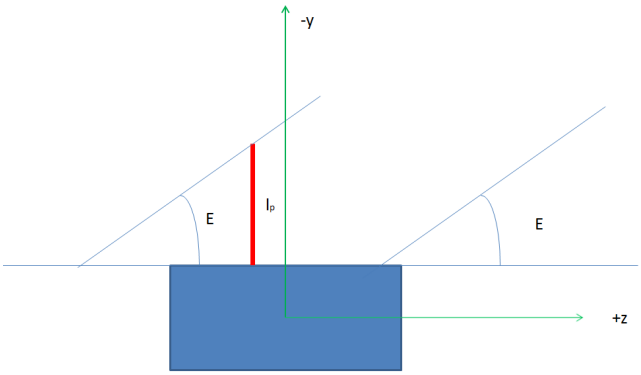

Figure 5.7: View of the problem in the y-z plane. l_p indicates the plate with the same length of the bracket, E is the elevation of the Sun on the orbital plane.

The length of the bracket in the y-direction is: 2.5±0.05m. The angle involved is the elevation of the Sun on the orbital plane that is the x-z plane. The y-surface is completely in the shadow of an hypothetical plate of the same size of the bracket if [26]:

$$l < \frac{l_p}{\tan E}. \tag{5.32}$$

In the lowest case: l_p=2.45m and E= 20deg for the orbit normal mode, that is:

$$l < 6.7313\text{m}.$$

It is always true, therefore there is no shadows of the solar panels on the body.

6. MODEL VALIDATION IN ORBIT DETERMINATION

This Master's thesis work was developed at the *German Space Operations Center* GSOC of the *Deutches Zentrum für Luft und Raumfahrt* DLR in Oberpfaffenhofen, near Munich, Germany. The work of thesis proceeded in parallel with the research of the GNSS group at DLR. In this chapter will be presented how the work of this thesis has been inserted in the work of the aforementioned group in the modeling of the Solar Radiation Pressure and the improvements which it can give on the quality of the orbit determination of the QZS-1 satellite. In particular the analytical model presented in Chapter 5 has been validated in NAPEOS by DLR.

6.1 Box-wing model parameter adjustment

The analytical model presented in Chapter 5 has to be validated in a real orbit determination process. It means that it has to check if the addition of an a priori model of the SRP can give benefits to the orbit determination performances. In order to do it the best set of parameters which describes the SRP model is investigated. The resulting parameters are called *adjusted parameters*. The software used for the Precise Orbit Determination is NAPEOS.

6.1.1 NAPEOS

NAPEOS (NAvigation Package for Earth Orbiting Satellites) is portable navigation software for Earth Orbiting satellite missions. It provides orbit determination and prediction, manoeuvre optimization and global parameter estimation capabilities and is able to process a wide variety of observation data, including: angles, range, range-rate, altimetry, satellite-to-satellite links and GNSS data [13]. The version v3.3.1 of Napeos was upgraded by DLR in order to consider the addition of a priori box-wing model and the $\overline{DYB}$-frame for orbit-normal mode [28]. In fact NAPEOS has to be able to switch from YS mode to ON mode depending on the elevation of the Sun above the orbital plane, that is the β angle. It is recalled that for $|\beta|$>20 deg the satellite is in YS mode, while for $|\beta|$<20 deg it is in ON mode. The *data arc* considered in this implementation is three days with a step-size of five minutes, furthermore the days with orbit maneuvers were excluded from the analysis [28]. The period selected for the computation is from 2 January 2015 until 18 December 2016, that is almost two full cycles of β angle[28]. The empirical accelerations obtained without an a priori model were compared to the QZS-1 results generated by Technische Universität München (TUM) within the frame of the IGS Multi-GNSS project [28]. Therefore a first effort was spent by DLR to overcome this difference in order to compare the two sets of results. The set of parameters proposed in the previous chapter was used as *first guess* of the possible values of the partial accelerations: It does not give the expected improvements and so iteratively they have

Table 6.1: First guess of the partial accelerations. All values in nm/s^2.

partial acc	value
$a_{zx}^{\alpha\delta}$	+20.0
$\Delta a_{zx}^{\alpha\delta}$	-3.2
$a_{y}^{\alpha\delta}$	+6.0
a_{y}^{ρ}	+15.0
$a_{sp}^{\alpha\delta}$	+75.0
a_{sp}^{ρ}	+20.0
a_{sp}^{δ}	+3.0
bias$_y$	-0.9

to be *adjusted*.

6.1.2 Model Adjustment with NAPEOS

The work presented in [28] shows as, especially in the orbit normal mode, the shape of the function related to ρ or $\alpha+\delta$ are very similar (see Fig. 6.1). It improves the difficulty in distinguishing the two different effects. Furthermore, as already mentioned, the reflective component has an important role in particular considering the ± y panels. It means that the reflective contribution con be neglected for x and z (and hence for the yaw steering mode) with an important role only for the y contribution.

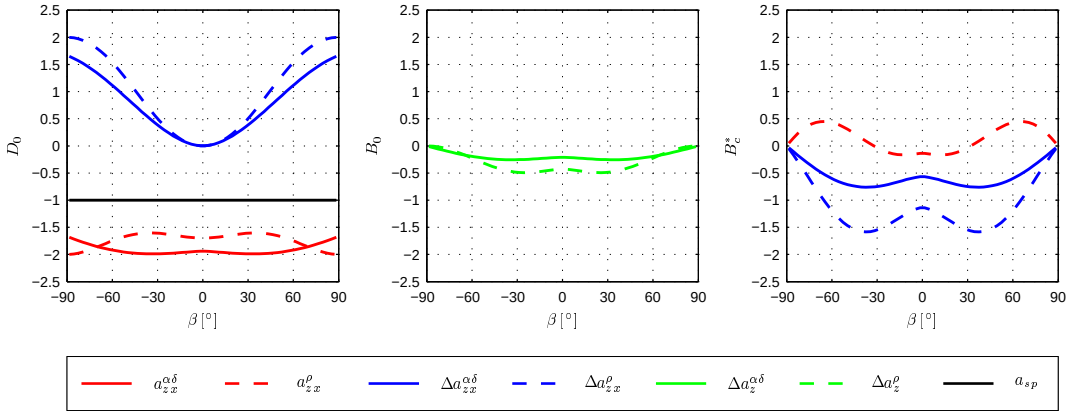

(a) *Yaw Steering mode.*

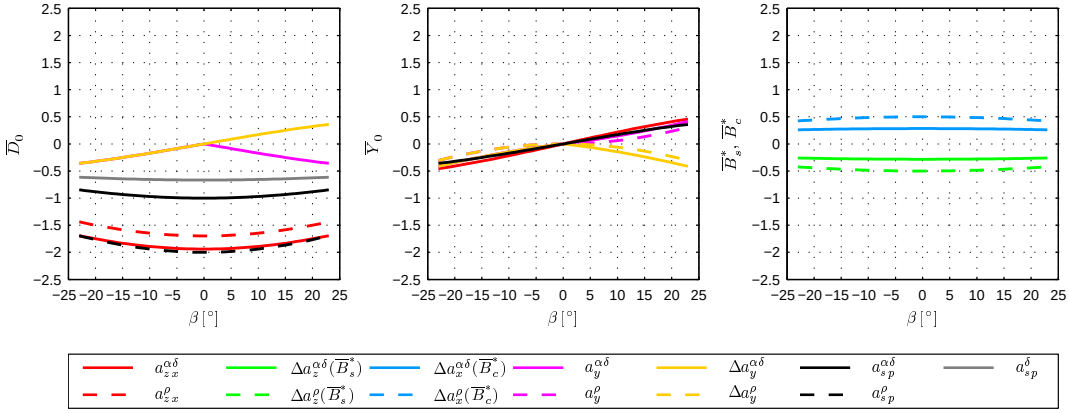

(b) *Orbit Normal mode.*

Figure 6.1: Different contribution of the partial accelerations of the box-wing model on the ECOM parameters. In particular itunderlines the different impacts of the $\alpha+\delta$ and ρ components. Reproduced from [28].

The adjustment of the parameters of the model is done iteratively in order to minimize the amplitude and variation of the remaining empirical ECOM-YS/ON parameters with β angle over the period considered [28].

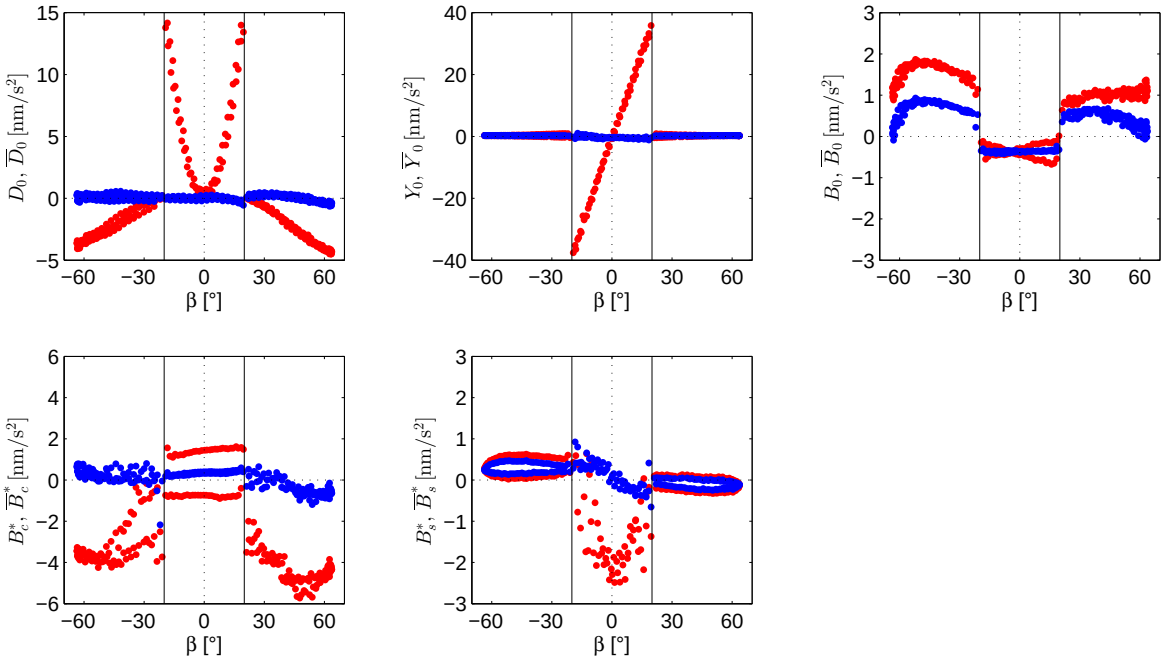

Figure 6.2: Estimate ECOM parameters with (blue) and without (red) the addition of an a priori model with respect to the β angle. In order to have the true amount of the parameters without the box-wing model a mean value of 156 nm/s^2 has to be added to the D0 and the $\bar{D}0$ estimates. The two central vertical lines divide the YS mode application range from the ON mode. Reproduced from [28].

The adjustment of the parameters shows that also the ±y asymmetry can be neglected. Table 6.2 shows the characteristic acceleration of the adjusted model compared to the expected values of the box-wing model proposed in [28].

Table 6.2: The table illustrates the results of the model adjustment with Napeos and it compares these results with the expected values of the box-wing model [28].

Parameter	Adjusted	Expected
$a_z^{a\delta}$	13.0	13.25
$a_x^{a\delta}$	27.0	27.3
$a_{zx}^{a\delta}$	20.0	20.3
$\Delta a_{zx}^{a\delta}$	-7.0	-7.0
$a_y^{a\delta}$	7.0	18.0
a_y^{ρ}	15.0	10.7
$a_{sp}^{a\delta}$	70.5	72.1
a_{sp}^{δ}	0.0	3.6
a_{sp}^{ρ}	21.0	19.2

Hence the final adjusted model is defined by six parameters as summarized in Table 6.3.

Table 6.3: Partial accelerations that define the adjusted model [28].

Parameter	value [nm/s^2]
$a_{zx}^{a\delta}$	20.0
$\Delta a_{zx}^{a\delta}$	-7.0
$a_y^{a\delta}$	7.0
a_y^{ρ}	15.0
$a_{sp}^{a\delta}$	70.5
a_{sp}^{ρ}	21.0

6.2 Improvements by using an a priori model

The improvements obtained by the addition of the a priori QZS-1 box-wing model on the orbit quality is evaluated considering three factors [28]:

- the Day Boundary Discontinuities (DBDs), derived as the 3D distance of the midnight epochs at the boundaries of two consecutive 3-day orbital arcs [28]. These discontinuities should be close to zero and they should not show a β dependence.
- The SLR residuals. The Satellite Laser Ranging is a technique to obtain instantaneous range measurements. In particular the element for the comparison is the Standard Deviation (STD) of the SLR residuals. For the validation of GNSS satellite orbits can be used the SLR measurements collected by the International Laser Ranging Service (ILRS) [28].
- The stability of GNSS satellite clocks. The function of the clock residuals with respect the time has to be close to zero and to not show great variations.

Considering these three factors the addition in NAPEOS of the box-wing model yields [28]:

1. a clear decrease of the DBDs dependence on the β angle: the a priori model reduces the peak values from 5m (ON mode) and 2.5 m (YS mode) to 0.5 m and the mean value from 0.9 m to 0.3 m. Therefore there is a consistent improvement concerning this topic.

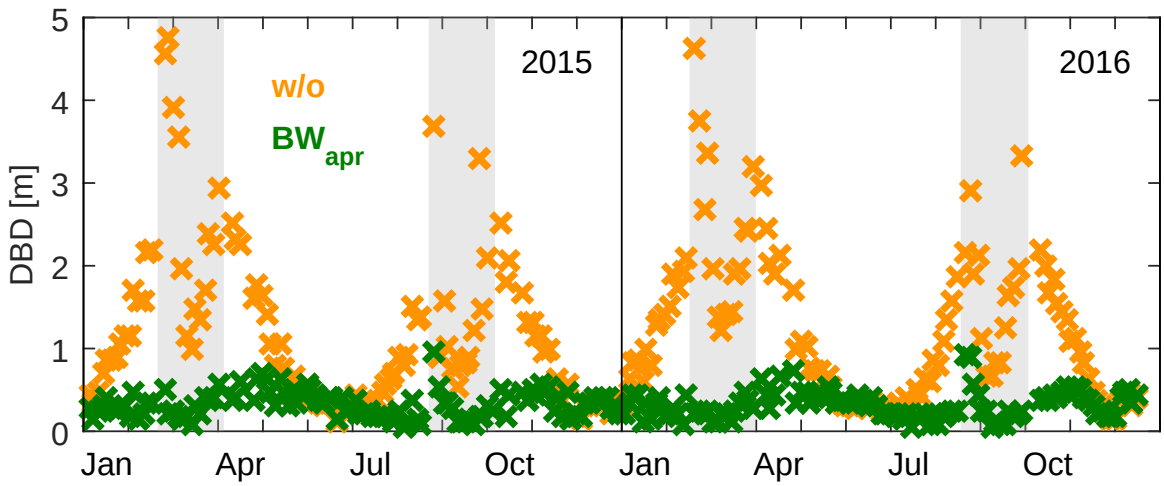

Figure 6.3: Effect of the a priori box-wing model on the Day Boundary Discontinuities DBDs. The orange time series represents the day boundary discontinuities without the a priori model, while the green one represents the DBDs with the box-wing model. Reproduced from [28].

2. A reduction of both the mean value and the standard deviation (STD) of the SLR residuals as shown in Table 6.4. The mean value of the SLR residuals in the YS mode decreases (in absolute value) from −5.4cm to −2.9cm while during the ON mode it decreases from 14.4cm to 2.1cm [28]. The STD of the SRL residuals is reduced by 75% during ON mode and by 43% during YS mode [28].

Table 6.4: SLR residuals for the QZS-1 estimated orbits without and with the a priori box-wing model. σ is the standard deviation. Reproduced from [28]

Attitude	w/o mean±σ [cm]	with mean ±σ [cm]
YS	-5.4±14.0	-2.9±8.0
ON	14.4±33.3	+2.1±8.3
all	-0.5±22.2	-1.6±8.4

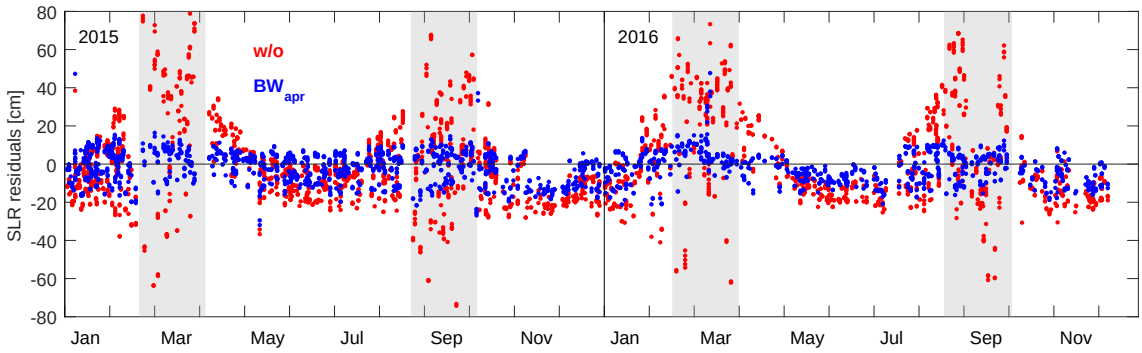

Figure 6.4: Satellite Laser Ranging. The gray series is the result without a priori model, the red and blue series represent respectively the a priori box-wing model during the orbit normal mode and the yaw steering mode. The shaded regions indicate the periods in which the ON mode is adopted. Reproduced from [28].

3. The variations of the apparent clock reduced from ±1m roughly speaking to ±15 cm in YS mode. It has to be noticed that there are twice-per-rev periodicities in the observed variations of the apparent clock in YS mode. It cannot be solved with this model proposed and it might be due to thermal variations of the atomic frequency standard or orbit errors. However the improvement is evident in the ON mode : the orbit-induced clock variations are reduced by up to 85 % [28].

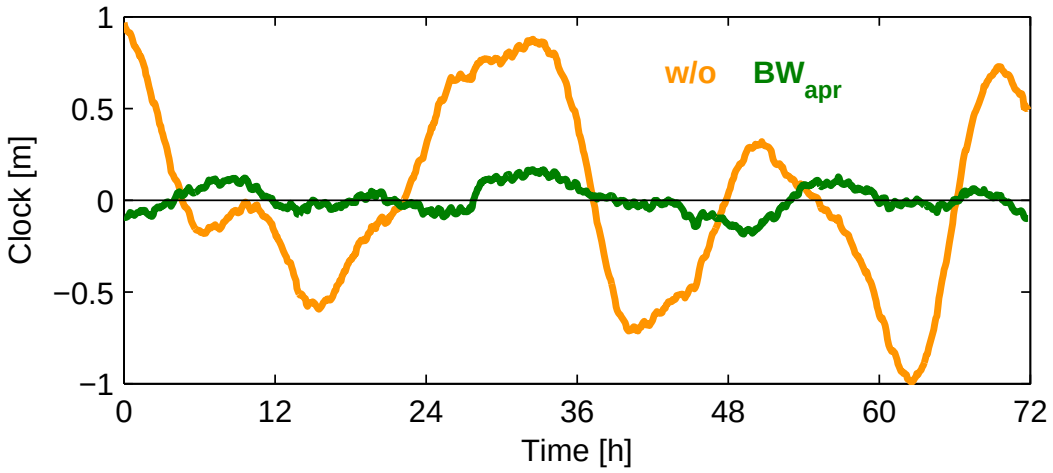

Figure 6.5: Michibiki clock residuals with and without a priori model for the period 23-25 September 2016 . The span involved represents an arc orbit (three days) . Reproduced from [28]

6.3 Observations

Eventually, in order to fixed the ideas and to take out a conclusion of this model validation, the following considerations can be listed:

- The addition of an a priori model in the orbit determination essentially improve the orbit quality in terms of day boundary discontinuities (DBDs), SLR residuals and clock residuals [28].
- The y-bias used for the least squares seems to be not necessary as well as the ±y asymmetry that can be neglected.
- As may be recognized from fig. 6.2 the estimated ECOM parameters with the introduction of the box-wing model are very small. It means that the simple model considered is a good

way to represent the reality because the *delta* to cover the discrepancy between model and reality (represented by the ECOM parameters) is little, or better is very smaller than without any a priori model. However it is true especially for the D_0, Y_0 and $\bar{D}_0$, $\bar{Y}_0$ parameters. In fact the B-parameters still show a β angle dependency. Particularly strange is the sort of *loop* that can be observed in the B_s^* parameter. It is something still not clear and that needs to be investigated. It is interesting to see if a more accurate model from a geometric point of view could help in explaining this particular behaviour of the B-parameters.

- If no a priori model is considered, in the Yaw-Steering mode, D_0 varies linearly with β changing its value of 4-5 nm/s^2 roughly speaking.

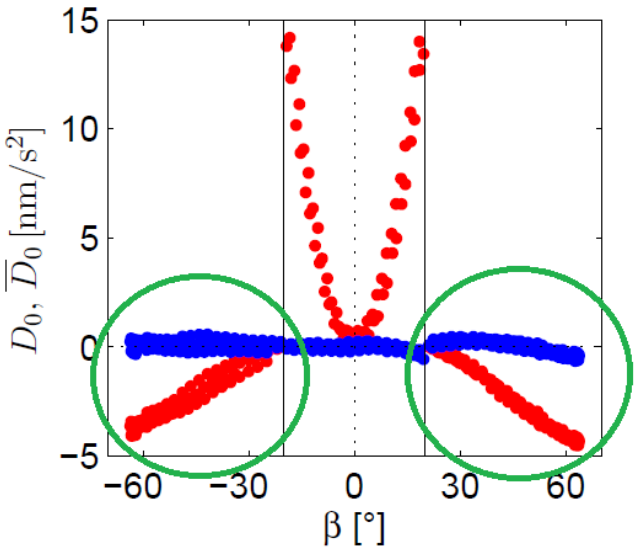

Figure 6.6: Estimate D_0 ECOM parameter for the YS mode [28]. It is a focus on the YS mode for D_0 of fig. 6.2 and as well as in that picture to have the true amount of the parameters without the box-wing model a mean value of 156 nm/s^2 has to be added.

This variation is directly connected to the $\Delta a_{zx}^{\alpha\delta}$ parameter, which is connected to the shape of the body of the spacecraft. Therefore an estimation exclusively based on the ECOM parameters without an a priori model has to give a value of $\Delta a_{zx}^{\alpha\delta}$ near to $-4\,\mathrm{nm/s^2}$. But it is in contrast with the real geometry of the satellite which shows a more stretched shape in the x-z direction. This problem is solved with the addition of the box-wing model and the iteration to find a refined solution. However it could be a problem for an estimation based only on the ECOM parameters also with a more accurate model that could be a ray-tracing model. It is because the ray tracing model is based on a refined geometry, but the ECOM parameters without any a priori model seem to be in contrast with what the geometry dictates.

- As may be observed the adjusted parameters are not so different from the expected values with the exception of the y-parameters. It may be due to the thermal re-radiation over the ± y panels, but it cannot be modeled because there are no information about the thermal exchanges of the spacecraft. Therefore there is a strong hypothesis about the presence of a force due to thermal considerations which is not possible to calculate with the published information so far.

- A more accurate model, as could be obtained with ray-tracing technique, could improve the results, but it has to be investigated. In fact the improvement offered by the ray tracing is to consider a detailed geometry and to associate the right (however still assumed) optical properties to the precisely surfaces, but it could be that the differences found with the adjusted parameters will not solve also with the ray tracing because it is always based on geometry and optical properties as well as the box-wing model and if there is an interaction

with another kind of force, this new technique will not recognize it. However the ray-tracing technique has to be considered as tool of investigation and it is important to understand what is the difference between to use a simplified box-wing model and a ray-tracing model.

- The accuracy achieved considering a simplified box-wing model could potentially be improved with a detailed description of the true attitude of the spacecraft as well as the offsets between the nominal and actual solar panel angle [28].

7. RAY-TRACING ANALYSIS

The ray-tracing analysis is considered in order to better understand the importance of all the components of the satellite and its optical properties and to calculate the acceleration due to the solar radiation pressure with a good accuracy with the few data available about the geometrical and optical properties. The softwares used to do this operation, already mentioned, are the optical commercial software ZEMAX and ARPA — Aerodynamics and Radiation Pressure Analysis — which is the software designed and implemented at the University of Padova to compute forces and torques on satellites due to the non-gravitational perturbations: Solar Radiation Pressure (SRP), Earth Radiation Pressure (ERP) for the albedo and infrared components, the satellite Thermal Re-Radiation (TRR), and the aerodynamics. In this particular case ZEMAX is used only for the ray-tracing and ARPA for the calculation of the SRP. Concerning the ray-tracing technique this works follows Gini's PhD thesis [19].

7.1 ZEMAX

The ray-tracing tool adopted is the commercial software ZEMAX [38]. Of course, the purpose of this software in relation to the current work is extremely different from its designed scopes, and this approach is the same used in Gini's work [19]. As already explained the ray-tracing technique in this case considers a CAD geometry (made up of different simplified geometries) of the spacecraft and a pixel array which represents the Sun. The software ZEMAX has to be setup in order to import the CAD geometries in the standard ACIS text (SAT) or stereolithography (STL) formats. Once the CAD geometry has been imported, the surfaces are automatically identified and numerated. The three main topics of the work with ZEMAX are:

- CAD geometry;
- ray source;
- macro in the programme language of ZEMAX for the interaction spacecraft-ray source in order to cover all the relative position between the two objects.

7.1.1 CAD geometry

The satellite CAD model is the input of the ray-tracing software. The computer aided design program chosen for this analysis is SolidWorks. The satellite is divided into simplified components:

- the box-shaped body;
- the solar panels;
- the *under-antenna* component;
- the antenna.

All the components are introduced in the software as singular objects and it is very important that all of them are already in the right position in the xyz reference system (the manufacturing reference frame, see Fig. 2.5), only in this way ZEMAX can consider the correct configuration. Therefore the x,y,z frame of ZEMAX corresponds to the spacecraft x,y,z frame as defined in Fig. 2.5 (the red one).

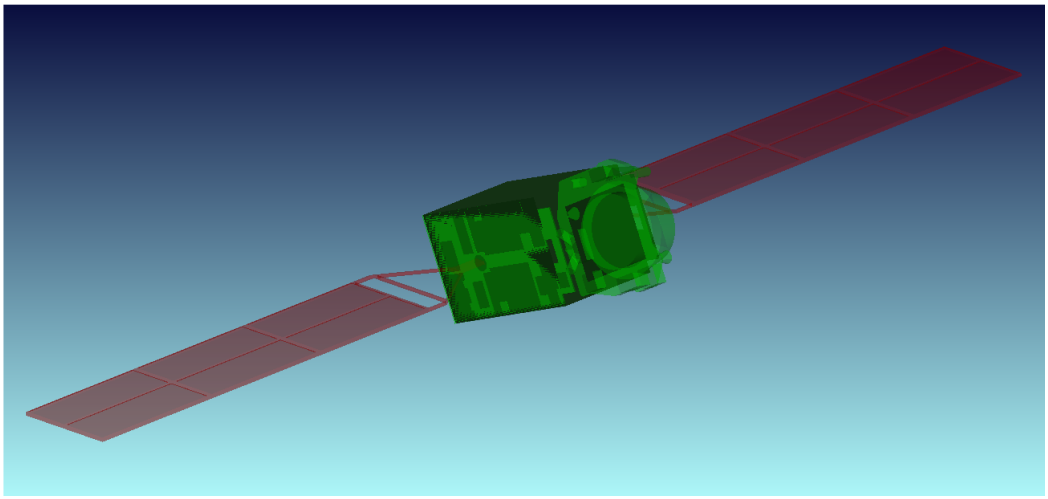

Figure 7.1: Visualization of the CAD model for QZS-1 in ZEMAX.

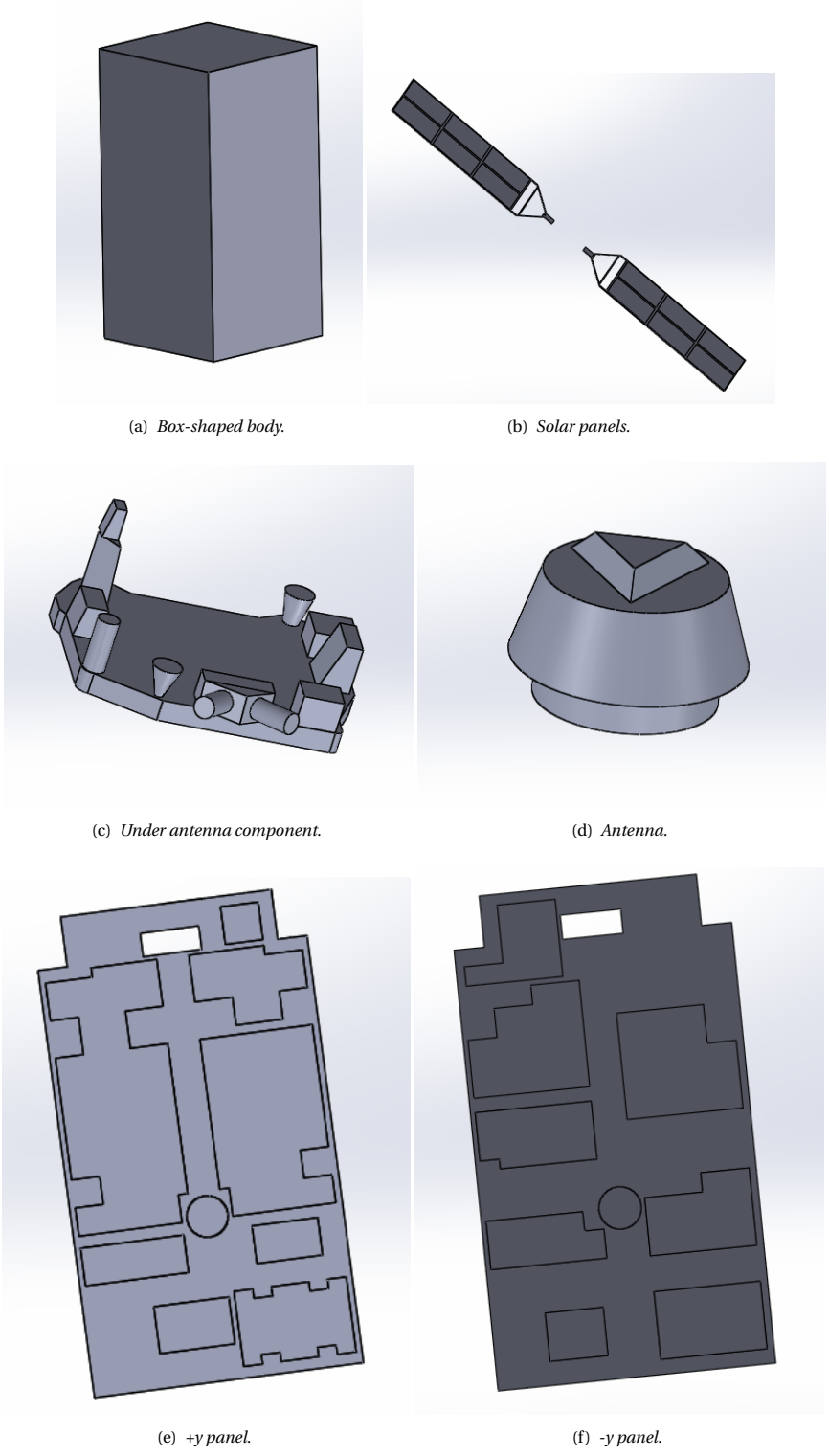

(a) *Box-shaped body.* (b) *Solar panels.*

(c) *Under antenna component.* (d) *Antenna.*

(e) *+y panel.* (f) *-y panel.*

Figure 7.2: Representation of the CAD components of QZS-1. As may be observed there are no the proper colours associated to the surfaces of the components. It is to not increase the computational effort of ZEMAX. Moreover the colours do not have importance in ZEMAX for the ray-tracing computation.

7.1.2 Ray-source

The source of the rays is a planar rectangle divided in identical pixels. From the source the parallel rays are traced (one ray per pixel). The dimension of the source has to be large enough to cover

the biggest dimension of the satellite. In ZEMAX the resolution and the dimension of the source are set as:

- resolution = 1 dm^2;
- side-length = 26000 mm.

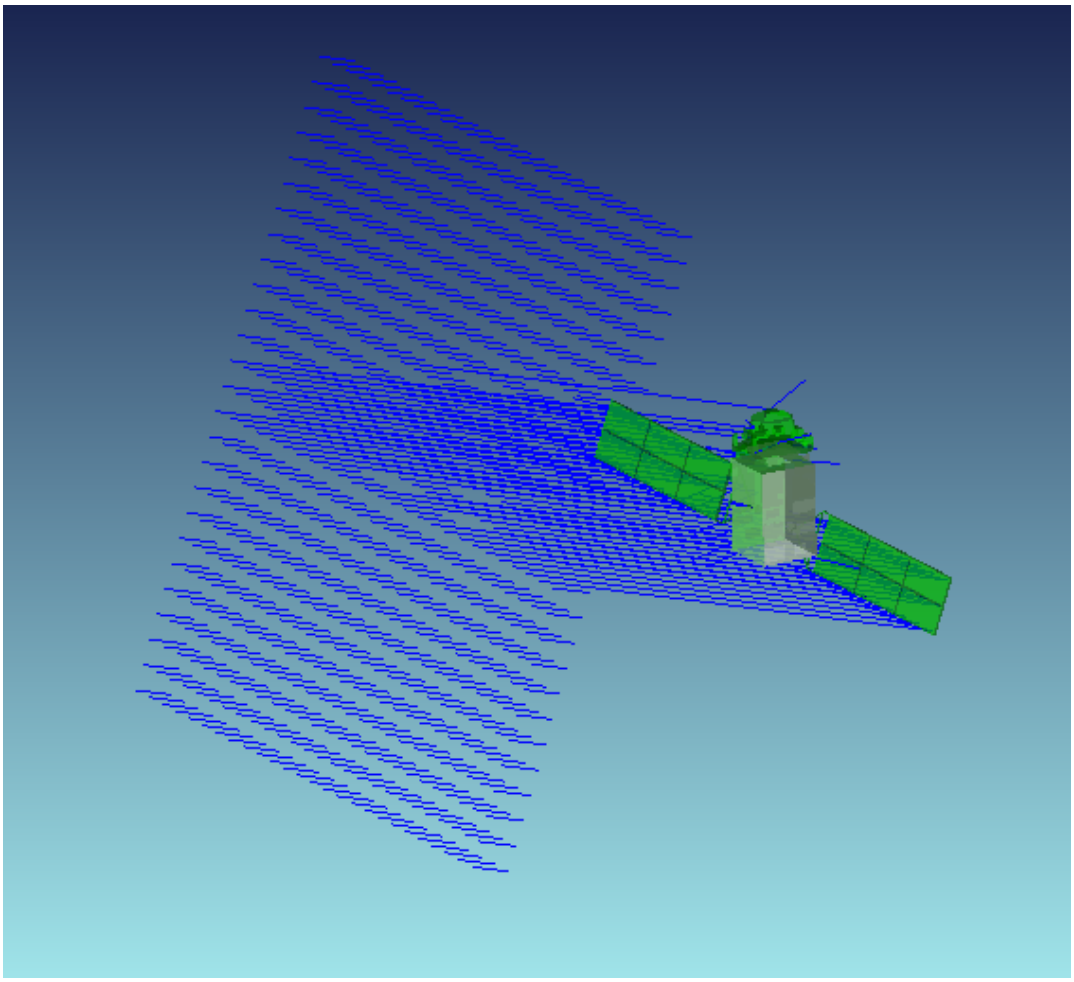

Figure 7.3: Representation of the ray-tracing in ZEMAX. In this figure the resolution is not that used in the work, but it is bigger in order to give a more clear idea of the description of the problem.

The resolution is the side of the quadratic singular pixel while the side-length is the size of the side of the quadratic array of pixels. The source is programmed to rotate around the spacecraft in order to represent all the relative configurations. In order to do it in ZEMAX, a macro programmed in the language of ZEMAX is used.

7.1.3 ZEMAX MACRO

The ZEMAX macro has two main objectives:

- to simulate the relative configuration between spacecraft (CAD geometry) and Sun (ray source);
- to save the results of the ray tracing into files which are then used by ARPA to calculate the SRP force.

The relative configuration is defined by the two angles azimuth A (angle between the z-axis and the projection of the Sun on the satellite x,z plane) and the elevation E which is the angle between the sun vector and the plane defined by the x-z axes of the spacecraft (Fig. 5.1). With the two

angles both the attitude modes of the satellite can be described as well as in the analytical case. The YS mode is defined by $E = 0$ and, since the ON mode is used in the range $\beta \in [-20, 20]$deg and, in the ON mode, $E = \beta$, the two angles A and E are defined in the following intervals:

- $A \in [0, 360]$deg;
- $E \in [-20, 20]$deg.

In ZEMAX the ray source rotates with A around the perpendicular axis to the satellite x,z plane and it has an elevation of E on the satellite x,z plane, while the solar panels just rotate with A around the perpendicular axis to the satellite x-z plane (y). The macro is written in order to :

- select the two ranges of A and E;
- select the step-size in which the range of A and E are divided;
- consider both the YS mode and ON mode and therefore to rotate the solar panels of a desired angle;
- decide the name of the output file from Zemax.

The name of the output file has to be written in a specific way because it has to be read by the software ARPA. The standard naming of the file is (following what proposed by Gini):
Satellite_name+"_"+*Resolution*+"_"+*analysis*+*direction*+"_"+*AZ*+"_"+*EL*+".ZRD".
Where:

- *Satellite_name* = name of the object simulated (5 letters, e.g., "QZS__").
- *Resolution* = number from 1 to 8, representing the dimension of each ray-source pixel:
  1. 1 mm^2;
  2. 2 mm^2;
  3. 5 mm^2;
  4. 1 cm^2;
  5. 2 cm^2;
  6. 5 cm^2;
  7. 1 dm^2;
  8. 25 mm^2.
- *Analysis* = Non-gravitational force to be considered: 2) Solar Radiation Pressure (ARPA considers also other non-gravitational forces but in this work only SRP is considered) .
- *Direction* = specifies whther the rays are coming from front or the back (leave this flag 0 = rays only from the front).
- *AZ* and *EL* = identify the azimuth and elevation of the incoming rays in degrees:
  1. AZ = SXXXXXX:
     - S represents the sign of the angle (m =minus and p=plus);
     - XXXXXX represents the value of the angle, 3 digits for the units and 3 for the decimals.
  2. EL = SXXXXX. Identical to AZ, but only 2 digits for units.

7.1.4 The output of ZEMAX

The output files of Zemax are binary files (format .ZRD) that contain some important information about all the rays for every combination of A and E. The information that ARPA needs and ZEMAX gives in output are:

- *Object-ID*: the number which identifies the CAD object;
- *Face-ID* : number which identifies a particular face of a CAD object;
- **N** =(N_x, N_y, N_z) : vector which represents the normal to the surface impinged by a particular ray, expressed in the ZEMAX reference frame;
- **-S** =(L, M, N) : vector of the ray before the reflection on the object, expressed in the ZEMAX reference frame.

Zemax gives in output also other parameters as the position of the incident ray in the Zemax reference frame, but ARPA does not need them.

7.2 ARPA

ARPA is a Fortran software which needs in input the output files of ZEMAX and the optical properties for each face of each object. ARPA's output is adimensional force and torque coefficients of the non gravitational forces. In this work it calculates the adimensional force and torque coefficients due to the Solar Radiation Pressure. In particular this thesis is interested in the force because there are not enough published information (like the materials involved and their characteristics) and therefore the center of mass cannot be calculated to compute the torque. As already explained in the previous section ZEMAX associates a number to each face of the CAD objects. ARPA has to associate an optical property to each face of each object and therefore it needs an input file with the correct optical properties.

Surface Name	ID	ObjID	FaceID
panels	1	2	0
panels	2	2	1
panels	3	2	2
panels	4	2	3

(a) *Identification of the face.*

alpha_BOL	alpha_EOL	eps_BOL	specularity
0.7500	0.7500	0.7500	0.8400
0.7500	0.7500	0.7500	0.8400
0.7500	0.7500	0.7500	0.8400
0.7500	0.7500	0.7500	0.8400

(b) *Association of the correct optical property.*

Figure 7.4: Representation of the input file of the properties of the faces proposed in [19]. In the example above the object involved is the solar panels.

Figure 7.4 shows how the input file is built. The optical properties involved in this work are:

- $\alpha_{BOL} = \alpha_{EOL}$ because there is no information about the decay of the materials and they have the meaning already explained in the subsection 3.4.1 [19];
- $\bar{\epsilon}_{EOL}$ has the same meaning of $\bar{\epsilon}$ introduced in the subsection 3.4.1. In this thesis it is not considered because it has no meaning for this SRP study;
- *specularity* represents the fraction of reflected incident radiation which is specularly reflected and it will be called γ.

In the context of the work of this thesis a new version of ARPA is developed. The new version of ARPA, updated for this particular work by Prof. S. Casotto of the Department of Astronomy of the University of Padova, takes into account the two different expressions of the force used respectively for the body and for the solar panels of the satellite as well as in analytical model. In order to simplify the problem and to recognize the different force models, the solar panels are always identified by *Obj-ID*=2. In this way ARPA uses the force model expressed by Eq. 3.12 if the object is recognized as solar panels otherwise it uses Eq. 3.15. Therefore using the specific notation of this thesis and considering the same kind of input files of the previous version, ARPA calculates the three fractions of absorption, diffuse reflection and specular reflection as:

$$\alpha = \alpha_{BOL} = \alpha_{EOL}, \tag{7.1a}$$

$$\delta = (1-\alpha)(1-\gamma), \tag{7.1b}$$

$$\rho = (1-\alpha)\gamma. \tag{7.1c}$$

From the computational point of view, since the output of ZEMAX directly provides the direction of the incoming radiation $\boldsymbol{e}_\odot$ and local outward normal to the surface $\mathbf{e}_n$, it is faster and easier to compute the force in these directions. Hence, considering the equation 3.12 for the solar panels the force in ARPA in the aforementioned directions is given by:

$$\begin{aligned} \mathbf{F_n} &= F_{pixel}\left(\frac{2}{3}\delta + 2\rho\cos\theta\right)\mathbf{n}, \\ \mathbf{F}_\odot &= F_{pixel}(1-\rho)\boldsymbol{e}_\odot. \end{aligned} \tag{7.2}$$

While for the body yields:

$$\begin{aligned} \mathbf{F_n} &= F_{pixel}\left(\frac{2}{3}(1-\rho) + 2\rho\cos\theta\right)\mathbf{n}, \\ \mathbf{F}_\odot &= F_{pixel}(1-\rho)\boldsymbol{e}_\odot, \end{aligned} \tag{7.3}$$

where F_{pixel} is calculated in the following way [19]:

$$\frac{\Phi A\cos\theta}{c} = \frac{\Phi A_{pixel}}{c} = F_{pixel}. \tag{7.4}$$

As already mentioned the instantaneous sun direction ($\boldsymbol{e}_\odot$) and the normal to the surface impinged are given by the output of ZEMAX which contains the aforementioned **N** and **S**. Hence ARPA has all the instruments to calculate the force. Multiple reflections are also modeled by ARPA. In the work of this thesis it was assumed that the effects of the second and further reflections due to the diffusive component is small with respect to the specularly refected component of the radiation, and hence can be neglected. This is done because the diffuse reflection takes place in a Lambertian way, which therefore results in a distribution in space of the total energy of the reflecting rays, while the component of radiation that is specularly reflected maintains a high level of energy and hence the reflected radiation can give an extra contribution to the total force due to SRP [19]. Neglecting the diffuse radiation and subtracting the absorbed radiation component, the force per pixel associated to each specularly reflected ray after the n-th reflection is [19]:

$$F_{pixel-n^{th}refl} = \frac{\Phi A_{pixel}}{c}\prod_{j=1}^{N}\rho_j\gamma_j. \tag{7.5}$$

The maximum number of multiple reflections considered in this thesis is three. As may be observed the force due to the multiple reflections is multiplied by a specular reflective factor that is always smaller than one and often lower than 0.5 therefore it does not make sense to consider more than three reflections. Eventually ARPA generates an output file with the adimensional force and torque coefficients for every couple (A,E).

Az (deg)	El (deg)	CX_srp	CY_srp	CZ_srp	CTX_srp	CTY_srp	CTZ_srp
0.000	-25.000	-3.509073E+01	7.417676E-02	-7.141957E+01	-9.266795E-01	-6.493017E+00	2.734595E-01
0.000	-24.000	-3.371194E+01	7.031409E-02	-7.196885E+01	-9.473374E-01	-5.933770E+00	2.797859E-01
0.000	-23.000	-3.244012E+01	9.530775E-02	-7.238604E+01	-1.000922E+00	-5.844659E+00	2.781994E-01
0.000	-22.000	-3.086042E+01	6.561314E-02	-7.275910E+01	-9.439161E-01	-6.051711E+00	2.560694E-01
0.000	-21.000	-2.949338E+01	1.234470E-01	-7.302579E+01	-1.151911E+00	-5.535993E+00	2.610186E-01
0.000	-20.000	-5.221290E-02	-1.546959E+01	-7.182435E+01	2.810051E+01	1.198326E-01	-4.598239E-02
0.000	-19.000	-4.025913E-02	-1.426975E+01	-7.222626E+01	1.979014E+01	9.414526E-02	-9.210949E-02
0.000	-18.000	-5.159864E-02	-1.389042E+01	-7.200291E+01	2.052543E+01	2.784475E-02	-6.400907E-02
0.000	-17.000	-3.301786E-02	-1.317517E+01	-7.321805E+01	1.570130E+01	1.332448E-01	-5.555128E-02
0.000	-16.000	-5.565358E-02	-1.226190E+01	-7.385286E+01	1.376712E+01	3.998528E-02	-7.182607E-02

Figure 7.5: Output of ARPA as conceived in [19]. The data presented here do not have a descriptive meaning, but they figure just to give the idea of the composition of the output.

The adimensional coefficient C_i_srp is a component of C_srp that is given by [19]:

$$C_{srp} = F_{srp}\frac{c}{\Phi A_{ref}}, \tag{7.6}$$

where A_{ref} is an arbitrary reference area adopted to adimensionalize the coefficients [19]. Furthermore it can be set in the setup of ARPA. Eventually from the output of ARPA the components of the acceleration can be tabulated as function of (A,E). In these tables (three tables for three components) the SRP acceleration is tabulated with respect to the two angles azimuth A and elevation E, in particular A varies along the columns and E varies along the rows.

7.3 Bidimensional interpolation

In order to be able to obtain the value of the acceleration for all the possible couples (A,E) a bidimensional interpolation [10] is considered. For every element i of each component of the acceleration it wants to estimate, by interpolation, the function $a_i(A,E)$ at some untabulated point (A,E). The approach used is the *bilinear interpolation*.

Bilinear interpolation

The grid square in which the point (A,E) falls is the four tabulated points that surround the desired interior point. For convenience it will number these points from 0 to 3, counterclockwise starting from the lower left[10]. More precisely, if:

$$A_l \le A \le A_u, \tag{7.7a}$$
$$E_l \le E \le E_u, \tag{7.7b}$$

then:

$$a_{i0} = a_{ll}, \tag{7.8a}$$
$$a_{i1} = a_{ul}, \tag{7.8b}$$
$$a_{i2} = a_{uu}, \tag{7.8c}$$
$$a_{i3} = a_{lu}. \tag{7.8d}$$

The simplest interpolation in two dimensions is bilinear interpolation on the grid square. Its formulas are:

$$t = \frac{A - A_l}{A_u - A_l}, \tag{7.9a}$$
$$u = \frac{E - E_l}{E_u - E_l}, \tag{7.9b}$$

so that t and u each lie between zero and one, and:

$$a_i(A,E) = (1-t)(1-u)a_{i0} + t(1-u)a_{i1} + tua_{i2} + (1-t)ua_{i3}. \tag{7.10}$$

In order to verify the accuracy of this instrument the results of the interpolation are compared with the ray tracing values for the query points of the interpolation. The step-size used in the ray-tracing to tabulate the value of the acceleration is one degree both for the azimuth angle and

for the elevation angle. Considering the computation effort of ZEMAX this step-size is little, but it is needed to have a good accuracy of the interpolation. It is due to the shape of the surface described by the components of the acceleration that have not a linear tendency. However with this step-size the RMS of the residuals calculated as difference between the interpolated values and the sample ray-tracing values is: $\approx 2 \times 10^{-6}\,\mathrm{nm/s^2}$. This precision is even better the tolerance expected for this work ($\approx 1 \times 10^{-3}\,\mathrm{nm/s^2}$). The program which provides the bilinear interpolation is written in the fortran language. As may be observed Eq. 7.10 gives problems if one between A and E ore both is/are tabulated values. If both are already tabulated the program gives in output the corresponding tabulated value of the acceleration. Moreover if only one of the two is a tabulated value the program switches in a *linear interpolation* in a direction or in the other. The linear interpolation is obtain from Eq. 7.10 setting t or u equal to zero (it depends on the direction considered).

7.4 Fit of the analytical model to the ray-tracing results

The purpose of this section is to find the best box-wing model which fits the acceleration obtained with the ray-tracing technique described by the minimum number of parameters. The reason of this analysis stems out from the potential possibility that a more accurate model,e.g. the ray-tracing model, could improve the quality of the estimated QZS-1 orbits presented in Chapter 6 (i.e. considering a box-wing model). Then the difference between the best box-wing model and the ray tracing model is used as SRP model for the orbit determination and its performances are compared to the results of Chapter 6 (SLR residuals and ECOM parameters). The ray-tracing results are computed considering the optical properties of Table 5.2. In order to understand in a simpler and clear way the effects, only the box-shaped body of the spacecraft and the YS mode are considered. The YS mode can give most information in terms of the performances of the POD as my be observed in the Figures 6.2 and 6.4. Moreover, considering the YS mode the problem is simplified and the analysis of the ON mode cannot give more information for the aim of this section. Furthermore, to consider also the solar panels would add other uncertainties about the optical properties, since there is even lower information regarding the solar panels than the body. The approach used to fit the analytical model to the acceleration resulting from the ray-tracing analysis is the least-squares method (see Appendix A). Moreover the box-wing model is chosen considering only the $\alpha + \delta$ contribution, which, for the optical properties assumed, is the most significant contribution. Therefore with these assumptions and considering Eqs. 5.13 and 5.1 the expression of the acceleration is given by:

$$\begin{aligned} \boldsymbol{a} \quad = \quad & -|\sin\epsilon| \cdot H(+\sin\epsilon) \cdot \left[a_x^{\alpha\delta} \cdot (\boldsymbol{e}_\odot + \tfrac{2}{3}\boldsymbol{e}_{+x})\right] \\ & -|\sin\epsilon| \cdot H(-\sin\epsilon) \cdot \left[a_x^{\alpha\delta} \cdot (\boldsymbol{e}_\odot - \tfrac{2}{3}\boldsymbol{e}_{+x})\right] \\ & -|\cos\epsilon| \cdot H(+\cos\epsilon) \cdot \left[a_{+z}^{\alpha\delta} \cdot (\boldsymbol{e}_\odot + \tfrac{2}{3}\boldsymbol{e}_{+z})\right] \\ & -|\cos\epsilon| \cdot H(-\cos\epsilon) \cdot \left[a_{-z}^{\alpha\delta} \cdot (\boldsymbol{e}_\odot - \tfrac{2}{3}\boldsymbol{e}_{+z})\right]. \end{aligned} \tag{7.11}$$

Therefore the partial acceleration that have to be estimate are three: $a_{+z}^{\alpha\delta}$, $a_{-z}^{\alpha\delta}$ and $a_x^{\alpha\delta}$. As already mentioned the approach used to estimate the parameters of the box wing model is the least-squares method. The normal equations (see Appendix A) of the least squares approach are:

$$\boldsymbol{x} = (\boldsymbol{H}^T\boldsymbol{H})^{-1}(\boldsymbol{H}^T\boldsymbol{y}), \tag{7.12}$$

where in this case:

- $\boldsymbol{x}$ is the 3×1 vector of the parameters to estimate;
- $\boldsymbol{H}$ is the $n \times 3$ design matrix (see Appendix A) of the considered least squares problem;

- $\boldsymbol{y}$ is the $n \times 1$ vector of the observed data, i.e. the acceleration obtained from the ray-tracing analysis.

Table 7.1: Partial acceleration best fitting the ray-tracing considering only the body contribution. All values in nm/s^2.

	value
$a_{+z}^{\alpha\delta}$	12.88
$a_{-z}^{\alpha\delta}$	13.92
$a_{x}^{\alpha\delta}$	28.22

The set of box-wing parameters which best fits the ray tracing is shown in Table 7.1 and the fit is shown in Fig. 7.6. In Fig. 7.6 the variation of the two components x and z is considered with respect to the azimuth angle A. As already explained in Sec. 5.1 the YS mode is described by the angles (A,E) when E is set to zero and therefore in this case $A = \epsilon$.

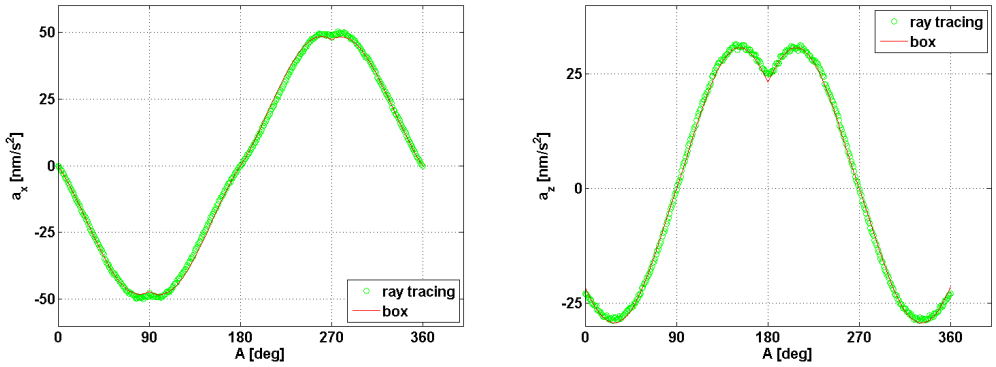

(a) *x-component of the acceleration.* (b) *z-component of the acceleration.*

Figure 7.6: Plot of the two components of the acceleration involved in the box-wing model fitting to ray-tracing results. These figures consider only the box contribution.

The RMS of the residuals, calculated as the difference between the box-wing model obtained and the ray-tracing model, is RMS = 0.99 nm/s^2. Looking at the correlation matrix (see Appendix A) it can be observed that the estimate parameters are uncorrelated.

$$\mathbf{C} = \begin{bmatrix} +1.00 & +0.12 & -0.35 \\ +0.12 & +1.00 & -0.35 \\ -0.35 & -0.35 & +1.00 \end{bmatrix} \tag{7.13}$$

The RMS shows that the difference between the two models can be roughly considered as 1nm/s^2 and it is interesting now to analyze what is the effect of this amount in the orbit determination.

Furthermore, considering the adjusted parameters from Chapter 6 (see Table 6.2 and Table 6.3) the box-wing model for the YS mode that best fit the observation data resulting from the analysis with NAPEOS is defined by only two parameters: $a_{zx}^{\alpha\delta}$ and $\Delta a_{zx}^{\alpha\delta}$. But from Eq. 5.18 these partial accelerations can be rearranged as: $a_{z}^{\alpha\delta}$ and $a_{x}^{\alpha\delta}$. Then from Eq. 5.16 the expression of the accel-

eration in the spacecraft reference frame is given by:

$$\begin{aligned} a_x &= -\tfrac{2}{3} a_x^{\alpha\delta} \cdot \cos\theta_x \\ &\quad -a_x^{\alpha\delta} |\cos\theta_x| \cos\theta_x \\ &\quad -a_z^{\alpha\delta} |\cos\epsilon| \cos\theta_x, \\ a_z &= -\tfrac{2}{3} a_z^{\alpha\delta} \cdot \cos\epsilon \\ &\quad -a_z^{\alpha\delta} \cdot |\cos\epsilon| \cos\epsilon \\ &\quad -a_x^{\alpha\delta} \cdot \cos\epsilon |\cos\theta_x|. \end{aligned} \tag{7.14}$$

This acceleration allows to estimate the best box-wing model which fits the ray-tracing results and that is the most similar to the model adjusted with the validation. Moreover it can be observed that the ϵ angle during the YS mode is always in the range [0 160] deg. It can be calculated from the relation that define ϵ, i.e. Eq. 2.5, and considering that the elevation of the Sun over the orbital plane is confined in the two intervals [-60 -20]deg and [20 60]deg. The least squares approach is applied as well as before and it gives results with an RMS=1.01 nm/s^2 of the residuals obtained also in this case as difference between the calculated value with the box-wing model and the ray-tracing model. Therefore the precision is basically the same and also the correlation matrix shows uncorrelated results.

$$\bar{\mathbf{C}} = \begin{bmatrix} +1.00 & -0.56 \\ -0.56 & +1.00 \end{bmatrix} \tag{7.15}$$

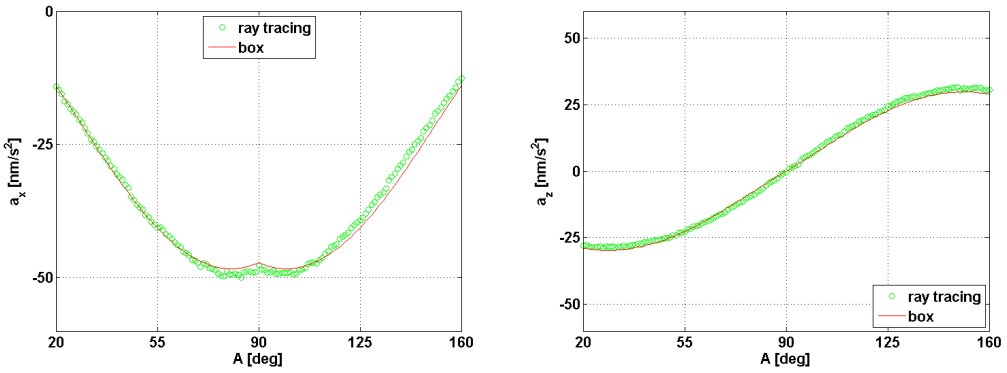

(a) *x-component of the acceleration.* (b) *z-component of the acceleration.*

Figure 7.7: Plot of the two components of the acceleration involved in the box-wing model fitting to ray-tracing results. These figures consider only the box contribution. It is calculated for the box wing model expressed by eq. 7.14

Therefore there are three different model: a reference model (the adjusted model) and two box-wing models defined respectively by three and two parameters that fit the ray-tracing results. It is interesting to see also what is the difference considering a model or another about the effects

Table 7.2: Partial accelerations best fitting the ray-tracing results considering only the body contribution. Two different models are introduced: the first consider three parameters and the second one only two as well as the reference model. All values in nm/s^2.

	ref. model	Model-1	Model-2
$a_z^{\alpha\delta}$	+13.00	+13.40	+13.13
$\Delta a_z^{\alpha\delta}$	+00.00	-00.52	+00.00
$a_x^{\alpha\delta}$	+27.00	+28.22	+28.31

on the orbit determination performances.

7.5 Orbit determination

This analysis has a precise purpose: to show if a ray-tracing model could improve the orbit determination performance compared to the box-wing model. The code for the orbit determination used is a program written in C++ language already used by DLR in the analysis of the SRP for the satellite GIOVE-B [26]. It uses the GHOST's library. GHOST is a powerful software package for GPS based orbit determination of satellites in low Earth orbit (LEO). GHOST comprises different modules for data preprocessing, kinematic positioning and reduced dynamic orbit determination using spaceborne GPS measurements. Satellite laser ranging data can, furthermore, be processed for orbit validaton purposes. All programs build up on a common library of C++ modules for GNSS data processing, spacecraft trajectory modeling, and estimation [31]. The GHOST library and application programs have been developed by DLR's German Space Operations Center (DLR/GSOC) in close cooperation with the Delft Institute of Earth Observation and Space Systems (DEOS) at TU Delft [31]. The programme used in this work has been modified in order to insert QZS-1 specifications and the results of the ray tracing analysis. It follows the principles presented in chapter 4 and for this particular case it is important to underline:

- the *observed* state vector is obtained by the propagation of the orbit considering the initial input data and the GHOST's without any model for the SRP;
- the system deviation vector (Eq. 4.13) is composed by the deviations of the state vector and five ECOM parameters: D0, Y0, B0, BC and BS;
- the SRP force model considered is the difference between the box-wing model and the ray-tracing model. It means that the SRP acceleration is given by the difference between Eq. 7.14 and the acceleration obtained from the ARPA computation;
- the residuals considered in this section are computed as the difference between the observed position and the calculated position (with the model of the SRP) expressed in the RTN frame (see Eq. 2.1).

The propagation considers an arc of three days with a step-size of five minutes. The input of the program is given by:

- time: initial date, final date, integration step;
- orbital elements: a, e, i , Ω, ω, M;
- PRN of the satellite, that is J01 for QZS-1;
- the box-wing parameters;
- the initial values of the ECOM parameters, that are set to zero;
- the a priori standard deviations.

It is important to notice that it does not deal with real observation data, but it is just a simulation to test the effect on the orbit of the difference between a simple box-wing model and a more accurate ray-tracing model.

The purpose of this analysis can be summarized in two main points:

- if the estimate ECOM parameters can supply the difference between the ray-tracing model and the box-wing model;
- the comparison between the radial residuals with respect to the β angle and the SLR residuals of Chapter 6 .

Looking at Fig. 6.2, Fig. 6.4 and Fig. 6.5 Chapter 6 shows that there is an improvement considering a simple a priori model as the box-wing model, but there are still errors that cannot be completely explained. The goal is to check if a more accurate geometric model can explain, in part or completely, those errors. The interest of the work is in the variation of the above mentioned quantities with respect to the β angle. There are two ways to change the elevation of the

Sun over the orbital plane: acting on the orbit or acting on the Sun position. The first one is obtained varying Ω the Right Ascension of the Ascending Node RAAN and the second one changing the starting date of the arch period. In order to consider the right combination of date and orbital elements the values of these quantities are taken from the output of NAPEOS. The interval of time considered is the year between October 2015 and October 2016. The analysis considers only the YS mode and only the contribution given by the body of the satellite without solar panels. It simplifies the problem and it is enough to understand if a more accurate model could improve the SRP modeling. It is due to the results of Chapter 6 which shows that the most important error involve the YS mode and the difficulty to estimate the properties of the solar panels even more than the body.

7.5.1 Ray-tracing model

As already mentioned the geometry involved for this analysis is the spacecraft without the solar panels, therefore considering: box-shaped body, ± surface components, the under antenna component and the antenna. The elevation E is set to zero degrees while the azimuth A varies between 0 and 360 degrees. The step-size considered is one degree. Considering the YS mode the software needs to calculate the ray-tracing acceleration for every ϵ angle. The connection between ray-tracing and box-wing description is that the ϵ angle correspond to the azimuth angle A. With a simple linear interpolation of the tabulated value resulting from ARPA it is possible to calculate the acceleration for the desired ϵ angle. It is because the YS mode is considered, hence there is only an angle which varies, otherwise a bidimensional interpolation needs to be taken into account. Calling y(x) the function of the tabulated values, x the variable of this function and x_1 the desired point in which the function has to be calculated, the linear interpolation calculation is [10]:

$$y(x_1) = y_j + \frac{x_1 - x_j}{x_{j+1} - x_j}\left(y_{j+1} - y_j\right), \tag{7.16}$$

where $x_j < x_1 < x_{j+1}$. Updating this relation for the problem considered it yields:

$$a(\epsilon) = a_j + \frac{\epsilon - A_j}{A_{j+1} - A_j}\left(a_{j+1} - a_j\right), \tag{7.17}$$

where $A_j < \epsilon < A_{j+1}$ and a represents a component of the acceleration.

7.5.2 Results

The orbit determination shows that considering the difference between the two models as SRP model the values of the ECOM parameters are low. In particular D0 and Y0 result to be very close to zero nm/s^2, while B0, BC and BS have a β dependency as could be expected from Fig. 6.2. However one of the most important things to notice is that there is a radial error with a β angle dependency. In particular this part of the work focuses on the mean value of the radial residuals over an orbit. This magnitude in fact can be compared to the SLR residuals obtain in the validation process of the box-wing model. The analysis considers both the box-wing models proposed in Table 7.2.

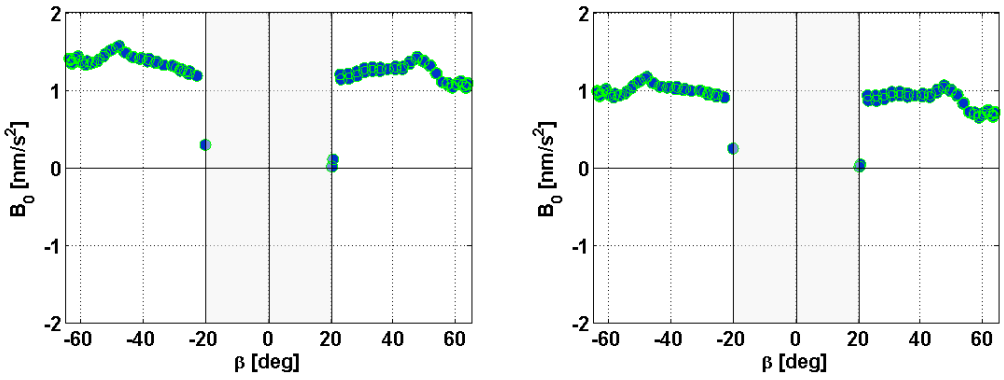

(a) *Model-1* (b) *Model-2*

Figure 7.8: Variation of B_0 with the β angle. The shaded areas represent the ON mode interval.

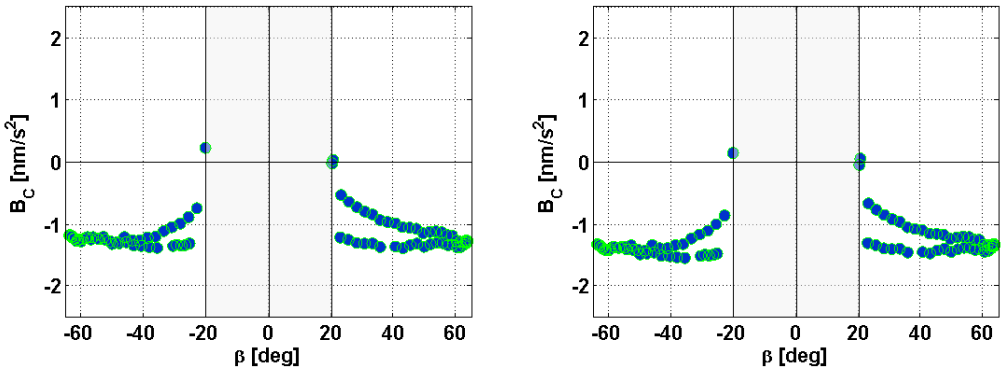

(a) *Model-1* (b) *Model-2*

Figure 7.9: Variation of B_C with the β angle. The shaded areas represent the ON mode interval.

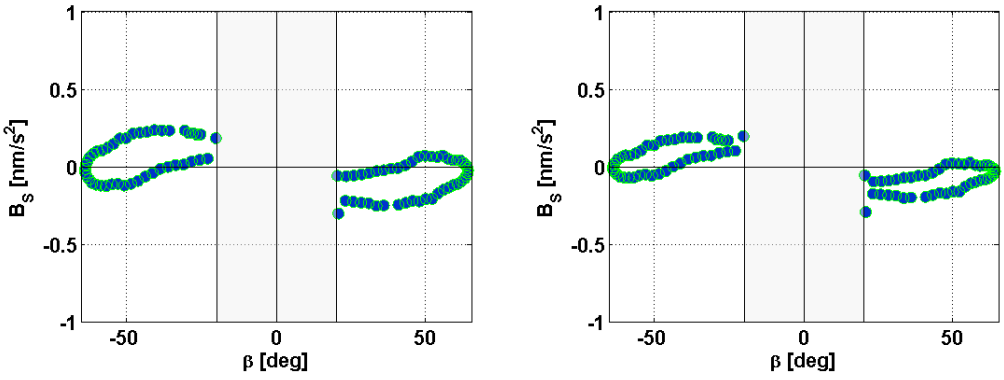

(a) *Model-1* (b) *Model-2*

Figure 7.10: Variation of B_S with the β angle. The shaded areas represent the ON mode interval.

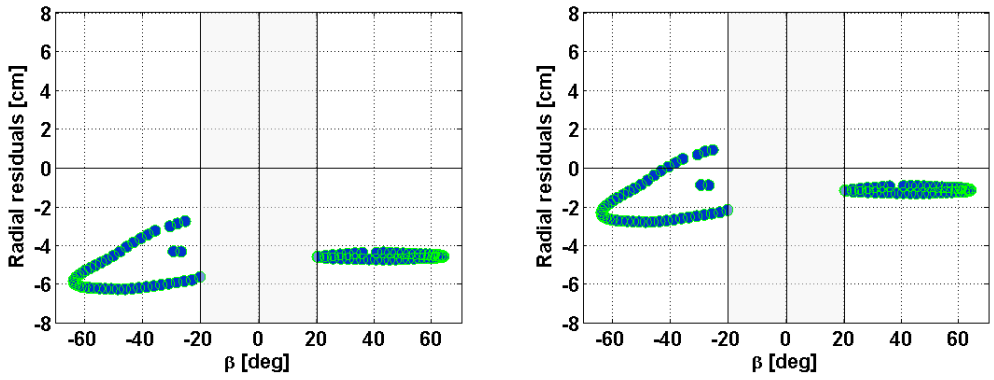

(a) *Model-1* (b) *Model-2*

Figure 7.11: Variation of radial residuals with the β angle. The shaded areas represent the ON mode interval and therefore they are not considered.

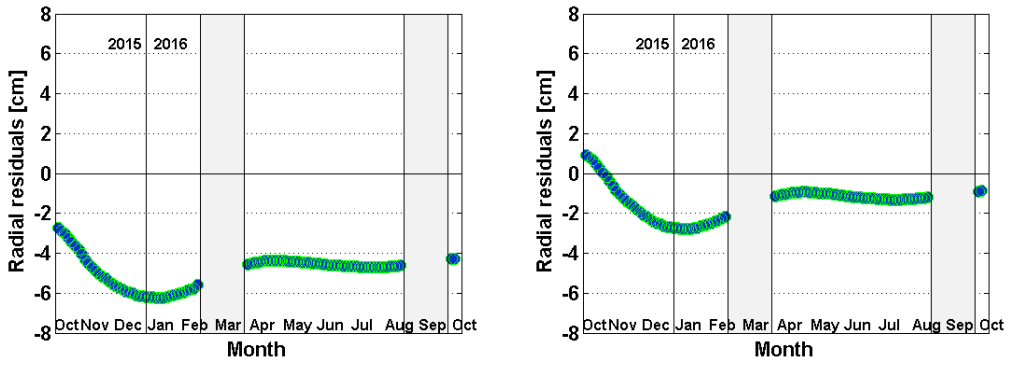

(a) *Model-1* (b) *Model-2*

Figure 7.12: Variation of the radial residuals with the time. The period considered is from October 2015 to October 2016 The shaded areas represent the ON mode interval and they are not considered.

Looking at the figures above it can be observed that there is not a significant difference between the application of the two models, but Model-2 gives slightly lower values for all the quantities considered, therefore a box-wing model with only two parameters seems to be enough to describe the SRP acceleration. It is clear that there are different profiles depending on if β is increasing or decreasing and it is something that can be observed also in Fig. 6.2. The plots show also an asymmetry with respect to the zero value as expected from the considerations about the real observed data (see Chapter 6). The radial residuals here are considered as the mean value of the residuals over the three-days arc. As can be observed Model-2 gives lower residuals in absolute value while the maximum value reached is $\approx 10\,\text{cm}$ in module in the both cases. Furthermore as can be recognized from Fig. 7.11 and Fig. 7.12 the consideration of the $\pm z$ asymmetry (i.e. Model-1) introduces a shift of the curve of $\approx -4\,\text{cm}$ while the shape is conserved.

Conclusion

The analysis of the effect of the difference between an accurate ray-tracing model of the spacecraft and a simple box-wing model in the orbit determination leads to some interesting results:

- a difference of roughly $1\,\text{nm/s}^2$ between the box-wing and ray-tracing models involves effects on the orbit determination that cannot be neglected;
- two parameters (that represent the so called Model-2) are enough to describe a box-wing model which fits a ray-tracing model;

- the comparison between the estimate ECOM parameters obtained in this section with those of Fig. 6.2 suggests that the implementation of a ray-tracing model in a software for POD like NAPEOS could give an improvement of the orbit quality. It could explain why the B_0, B_C and B_S parameters are not zero partially or maybe completely.
- Comparing the SLR residuals obtained with Fig. 6.4 and the radial residuals obtained in this analysis, a ray-tracing model seems to be able to explain part of the residuals shown in the validation process for the box-wing model but not completely. In fact the residuals of Chapter 6 are higher in magnitude. However it is something that should be check in Precise Orbit Determination with real observed data considering the ray-tracing model for the SRP.

7.6 Optical properties estimation

Since the real value of the optical properties of the surfaces is unknown and so far the properties used are based on reasonable assumptions it would be useful to estimate the values of these elements. As already mentioned four different materials are considered: black, silver, radiator for the y panels and the solar panels. The new version of ARPA, in fact, has another functionality: it calculates the partial derivatives of the optical coefficients of the materials. It allows to calculate the design matrix **H** of the fitting problem that in this case is the Jacobian defined by:

$$\boldsymbol{H} = \frac{\partial \boldsymbol{a}}{\partial x_i} \qquad i = 1, ..., k, \tag{7.18}$$

where $\boldsymbol{a}$ is the acceleration described by the model, **x** is the $k \times 1$vector of the partial accelerations that have to be estimated and k is the number of partial accelerations to estimate. ARPA will calculate for each pixel the partial derivatives and then the sum over all the pixels will give the set of partial derivatives for that combination of A and E. Repeating it for all the output files of ZEMAX the design matrix is complete. The five partial derivatives (three for the Eq. 3.15 and two for Eq. 3.12) are divided into three types: partial derivative for ρ with the model with re-radiation Eq. 3.15, partial derivatives for ρ and δ with the model without re-radiation used for the solar panels Eq. 3.12. For each pixel they are given by:

$$\frac{\partial \boldsymbol{a}}{\partial \rho_{bl\,i}} = -\frac{\Phi}{mc} A_{pix}\Big[-(\boldsymbol{e}_{\odot i} + \frac{2}{3}\boldsymbol{e}_{ni}) + 2\cos\theta_i \boldsymbol{e}_{ni}\Big], \tag{7.19a}$$

$$\frac{\partial \boldsymbol{a}}{\partial \rho_{sl\,i}} = -\frac{\Phi}{mc} A_{pix}\Big[-(\boldsymbol{e}_{\odot i} + \frac{2}{3}\boldsymbol{e}_{ni}) + 2\cos\theta_i \boldsymbol{e}_{ni}\Big], \tag{7.19b}$$

$$\frac{\partial \boldsymbol{a}}{\partial \rho_{ra\,i}} = -\frac{\Phi}{mc} A_{pix}\Big[-(\boldsymbol{e}_{\odot i} + \frac{2}{3}\boldsymbol{e}_{ni}) + 2\cos\theta_i \boldsymbol{e}_{ni}\Big], \tag{7.19c}$$

$$\frac{\partial \boldsymbol{a}}{\partial \rho_{sp\,i}} = -\frac{\Phi}{mc} A_{pix}\Big[-(\boldsymbol{e}_{\odot i}) + 2\cos\theta_i \boldsymbol{e}_{ni}\Big], \tag{7.19d}$$

$$\frac{\partial \boldsymbol{a}}{\partial \delta_{sp\,i}} = -\frac{\Phi}{mc} A_{pix} \cdot \frac{2}{3}\boldsymbol{e}_{ni}. \tag{7.19e}$$

Where:

- $\cos\theta_i = \boldsymbol{e}_{\odot i} \cdot \boldsymbol{e}_{ni}$
- *bl* indicates the black material;
- *sl* indicates the silver material;
- *ra* indicates the radiator material.

Furthermore ARPA has to recognize if the surface is black, silver or radiator. A way to do it, without changing the input-files in ARPA, is to consider three different ranges of α:

- if $0.9 \leq \alpha \leq 1.0$ the surface is black;
- if $0.2 \leq \alpha < 0.9$ the surface is silver;

- if $0.0 \leq \alpha < 0.2$ the surface is radiator.

In order to use the data furnished by the orbit determination the acceleration and the partial derivatives should be projected in the DYB and $\overline{DYB}$ frames respectively for YS mode and ON mode. The observed values are the empirical acceleration calculated as in Eq. 3.21. Then considering the reference initial values based on reasonable assumptions, using the least squares method, the best set of optical properties that fits the data is estimated:

$$\mathbf{x}^{ls} = \mathbf{x}^{ref} + (\mathbf{H}^T\mathbf{H})^{-1}\mathbf{H}^T(\mathbf{y}-\mathbf{a}), \tag{7.20}$$

where $\mathbf{y}$ represents the vector of the observed data, $\boldsymbol{a}$ represents the vector of the calculated values of the acceleration and $\mathbf{x}^{ref}$ is the vector of initial reference parameters considered.

8. CONCLUSIONS AND FUTURE WORK

8.1 Conclusions

In this project two different ways to model the Solar Radiation Pressure have been investigated: the analytical derivation and the ray-tracing approach. The analytical model consists in a simple box-wing model in which the spacecraft is considered as the sum of a box made of plates, which represents the body, and wings (two flat plates) that are the solar panels. It is based on the previous work of DLR for the Galileo satellites [24] and upgraded in order to consider two different attitude modes: the Yaw Steering mode and the Orbit Normal mode. It implies the introduction of a new reference frame, the $\overline{DYB}$ frame [28] which is useful to estimate the coefficients of the empirical SRP model ECOM. The second approach is a ray-tracing technique which considers a detailed geometry of the spacecraft through a CAD model. It is based on the previous F.Gini's work at the University of Padova [19] using the commercial software ZEMAX for the ray-tracing and the program ARPA of the University of Padova to compute the forces. The present work considers a more complex satellite configuration with respect to the GOCE satellite considered in Gini's work. In the ZEMAX macros in fact an additional relative motion between the body of the spacecraft and the solar panels has been considered. Moreover, this work allows to consider both the two different attitude modes of QZS-1 (YS and ON mode). Furthermore, ARPA has been upgraded to a new version which considers also the SRP force model with a sort of instantaneous re-radiation of the absorbed fraction of the incident radiation. For a future work ARPA provides also the partial derivatives with respect to the optical properties to allow an estimate of the unknown optical properties. Eventually, concerning the ray tracing approach, tabulated values for the three components of the acceleration are given with respect to the angles which define the relative position between the body and the solar panels. Moreover, a Fortran routine for the bidimensional interpolation is developed in order to calculate the SRP acceleration for all the relative configurations.

The validation of the simple analytical box-wing model into the NAPEOS software gives an adjusted model which provides benefits to the quality of the orbit determination [28]. These improvements are listed below:

- the values of the day boundaries discontinuities decrease their value by a factor of two thirds;
- the SLR residuals are substantially improved of a factor two in the YS mode and of a factor four in the ON mode;
- a reduction of $\approx 85\%$ of the orbit-induced clock variations during the ON mode;
- the use of the empirically adjusted box-wing parameters reduces the amplitude of complementary ECOM parameters estimated in the orbit determination.

Hence, the a priori box-wing model decreases both the orbit errors and empirical SRP parameters, but it does not fully removed them [28]. Furthermore the adjusted parameters are consistent with the expected values calculated from geometrical and optical assumption with the exception of the y-components. This discrepancy in the y-direction could be related to the thermal exchanges that involve the y-surfaces caused by the heat pipes. However it is something difficult to understand and explain since a limited amount of official information about the thermal evolution of the spacecraft is available.

The orbit determination using the GHOST's library shows that the difference between a ray-tracing model based on a detailed geometry and the box-wing model causes orbital position errors and the need of empirical SRP parameters. Therefore it suggests that the ray-tracing modeling could explain part of the SLR residuals and the presence of the ECOM parameters that the validation process of the box-wing model shows, even if not completely.

In conclusion the box-wing model provides a good model of the SRP and it improves the orbit quality. A ray-tracing could increase even more the orbit determination performances but

it cannot explain completely the results obtained from the orbit determination with NAPEOS. However it would be interesting to use the ray-tracing results directly into the NAPEOS software. Additionally, a complete and accurate analysis requires more detailed information related the optical/thermal properties and the true attitude as well as offsets between the nominal and actual solar panel angle. These information would be required from the provider and the operator of QZS-1 spacecraft.

8.2 Future work

As already mentioned the next step would be to implement the ray-tracing model into NAPEOS. The ray-tracing model is represented by tables of the components of the acceleration with respect to the azimuth and elevation angles. In order to do it the acceleration for any couple of azimuth and elevation is required and this work provides the needed bidimensional interpolation. It would be interesting to notice the differences with a simple box-wing model employing real observed data. Moreover, if more detailed information will not be provided, using the tabulated values of the partial derivatives calculated by ARPA, the optical properties of the three materials considered could be estimated iteratively inside the NAPEOS software. On the contrary, if the optical and thermal properties will be furnished, the upgraded ARPA program is a very efficient tool to provide an accurate model of the forces involved since it considers the SRP, as well as the Earth Radiation Pressure and Thermal Re-Radiation.

A. General Linear Least Squares

The least squares approach is often used to condense and summarize a set of observed data by fitting it to a model that depends on adjustable parameters. It can also be used as a kind of constrained interpolation with the purpose to extend a few data points into a continuous function, but with some underlying idea of what that function should look like. The idea is to design a *merit function* [10] that measures the agreement between the data and the model with a particular choice of parameters. The parameters of the model are then adjusted to find the minimum of the merit function, yielding *best fit parameters*. It is also important to take into account that data are generally not exact, they are in fact subject to *measurement errors*. It may happen that the data do not fit the model even if the model is correct. It is useful therefore to test the *goodness of fit* considering statistical parameters.

In order to describe the least squares method some statistical basics have to be introduced. In particular the ideas of *standard deviation, RMS, covariance matrix* and *correlation matrix* need to be explain.

Standard deviation Given a set of N values $x_1, ..., x_N$ the mean of the values is given by [10]:

$$\bar{x} = \frac{1}{N}\sum_{j=1}^{N} x_j. \tag{A.1}$$

This value characterized the distribution's central value. In order to analyze a distribution of data it is important to characterized also the *variability* around the mean value. Therefore another magnitude is introduce: the *variance* [10]:

$$Var(x_1, ..., x_N) = \frac{1}{N}\sum_{j=1}^{N} (x_j - \bar{x})^2, \tag{A.2}$$

which estimates the mean squared deviation of x from its mean value. Often instead of the variance it is considered its square root, the *standard deviation* [10]:

$$\sigma(x_1, ..., x_N) = \sqrt{Var(x_1, ..., x_N)}. \tag{A.3}$$

Root Mean Squares (RMS) Given a set of N values $x_1, ..., x_N$ the root mean squares is given by the arithmetic mean of the squares of the set:

$$RMS = \sqrt{\frac{1}{N}\left(x_1^2 + ... + x_N^2\right)}. \tag{A.4}$$

Covariance matrix The *covariance* C can be defined as a measure of the joint variability of two random variables. In particular in the least squares problem the covariance gives the idea of the joint variability of two fitted parameters. The *Covariance matrix* $\mathbf{C}$ is a matrix whose diagonal elements are the variances of the fitted parameters and the off - diagonal elements are the covariances between the different fitted parameters [10].

Correlation matrix In the least squares approach the *correlation* is a statistical relationship between two estimated parameters and it is given by:

$$\bar{C}_{j,k} = \frac{C(a_j, a_k)}{\sigma(a_j)\sigma(a_k)}, \tag{A.5}$$

where $C(a_j, a_k)$ is the covariance of two random fitted parameters and $\sigma(a_j), \sigma(a_k)$ are the corresponding standard deviations. The correlation is a number in the range [-1,1] and the *correlation matrix* $\bar{\mathbf{C}}$ is a matrix whose elements are $\bar{C}_{j,k}$.

Given this brief introduction about significant statistical elements, the *general linear least squares method* can be described. It is given a set of N observed data $y_1, ..., y_N$ and a model whose general form is [10]:

$$y(x) = \sum_{k=1}^{M} a_k X_k(x), \tag{A.6}$$

where the quantities $X_1(x), ..., X_M(x)$ are arbitrary fixed functions of x. The functions $X_k(x)$ can be wildly nonlinear functions of x, the attribute linear above used refers only to the model's dependence on its parameters a_k [10]. For these linear models the merit function previously mentioned is given by [10]:

$$\chi^2 = \sum_{i=1}^{N} \left[\frac{y_i - \sum_{k=1}^{N} a_k X_k(x_i)}{\sigma_i} \right]^2. \tag{A.7}$$

σ_i is the *measurement error*, i.e. standard deviation of the i_{th} data point, presumed to be known. If it is unknown it is set to one. Let $\mathbf{H}$ a $N \times M$ matrix whose components are defined in the following way [10]:

$$H_{ij} = \frac{X_j(x_i)}{\sigma_i}. \tag{A.8}$$

The matrix $\mathbf{H}$ is called *design matrix* of the fitting problem. The best set of parameters is those that minimizes the merit function χ^2. The minimum is obtained when the derivative of χ^2 with respect to all M parameters a_k vanishes, which means:

$$0 = \sum_{i=1}^{N} \frac{1}{\sigma_i^2} \left[y_i - \sum_{i=1}^{M} a_j X_j(x_i) \right] X_k(x_i) \qquad k = 1, ..., M. \tag{A.9}$$

Equation A.9 can be rewritten as [10]:

$$\sum_{j=1}^{M} a_{kj} a_j = \beta_k, \tag{A.10}$$

where:

$$\alpha = \mathbf{H}^T \cdot \mathbf{H}, \tag{A.11a}$$

$$\beta = \mathbf{H}^T \cdot \mathbf{b}. \tag{A.11b}$$

$\mathbf{b}$ is a vector of length N defined by:

$$b_i = \frac{y_i}{\sigma_i}. \tag{A.12}$$

Hence Eq. A.9 can be written as:

$$\left(\mathbf{H}^T \cdot \mathbf{H}\right) \cdot \mathbf{a} = \mathbf{H}^T \cdot \mathbf{b}. \tag{A.13}$$

These are called *normal equations* of the least squares problem [10] and $\mathbf{a}$ is the vector of the best estimate parameters. The covariance matrix is defined as the inverse matrix $\mathbf{C} = \alpha^{-1}$. The variance associated with the estimate a_j can be computed in the following way:

$$\sigma^2(a_j) = \sum_{i=1}^{N} \sigma_i^2 \left(\frac{\partial a_j}{\partial y_i} \right)^2. \tag{A.14}$$

From $\mathbf{C}$ the *correlation matrix* can be calculated in the following way:

$$\bar{\mathbf{C}} = \mathbf{D}^{-\frac{1}{2}} \mathbf{C} \mathbf{D}^{-\frac{1}{2}}, \tag{A.15}$$

where $\bar{\mathbf{C}}$ is the mentioned correlation matrix and $\mathbf{D}$ is a matrix with the same diagonal element of $\mathbf{C}$, i.e. the variance associated with the fitted parameters.

It may happen that an a priori information $\mathbf{a}_0$ about the best set of parameters and the associated covariance matrix $\mathbf{C}_0$ are furnished. In this case the normal equations of the least squares become:

$$\left(\mathbf{H}^T \cdot \mathbf{H} + \mathbf{C}_0^{-1}\right) \cdot \mathbf{a} = \mathbf{H}^T \cdot \mathbf{b} + \mathbf{C}_0^{-1} \mathbf{a}_0, \tag{A.16}$$

where $\mathbf{C}_0^{-1}$ represents the weight matrix associated to the a priori information which is a diagonal matrix whose diagonal elements are defined by:

$$C_{0,jj}^{-1} = \frac{1}{\sigma_{0,j}^2} \qquad j = 1, ..., M. \tag{A.17}$$

Where σ_0 is the standard deviation associated with the a priori information. Eventually the covariance matrix in this case is computed as:

$$\mathbf{C} = \left(\mathbf{H}^T \cdot \mathbf{H} + \mathbf{C}_0^{-1}\right)^{-1}. \tag{A.18}$$

BIBLIOGRAPHY

[1] A. Milani, A.M. Nobili, and Farinella P. *Non-gravitational perturbations and satellite geodesy*. Adam Hilger Ltd., Bristol, 1987.

[2] G. Beutler et al. “Extended orbit modeling techniques at the CODE processing center of the international GPS service for geodynamics (IGS):Theory and initial results. ” In: *Manusc Geodesy* 19 (1994), pp. 367–386.

[3] H. F. Fliegel and T. E. Gallini. “Solar force modeling of block IIR Global Positioning System satellites”. In: *J. Spacecraft and Rockets* 33.(6) (1996), pp. 863–866. DOI: http://dx.doi.org/10.2514/3.26851.

[4] O. Montenbruck and E. Gill. *Satellite Orbits, Models Methods Applications*. Astronomy/Astrophysics. Springer, 2000. ISBN: 978-3-540-67280-7.

[5] M. Ziebart. *"High Precision Analytical solar radiation pressure modelling for GNSS spacecraft", Ph.D. thesis, University of East London*. 2001.

[6] M. Ziebart and P. Dare. “Analytical solar radiation pressure modelling for GLONASS using a pixel array”. In: *Journal of Geodesy* 75 (2001), pp. 587–599.

[7] R. H. Lyon. *"Geosynchronous Orbit Determination using Space Surveillance Network Observations and Improved Radiative Force Modeling", Master of Science in Aeronautics and Astronautics, Massachusetts Institute of Technology*. 2002.

[8] M. Ziebart. “Generalized Analytical Solar Radiation Pressure Modeling Algorithm for Spacecraft of Complex Shape”. In: *Journal of Spacecraft and Rockets* 41.5 (2004).

[9] S. Adhya. *"Thermal re-radiation modelling for the precise prediction and determination of spacecraft orbits." Ph.D. thesis, University of London*. 2005.

[10] W. H. Press et al. *Numerical Recipes, The Art of Scientific Computing*. Cambridge University Press, 2007. ISBN: 978-0-521-88068-8.

[11] N. Inaba et al. “Design concept of Quasi Zenith Satellite System”. In: *Acta Astronautica* 65 (2009), pp. 1068–1075. DOI: http://dx.doi.org/10.1016/j.actaastro.2009.03.068.

[12] Y. Ishijima et al. “Design and Development of the first Quasi-Zenith Satellite attitude and orbit control system”. In: *IEEE Aerospace conference* (2009), pp. 1–8. DOI: http://dx.doi.org/10.1109/AERO.2009.4839537.

[13] T. Springer. *NAPEOS mathematical models and algorithms*. 2009, publisher=Tech. Rep. DOPS-SYS-TN-0100-OPS-GN, ESA/ESOC, Darmstadt, keywords =.

[14] L. Cerri et al. “Precision orbit determination standards for the Jason series of altimeter missions.” In: *Marine Geod.* 33 (2010), pp. 379–418. DOI: http://dx.doi.org/10.1080/01490419.2010.488966.

[15] C. J. Rodriguez-Solano, U. Hugentobler, and P. Steigenberger. “Adjustable box-wing model for solar radiation pressure impacting GPS satellites.” In: *Adv. Space Res.* 49.7 (2010), pp. 1113–1128. DOI: http://dx.doi.org/10.1016/j.asr.2012.01.016.

[16] Japan Aerospace Exploration Agency. *"Interface Specification for QZSS"*. 2012.

[17] S. Casotto. *Introduzione alla Meccanica Celeste-Lecture notes*. 2012.

[18] A. Hauschild, P. Steigenberger, and C. Rodriguez-Solano. “QZS-1 yaw attitude estimation based on measurments from the CONGO network”. In: *Navig. J. ION* 59.(3) (2012), pp. 237–248. DOI: http://dx.doi.org/10.1002/navi.18.

[19] F. Gini. *"Goce Precise Non-Gravitational Force Modeling for POD Applications", PHD thesis, University of Padova, CISAS*. 2014.

[20] C.J. Rodriguez-Solano. *"Impact of non-conservativeforce modeling on GNSS satellite orbits and global solutions", PHD thesis, Technische Universität München*. 2014.

[21] RUAG Space. *"Thermal Insulation products"*. 2014.

[22] P. Steigenberger and S. Kogure. *IGS-MGEX: QZSS Orbit and Clock Determination*. IGS Workshop, Pasadena, 2014.

[23] QZSS-Cabinet Office (Japan). *Project Overview of The Quasi-Zenith Satellite System*. 2015.

[24] O. Montenbruck, P. Steigenberger, and U. Hugentobler. “Enhanced solar radiation pressure modeling for Galileo satellites”. In: *Journaly of Geodesy* 89 (2015), pp. 283–297. DOI: http://dx.doi.org/10.1007/s00190-014-0774-0.

[25] O. Montenbruck et al. “GNSS satellite geometry and attitude models”. In: *Advances in Space Research* 56 (2015), pp. 1015–1029. DOI: http://dx.doi.org/10.1016/j.asr.2015.06.019.

[26] P. Steigenberger, O. Montenbruck, and U. Hugentobler. “GIOVE-B solar radiation pressure modeling for precise orbit determination”. In: *Advances in Space Research* 55 (2015), pp. 1422–1431. DOI: http://dx.doi.org/10.1016/j.asr.2014.12.009.

[27] S. Kogure. *Status Update on the Quasi-Zenith Satellite System*. 2016.

[28] O. Montenbruck, P. Steigenberger, and F. Darugna. “Semi-Analytical Solar Radiation Pressure Modeling for QZS-1 Orbit-normal and Yaw-Steering Attitude”. In: *Advances in Space Research* 59.8 (2017), pp. 2088–2100. DOI: http://dx.doi.org/10.1016/j.asr.2017.01.036.

[29] ChineseGovernment. *BeiDou Navigation Satellite System*. URL: http://en.beidou.gov.cn/introduction.html.

[30] eoPortal directory. *Sharing Earth Observation Resources*. URL: https://directory.eoportal.org/web/eoportal/satellite-missions/q/qzss.

[31] DLR. *GPS High Precision Orbit Determination Software Tools (GHOST)*. URL: http://www.dlr.de/rb/desktopdefault.aspx/tabid-10749/10536_read-23371/.

[32] EuropeanSpaceAgency. *Galileo*. URL: http://www.esa.int/Our_Activities/Navigation/Galileo/What_is_Galileo.

[33] S. Ikari et al. *An Evaluation of Solar Radiation Pressure Models for QZS-1 Precise Orbit Determiantion (Department of Aeronautics and Astronautics, The University of Tokyo, Japan)*.

[34] Jaxa. *QZ-Vision*. URL: http://qz-vision.jaxa.jp/READ/qz-navi04.html.

[35] 2010 JAXA. *QZ 1:50 scale paper craft*. URL: http://qz-vision.jaxa.jp/READ/qz-craft.html.

[36] Japanese Aerospace Exploration Agency (JAXA). *Presskit Michibiki*.

[37] Japan Cabinet Office. *Quasi Zenith Satellite System*. URL: http://qzss.go.jp/en/overview/services/sv02_why.html.

[38] OpticStudio. *OpticStudio-Zemax*. URL: http://www.zemax.com/os/opticstudio.